Study of Thermoresponsive Hybrid Polymer for Oil Sands Applications

by

Jason K.H. Ng

A thesis submitted in partial fulfillment of the requirements for the degree of

Master of Science

in

Chemical Engineering

Department of Chemical and Materials Engineering
University of Alberta

Abstract

Many tailings treatment technologies rely on the use of water-soluble polyacrylamides (PAM) to flocculate fine solids. However, PAM-induced flocs are often loosely-structured and retain significant volume of water due to the hydrophilicity of PAM and fine clays in oil sands fine tailings. Thermoresponsive polymers and inorganic-organic hybrid polymers are both promising alternative flocculants to accelerate solids settling and improve sediment consolidation. As such, a multifunctional hybrid polymer (Al-NIPAM) was synthesized in this study by integrating inorganic $Al(OH)_3$ colloidal particle into the organic molecular structure of poly(*N*-isopropylacrylamide) (poly(NIPAM)) for the flocculation of mature fine tailings (MFT) suspension. The hybrid polymer responded to temperature changes, with a lower critical solution temperature (LCST) transition from hydrophilic coils to hydrophobic globules close to poly(NIPAM).

Zeta potential measurements showed that Al-NIPAM reduced the surface charges of fine solids in MFT, indicating polymer-particle adsorption interactions. The hybrid polymer exhibited charge selective adsorption in QCM-D with strong electrostatic attraction between the cationic $Al(OH)_3$-core in hybrid polymer and the negatively-charged surface. Furthermore, the adsorbed Al-NIPAM polymer layer became dehydrated and collapsed upon heating. Results from the adsorption and conformation experiments provided a basis for the use of Al-NIPAM as a flocculant in oil sands tailings treatment, where the cationic $Al(OH)_3$-cores in the hybrid molecules attract and bind negatively-charged fine clays while the poly(NIPAM) chains provide the thermal response for enhanced floc densification.

Laboratory settling tests and FBRM experiments showed that Al-NIPAM outperformed poly(NIPAM) and its respective mixture blend of $Al(OH)_3$ and poly(NIPAM) in flocculation of MFT suspension, producing larger and more shear-resistant flocs that lead to higher settling rate, clearer supernatant and better sediment consolidation due to synergism of the hybrid polymer structure. Furthermore, two settling temperatures were investigated: 21°C (below LCST) and 40°C (above LCST). At elevated temperature, the coil-globule transition of thermoresponsive polymers resulted in accelerated settling and improved consolidation due to floc densification and hydrophobic interaction.

The potential effects of the hybrid Al-NIPAM on bitumen extraction were also studied. The hybrid polymer was interfacially-active at the model toluene-water interface due to the amphiphilic nature of poly(NIPAM). Preliminary results showed that Al-NIPAM increased the degree of bitumen liberation and reduced the induction time for bitumen-bubble attachment in the presence of fines. This study presented some insights on the potential benefits of thermoresponsive hybrid polymer for oil sands mining applications.

Acknowledgment

First and foremost, I would like to express my deepest gratitude to my supervisors, Prof. Zhenghe Xu and Prof. Qingxia (Chad) Liu, for their guidance and support throughout the course of my Master of Science program. Not only have they guided me through this research project, but also they have taught me to think critically and embrace challenges. Without their expertise and patience, this research thesis would not be achievable. It has been my great privilege to study under their supervision.

I would like to thank Dr. Chen Wang for his enthusiasm to discuss and contribute to this research project and various tailings-related topics. I give special thanks to Miss Qing Yao for her invaluable assistance as a summer student in the laboratory. I acknowledge Mr. Shiraz Merali for his help with the AAS experiments. I also extend my appreciation to all the members of the oil sands research group and CMPT for the collaboration within the groups.

I offer many thanks to Mr. Jim Skwarok and Ms. Jie Ru for their dependable technical and equipment support that has been instrumental to my research progress. My appreciation also goes to Ms. Lisa Carreiro, Ms. Pat Silfield and Mr. Carl Corbett for their timely administrative support.

The financial support from Natural Sciences and Engineering Research Council of Canada (NSERC) Industrial Research Chair in Oil Sands Engineering is gratefully appreciated. I would also like to acknowledge the scholarship support received through the Faculty of Graduate Studies and Research and Student Aid Alberta.

Last but not least, I would like to recognize my family and friends for their encouragement, especially my mom, dad and brother for their unconditional love. I sincerely thank Miss Elsie Chang for her companionship. Finally, I give praises to God the Almighty for all His blessings and provisions.

Table of Contents

List of Tables

List of Figures

Nomenclature

AAS: atomic absorption spectrophotometer

AER: Alberta Energy Regulator

Al-NIPAM: $Al(OH)_3$-poly(*N*-isopropylacrylamide) hybrid polymer

CHWE: Clark's hot water extraction

CNRL: Canadian Natural Resources Limited

COSIA: Canada Oil Sands Innovation Alliance

DLVO: Derjaguin-Landau-Verwey-Overbeek

FBRM: focused beam reflectance measurement

FFT: fluid fine tailings

ISR: initial settling rate

LCST: lower critical solution temperature

MFT: mature fine tailings

NTU: nephelometric turbidity units

OSPW: oil sands process water

PAM: polyacrylamide

Poly(NIPAM): poly(*N*-isopropylacrylamide)

Poly(NIPAM)+Al: blend of poly(*N*-isopropylacrylamide) + $Al(OH)_3$ colloids

QCM-D: quartz crystal microbalance with dissipation

UCST: upper critical solution temperature

Chapter 1: Introduction

1.1 Canada's Oil Sands

Oil sands are a mixture of bitumen, sand, clay minerals and water that can be found naturally in several locations around the world including Canada, United States, Russia and Venezuela.[1] The largest and the most developed oil sands deposits known in the world are located in the Athabasca, Peace River and Cold Lake regions of Alberta, Canada with approximately 165 billion barrels (bbl) of proven recoverable bitumen.[1] Bitumen, which is classified as a heavy and viscous form of petroleum, can be upgraded into synthetic crude and refined into various fuels such as gasoline, diesel and kerosene, as well as products such as lubricants and asphalts.[1-2] According to the Alberta Energy Regulator (AER), the total crude bitumen production from Alberta's oil sands amounted to ~2.8 million bbl/d in 2017.[3] Despite the most recent 2014 global oil crash, the revised production forecast is still expected to reach 3.7 million bbl/d by 2027.[3] The oil sands and supporting sectors have generated significant economic contributions across Canada with combined investment amounting to $290 billion from 1997 to 2012.[4] Looking forward, Canada's oil sands remain a strategic resource for Canada, representing an important and secure source of energy for today and the future.

1.2 Oil Sands Separation Processes

There are two main separation methods to extract bitumen from oil sands: in-situ and surface mining.[1-2] In 2017, the breakdown of bitumen production from in-situ and surface mining is almost evenly split, with 53% from in-situ and 47% from surface mining.[3] The method used to extract bitumen from the deposits mostly depends on the depth of the deposit. For deposits situated near the surface (< 50 m below surface), the oil sands can be mined and directly processed at an extraction plant. However, about 80% of Alberta's bitumen reserves are too deep to be mined.[1, 5] In-situ methods are appropriate to recover bitumen for deposits that are more than 75 m below surface. Depending on the extraction method, the bitumen recovery rates vary.

1.2.1 In-situ

The most commonly applied in-situ technologies are steam-assisted gravity drainage (SAGD), cyclic steam stimulation (CSS) and other steam drive techniques.[2] Because oil sands do not flow like conventional crude oil, the bitumen reservoir must be heated to reduce the viscosity of bitumen to fluid-like properties. Typically, high pressure steam is generated and injected into the subsurface to heat up the reservoir. When bitumen begins to liquefy, the emulsion of bitumen and condensed water is pumped to the surface and processed at a separation plant, where water is separated from bitumen. The choice between CSS and SAGD technology is mainly dependent upon the geology of the reservoir, where the Cold Lake deposit is more suitable to CSS and the Athabasca deposit works better with SAGD.[2] In-situ techniques have a smaller footprint and can be built in smaller scales compared to surface mining techniques.[1] However, the recovery rates are typically lower (35-60%), and enormous amount of energy is required for steam generation, contributing to more greenhouse gas (GHG) emissions per barrel of bitumen produced compared to surface mining operations.

1.2.2 Surface Mining

In Alberta, about 4800 km^2 of oil sands area is accessible via surface mining techniques.[1] The Athabasca oil sands in Northeastern Alberta is the only major mineable deposit, but it is also the largest known reservoir of crude bitumen in the world. Back in the 1920s, Dr. Karl A. Clark has developed a method to separate bitumen from sand using hot water and caustics (NaOH), known as the Clark's hot water extraction (CHWE) process.[6] Currently, there are 9 approved oil sands mining projects in the Athabasca deposit.[1] Figure 1.1 shows a typical flowchart of bitumen extraction in a surface mining operation.[7] In an open-pit mine, the ore deposits are excavated and transported to the processing plant by haul trucks. At the plant, the oil sands lumps are crushed and mixed with hot water to produce a slurry. The slurry is introduced into the hydrotransport where chemical additives are added. With heat, mechanical and chemical conditioning, bitumen is liberated from the sand grains. To collect the liberated bitumen, air is introduced to the

conditioned slurry for bitumen-bubble attachment. Inside the primary separation cell (PSC), the lighter aerated bitumen floats to the top as froth and the heavier coarse solids settle to the bottom as tailings. The PSC middlings stream, which contains fines solids (< 44 μm) and clays (< 2 μm), is further treated with flotation cells or hydrocyclones for secondary bitumen recovery. The collected bitumen froth is sent to either a naphthenic or paraffinic froth treatment process to reduce the viscosity of bitumen, remove the solids and water, and produce the crude bitumen product. The waste coarse tailings are typically sent directly into containment areas known as tailings ponds while the fine tailings are sent to the thickener to recover warm water that can be recycled back to the extraction plant. The thickened underflow is pumped to the tailings ponds for tailings and water management.

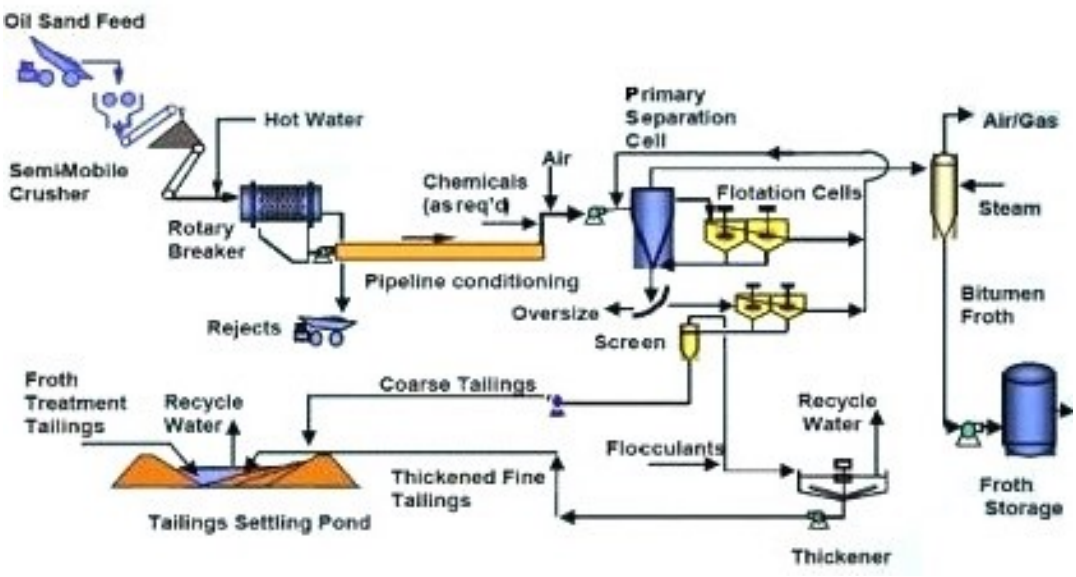

Figure 1.1. Schematic process flow of a typical CHWE operation.[7]

Mining operations have several advantages over in-situ operations, most notably high recovery rates (90%), long mine life, and lower GHG emissions per bitumen produced.[1] However, oil sands mines require massive scale operations to realize economy of scales, which are capital intensive projects. A larger footprint in surface mining also creates challenges such as tailings management and land reclamation.

1.3 Tailings and Water Management

Oil sands tailings, a mixture of mineral solids (sand, fines and clays), water and residual bitumen, are byproduct of the CHWE surface mining process.[1,5-6] Oil sands operators discharge tailings into engineered tailings ponds, which consist of dikes made of coarser solids to protect the surrounding environment. Tailings ponds play a critical role in storing solids and managing water for oil sands operations, as 80% of water is recycled during the production process.[5] Figure 1.2 shows the satellite images of an open-pit mine and tailings ponds in the Athabasca region of Alberta between 1984 and 2011.[8] The rapid oil sands expansions have led to a considerable growth of tailings ponds. As of 2013, tailings ponds and associated structures (e.g. dikes) have occupied 220 km^2 of land with liquid surface area of 88 km^2, making it one of the largest tailings storage units in the world.[1] With planned future production and long mine reserve life, tailings continue to accumulate at an alarming rate, discharging about 3.3 m^3 of tailings into tailings ponds for every bbl of produced bitumen.[5, 6] As such, accumulated tailings and tailings ponds raise significant environmental concerns.

Figure 1.2. Satellite images of the growth of open-pit mine and tailings ponds over Canada's oil sands.[8]

Extraction tailings discharged into tailings ponds contain a wide range of particle sizes and eventually separate into three different zones along the depth of the ponds, as illustrated in Figure 1.3.[6, 9] As coarse solids settle quickly, a sand bed is formed at the bottom of the pond. The coarse sand can also be used to form dikes and sand beaches. The top zone is a supernatant water layer that can be recycled back to the extraction plant. The middle transition zone is a layer of settling fine solids and clays known as fluid fine tailings (FFT) when initially deposited with unfavorable tailings characteristics. Over years of settling, FFT eventually consolidates to approximately 30 wt.% solids referred to as mature fine tailings (MFT).[6, 10] The ultra-stable MFT gel remains in fluid state and often resists further densification. To date, large volume of FFT/MFT has been produced and stored at tailings ponds, some of which are legacy ponds dating back to the 1960s.[11] As oil sands production grows, MFT tailings inventory continues to accumulate in tailings ponds, contributing to the growth of tailings ponds in size and number.

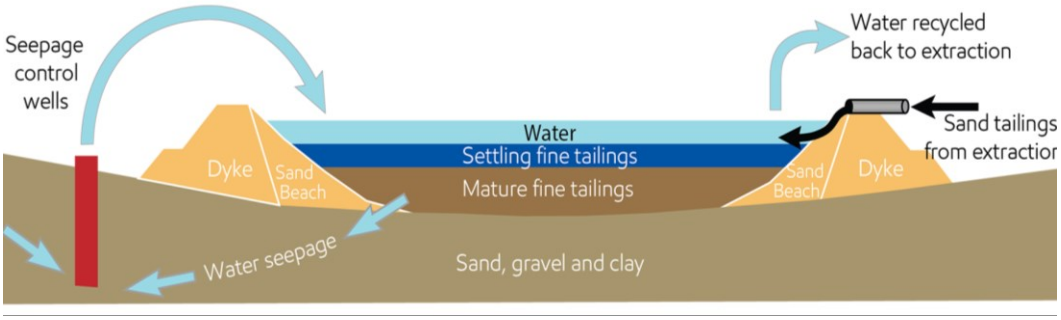

Figure 1.3. Schematic diagram of tailings pond.[9]

Strict regulations and monitoring programs are in place to mitigate the environmental impacts of FFT/MFT and tailings ponds.[5] By law (Directive 085), all fluid fine tailings associated with a project must be ready to reclaim 10 years after the closure of the mining project.[12] The oil sands producers are committed to improving environmental performance through organizations such as Canada's Oil Sands Innovation Alliance (COSIA) by collaborating and sharing research and technological innovations. Many research initiatives are also conducted by universities (e.g. University of Alberta), government agencies (e.g. AI-EES,

CanmetENERGY), technical institutes (e.g. NAIT) and independent companies.[5] COSIA's Tailings Environmental Priority Area (EPA) identifies the accumulation of FFT/MFT in tailings ponds and the urgency to accelerate reclamation of the tailings deposits as key issues to address within the industry.[13] As such, the Tailings EPA focuses on finding and developing innovative technologies and solutions that can reduce FFT/MFT inventory and accelerate land reclamation to minimize the environmental footprint of oil sands operations. Aside from environmental aspects, efficient tailings technologies to recover process water from tailings are also economic, as the annual fresh water withdrawals cannot exceed 3% of the Athabasca River flow.[14] Currently, there is no single 'silver bullet' technology that can completely eliminate the impacts of large volume of accumulated FFT/MFT. However, advances in fundamental knowledge and tailings research have led to technologies or combination of technologies that show promising potential to resolve the decades-old tailings problem. In summary, the importance of tailings technology developments cannot be understated for the future reclamation success of existing and future tailings deposits.

1.3.1 Current Tailings Technologies

Considerable efforts have been made to identify and develop tailings technologies since the late 1960s. Detailed evaluations of these technologies are well-documented in the 'Oil Sands Tailings Technology Deployment Roadmap' and the 'Oil Sands Tailings Technology Review'.[15-16] In general, tailings treatment technologies can be classified into five categories: Physical/Mechanical (e.g. filtration, centrifugation), Natural (e.g. thin-lift drying, freeze-thaw), Chemical (e.g. thickening), Mixtures/Co-disposal (e.g. composite/consolidated tailings), and Permanent Storage (e.g. end pit lakes).[16] Chemical addition (e.g. coagulants and flocculants) to facilitate fine solids aggregation forms the basis of many tailings treatment technologies or complements them in some way.[15] Notable mature processes that have been implemented on a commercial-scale include the composite/consolidated tailings (CT) process and paste technology (PT),[6] which will be discussed in the following sections.

1.3.2 Composite or Consolidated Tailings

The composite/consolidated tailings (CT) process has been commercially implemented for MFT treatment since the 2000s.[6] Typically, MFT is mixed with coarse sand and then treated with coagulants (e.g. gypsum, lime, alum, etc.) to produce non-segregating CT tailings. The coagulants destabilize the suspension through charge neutralization mechanisms (see Section 2.2.1), causing the clays in the MFT to aggregate into structures with sufficient apparent viscosity to hold the sand.[11, 17] The CT, typically ~60 wt.% solids, is pumped to the self-draining deposit site that leads to quick recyclable water. About 30% of the water in the CT can be released within the first year of deposition, reaching up to 80 wt.% solids in less than 10 years.[11] However, the released water from CT contains high concentration of divalent ions (e.g. Ca^{2+} in gypsum and lime). These divalent ions effectively destabilize the tailings suspension, but they also facilitate the attachment of fines onto bitumen (i.e. slime coating) in flotation, detrimentally impacting bitumen recovery.[18-19] Other amendments such as CO_2 and polymers are also feasible to create CT.

1.3.3 Thickened Tailings or Paste Technology

The paste technology (PT) process has been implemented in fresh fine tailings treatment for its effectiveness to quickly recover warm water with negligible impact on the water chemistry (i.e. ions concentration).[6] The PT process is based on the flocculation mechanism (see Section 2.2.2), where the fine solids aggregate into flocs with larger apparent size and favorable settling characteristics. This is achieved by the addition and mixing of polymeric flocculants with the fine tailings feed inside a thickener process vessel (see Figure 1.1). The flocculated fine solids settle to the base of the thickener, eventually consolidating to an underflow paste with higher solids content (25-30 wt.% solids) referred to as thickened tailings (TT).[6] The thickener overflow is released process water that is reused in the extraction plant. The PT process has been first designed for wastewater treatment, paper making and mineral tailings applications, which utilizes commercial polymeric flocculants with high molecular weights such as polyacrylamides (PAM)

and hydrolyzed PAM (HPAM) to flocculate the particles.[20] Hence, the quality of the polymeric flocculants used in PT significantly influences the paste performance (e.g. water release, geotechnical properties).[6] Currently, PAM-based flocculants are also used in oil sands tailings treatment. Although these high molecular weight PAM are very effective in promoting high settling rates of medium and large solids, their efficiencies diminish for the large quantities of fines and clays present in oil sands fine tailings, resulting in TT with high fines content.[21] More importantly, the addition of PAM does not significantly improve consolidation performance as large volume of water remains trapped in the sediment after treatment. This can be attributed to the hydrophilicity of PAM and the fine solids in tailings, resulting in loosely-structured flocs with retained water not easily removable. Consequently, the residual PT sediments often have similar solids concentration as MFT and still experience slow consolidation without further treatment. As such, the PT process alone cannot be used to address existing MFT inventories. Since PAM-based flocculants are originally designed for mining and wastewater treatment applications, they are more susceptible to unique feed characteristics of oil sands fine tailings (e.g. alkaline pH, high fines content). As such, opportunities exist to further improve the thickening performance through research and development of new polymeric flocculants.

From a high-level perspective, flocculants that can accelerate settling followed by densification of the sediments (i.e. floc structures with less retained water) are highly desirable, alongside properties such as clays selectivity and shear resistivity. As polymers are versatile materials, various chemical and structural modifications are possible to create novel flocculants with tailored properties. Recent polymer research has studied novel alternative flocculants such as inorganic-organic hybrid flocculants[22-23] and thermoresponsive flocculants[24-25] for oil sands tailings treatment. A general comparison overview of these alternative flocculants and conventional PAM flocculants is well-described by Vedoy and Soares.[26] Several flocculation and dewatering studies have reported enhanced solid-liquid separation by utilizing the thermal switch of thermoresponsive polymers and synergism of inorganic-organic hybrid structures.[22-25, 27-29]

1.4 Objectives and Organization of Thesis

Researchers in tailings treatment have been developing progressively better polymeric flocculants and tailings technologies for flocculation and dewatering of oil sands FFT/MFT. Particularly, both thermoresponsive polymers and inorganic-organic hybrid polymers have been demonstrated to be promising alternatives to conventional PAM flocculants via the thermal response and the synergy of inorganic coagulation and organic flocculation in hybrid materials.[22-29] Although there have been many studies involving various thermoresponsive polymers and inorganic-organic hybrid polymers for solid-liquid separation, little research has been investigated for the combination of the two. By molecular design, it is possible to create a multifunctional polymer by selecting a thermoresponsive polymer as the organic component of the hybrid composite, which is the focus of the current study.

The main objectives of this study are to:

- Synthesize and characterize a thermoresponsive hybrid polymer,
- Understand the adsorption and conformational behaviors of thermoresponsive hybrid polymer with temperature,
- Evaluate the flocculation and consolidation potential of thermoresponsive hybrid polymer on MFT suspension,
- Explore the potential of using thermoresponsive hybrid polymer as a polymer aid in oil sands extraction.

This thesis comprises of nine chapters. Chapter 1 introduces the basic facts about oil sands, bitumen extraction processes, objectives and challenges of tailings management and an overview of the current tailings treatment technologies. Chapter 2 reviews the fundamentals of colloidal dispersion and surface chemistry and gives a state-of-the-art review of thermoresponsive polymers and inorganic-organic hybrid polymers in solid-liquid separation. Chapter 3 describes the materials and the experimental methodologies. Chapter 4 details the synthesis and characterization of the polymeric flocculants used in this study. Specifically, inorganic aluminum hydroxide colloidal particles ($Al(OH)_3$) and organic poly(*N*-

isopropylacrylamide) (poly(NIPAM)) are used to synthesis the thermoresponsive hybrid polymer, $Al(OH)_3$-poly(*N*-isopropylacrylamide) (Al-NIPAM). Chapter 5 explores the adsorption mechanism and temperature conformation behavior of Al-NIPAM. Chapter 6 presents the results and discussion on the flocculation and consolidation potential of the synthesized polymeric flocculants on MFT suspension. To better understand the synergy in the hybrid structure, the settling and consolidation performances of the Al-NIPAM are compared with linear poly(NIPAM) and the corresponding coagulant/flocculant mixture blend of poly(NIPAM) and $Al(OH)_3$ (poly(NIPAM)+Al). Also, the effects of mixing and temperature are investigated to determine the ideal processing condition for the polymers studied. Chapter 7 investigates the potential effects of the hybrid polymer in oil sands extraction. The interfacial properties of the polymer at a model oil-water interface are determined, and the effects of polymer in bitumen liberation and aeration processes are studied. Chapter 8 draws some conclusions based on the findings from this research study and Chapter 9 suggests some of the future work that should be done. This research study aims to provide some insights of using thermoresponsive hybrid polymers in the context of oil sands tailings treatment and bitumen extraction.

Chapter 2: Literature Review

2.1 Basics on Colloidal Dispersion and Surface Phenomena

The slow settling behavior of FFT/MFT can be explained by colloidal and surface chemistry as these tailings contain fine clays in the colloidal form. By definition, colloids are dispersion of fine particles ranging from 1 nm to 1 μm in size with a very large specific surface area.[30] As such, surface phenomena strongly influence the properties of a colloidal system and dominates over gravity forces. This section reviews the basic principles that govern the stability of colloidal system.

2.1.1 Clays and their Behavior in Aqueous Suspension

Clays (< 2 μm), a form of colloids, typically compose of tetrahedral silicon-oxygen sheets and octahedral hydroxide sheets, as illustrated in Figure 2.1.[30] Aluminosilicate clays (e.g. kaolinite) are plate-like minerals with two layers (1:1) consisting of unit layers of tetrahedral SiO_4 sheet and octahedral AlO_6 sheet. Three-layered clays (2:1), such as illite or smectite, have an octahedral sheet in between two tetrahedral sheets. The most abundant clay mineral in oil sands tailings is kaolinite, followed by illite and other layered clays.[21] The poor consolidation of FFT can be attributed to the gelation of ultrafine clays with sizes less than 0.1 μm (mostly kaolinite and mica), trapping coarser solids in the gel as it forms.[6]

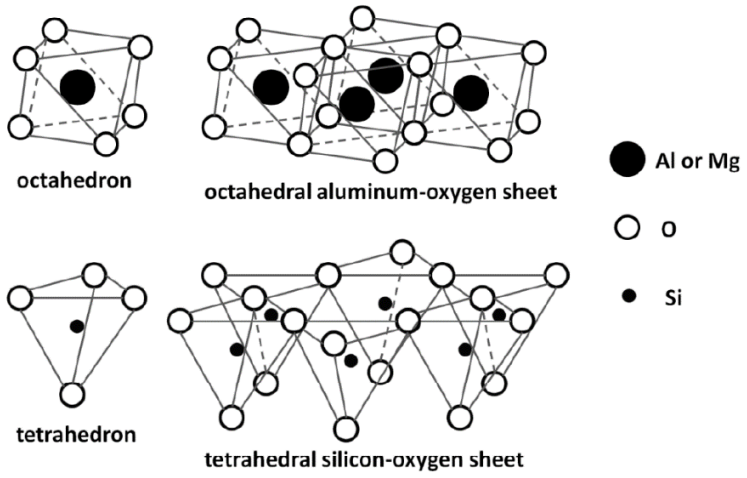

Figure 2.1. Basic building blocks of clay minerals.[30]

Due to Brownian motion, colloidal particles collide with each other, potentially resulting in destabilization if no repulsive forces are present to counteract the attractive short-range van der Waals forces between the particles.[6] However, particle repulsion arises from the surface charges of colloids. For instance, the dispersed clays in FFT/MFT are active with highly negative charges, thus repelling each other and stabilizing the suspension.[21, 30] Fine solids, especially clays, attain surface charges through isomorphous substitution, where cations (e.g. Si^{4+}, Al^{3+}) are exchanged by dissolved cations of equal or lower valence (e.g. Al^{3+}, Mg^{2+}, K^{+}).[30] Due to the cationic exchange, clays (e.g. kaolinite) exhibit anisotropic charge characteristic with permanent negative charge on the basal planes and pH-dependent charge on the edge planes. The pH-dependent charge on the edge planes arises from protonation (positively-charged) and deprotonation (negatively-charged) of surface hydroxyl groups. In acidic to intermediate pH medium, the clays form a 'house of cards' orientation due to the predominant interactions between positively-charged edge planes and negatively-charged basal planes of clays.[30] In alkaline medium, the charge repulsion between the negatively-charged basal and edge planes results in a staggered structure.

2.1.2 Electrical Double Layer

As mentioned earlier, fine solids and clays attain surface charges in aqueous solution, which promote suspension stability. The Stern model can be used to illustrate the electrical potential profile near a charged surface.[31] A negatively-charged surface and its surrounding ions distribution with the corresponding electrical potential profile (i.e. Stern model) are shown in Figure 2.2. The charged surface attains a surface potential because it attracts oppositely-charged ions (i.e. counter ions) in solution. The excess counter ions form an immobile layer on the surface, called the Stern layer, and the potential at the Stern plane is called the Stern potential (ψ_0). Further away from the particle surface, there exists a diffuse layer where the ions and solvents move freely. Therefore, the charged particle appears electrically neutral in bulk, forming the basis of the electric double layer. When two charged particles approach each other, they experience an electrostatic repulsion

due to the overlapping of electrical double layers, where higher surface charges also lead to stronger interparticle repulsion.

From the particle surface, the electrical potential decreases linearly within the Stern layer and then decreases exponentially through the diffuse layer.[31] The Shear plane is a no-slip boundary where the ions and solvent move around the surface. Since a charged colloidal particle moves at a fixed velocity inside an electric field, the particle's mobility can be related to the electrical potential at the shear plane. This phenomenon is known as electrophoresis. The potential at the point between the shear plane and the diffuse layer is called zeta potential (ζ), which is a measurable quantity that is often used to determine stability of the colloidal suspension.

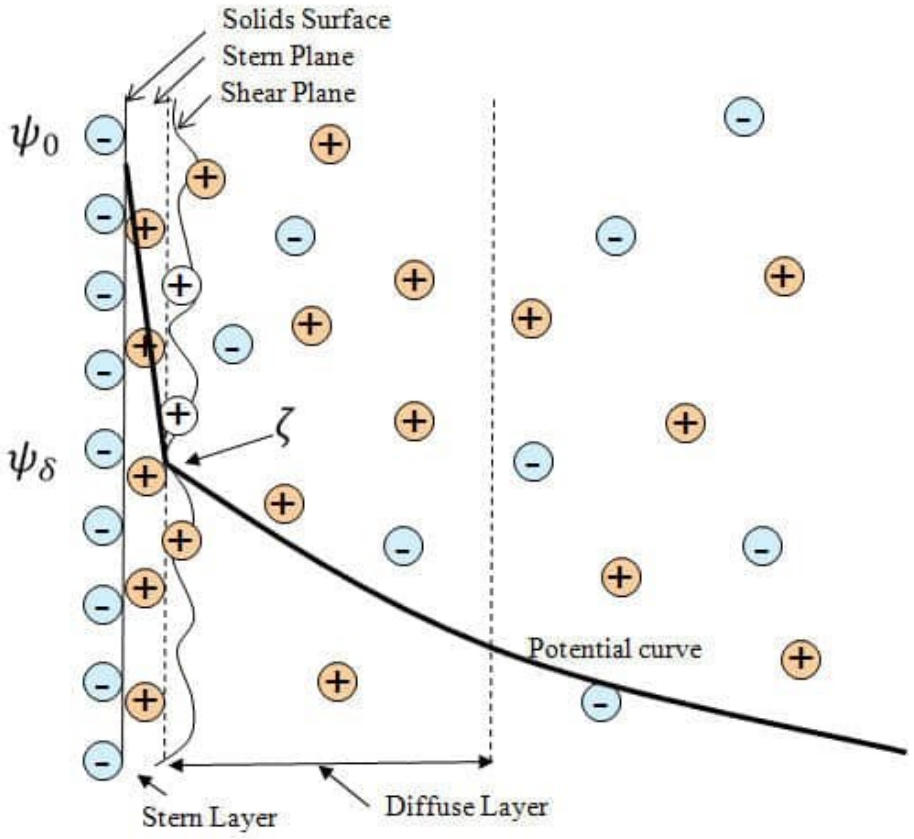

Figure 2.2. Schematic illustration of the electrical double layer in Stern model and its corresponding electrical potential profile.[31]

2.1.3 DLVO Theory

Since the 1940s, the DLVO (Derjaguin-Landau-Verwey-Overbeek) theory has been the foundation of colloidal science.[6, 30] The theory describes the interaction forces between charged surfaces in a suspension, mainly the effects of van der Waals attraction forces (W_{VDW}) and electrostatic repulsion forces (W_{EDL}). W_{VDW} describes the short-range attractive forces between the particles arising from the interaction of dipole moments. On the other hand, W_{EDL} describes the repulsion between charged particles due to the overlap of electrical double layers. As the theory assumes two principle forces only, the net interaction (W_{DLVO}) between the particles quantitatively describes the colloidal stability of a system, as shown in Equation 2.1. If W_{DLVO} is repulsive (i.e. $W_{VDW} < W_{EDL}$), the colloidal system remains stable. On the contrary, if W_{DLVO} is attractive (i.e. $W_{VDW} > W_{EDL}$), the system becomes unstable and thus promotes particle aggregation.

$$W_{DLVO} = W_{VDW} + W_{EDL} \tag{2.1}$$

2.1.4 Non-DLVO Forces

In some colloidal systems, there are addition interaction forces (i.e. non-DLVO forces) that are significant but are excluded in the classical DLVO theory. For instance, solids in aqueous solution can be generally characterized as either hydrophilic or hydrophobic, depending on their relative water affinity.[32] The hydrophobicity of clay minerals has been found to influence colloidal stability, where attractive hydrophobic force exists for hydrophobic surfaces.[33-34] Even though the origin of hydrophobic force are not entirely understood, this interaction is commonly believed to be long-range.[6, 35] Other non-DLVO forces include repulsive hydration pressure for hydrophilic surfaces and steric force for polymer-covered surfaces.[6] As the theories for describing these non-DLVO forces are less developed, these interaction forces are generally inferred from the deviation of the experimentally measured colloidal forces (e.g. atomic force microscopy AFM) from those predicted by the classical DLVO theory.[36]

2.2 Particle Aggregation Mechanisms

As mentioned earlier, colloidal forces play a critical role in tailings stability. In a stable suspension of fine clays, the primary solids are stabilized by repulsive forces. For particle aggregation to occur, it is necessary to overcome the energy barrier keeping the solids apart. This can be achieved by coagulation and flocculation. In these processes, the primary solids aggregate into larger-sized aggregates known as flocs. In literature, the terminologies of 'coagulation' and 'flocculation' are sometimes used interchangeably. However, it is important to differentiate the mechanisms behind these processes, which are discussed in this section.

2.2.1 Coagulation

Coagulation refers to processes that reduce repulsive forces between the particles by altering the charge characteristics (e.g. double layer compression, charge neutralization).[6, 30] Double layer compression can be achieved via ionic strength manipulation. As ionic strength increases (e.g. increased salinity), a higher concentration of counter ions is formed in the diffuse layer. This effectively compresses the thickness of the electrical double layer and causes aggregation when the repulsive energy barrier is overcame. On the other hand, coagulation by charge neutralization can occur via pH adjustment or adsorption of ions. The surface charge of clays becomes less negative as pH decreases. Charge neutralization also occurs when counter ions specifically adsorb on particle surfaces, reducing or reversing the surface potential. Since most clays in aqueous solution carry negative charges, multivalent cations with specific clay affinity (e.g. Al^{3+}, Fe^{3+} and Ca^{2+}) are very effective in suspension destabilization. As such, aluminum- and iron-based coagulants, gypsum and lime have been used extensively in wastewater and mineral tailings treatment.[37] Once the repulsion forces are neutralized or sufficiently reduced with coagulant addition, the van der Waals attractive forces become predominant, causing the primary particles to aggregate into micro-flocs. Micro-flocs are reversibly broken when subjected to intense shear but can be reformed under low shear. When excess doses of aluminum and iron-based coagulants are added, metal hydroxides (e.g. $Al(OH)_3$, $Fe(OH)_3$) precipitates can also form,

dragging the primary particles along with the precipitates as they settle (i.e. sweep flocculation).[38] The coagulation mechanism is especially important for aggregation of fine solids and clays due to their surface charges.[21]

2.2.2 Flocculation

Flocculation involves the aggregation of primary particles into large flocs by the addition of polymeric flocculants.[39, 40] Compared to coagulation, flocculation produces larger and stronger flocs, but the formed flocs generally have more open structures with significant volume of trapped water. Flocculation performance can be strongly influenced by polymer characteristics, such as molecular weight, ionic charge (non-ionic, anionic or cationic), architecture and dosage. Figure 2.3 shows the flocculation mechanisms via polymer bridging and charge patching.[41] Bridging flocculation occurs when segments of polymer chain adsorb on particle surfaces at one or more sites, resulting in interparticle bridging.[40] This is often achieved with high molecular weight polymers, such as non-ionic PAM and HPAM, that have long polymer chains with large numbers of active adsorption sites capable of extending beyond the electrical double layer to form interparticle bridges. Such adsorption interactions are mainly hydrogen bonding and van der Waals forces. For anionic PAM (e.g. PAM-sodium acrylate), the anionicity of the polymer also promotes polymer chain extension in solution and enhances bridging adsorption. The adsorption and bridging interactions between polymers and particle surfaces allow the primary particles to aggregate to large flocs suitable for gravity settling. Unlike micro-flocs formed by coagulation, the interparticle bridges undergo irreversible breakage when subjected to intense shear.

If the polymers and particle surfaces have opposite charges, an electrostatic attraction also exists.[40] As fine solids and clays in solution typically carry negative charges, cationic polymers are appropriate. For low molecular weight cationic polymers (e.g. polyelectrolytes), flocculation occurs mainly through charge-patching, where the cationic polymers attach on parts on the surfaces of negatively-charged particles (Figure 2.3b). Strong electrostatic attraction also increases the chance of polymer adsorption on particle surfaces. Subsequently, these surface

regions with reduced repulsion facilitate particle aggregation. Cationic polymers are used primarily for clays flocculation due to their effectiveness in charge neutralization of suspended fine clays. Excess polymers can re-stabilize the suspension by charge reversal of the particles.

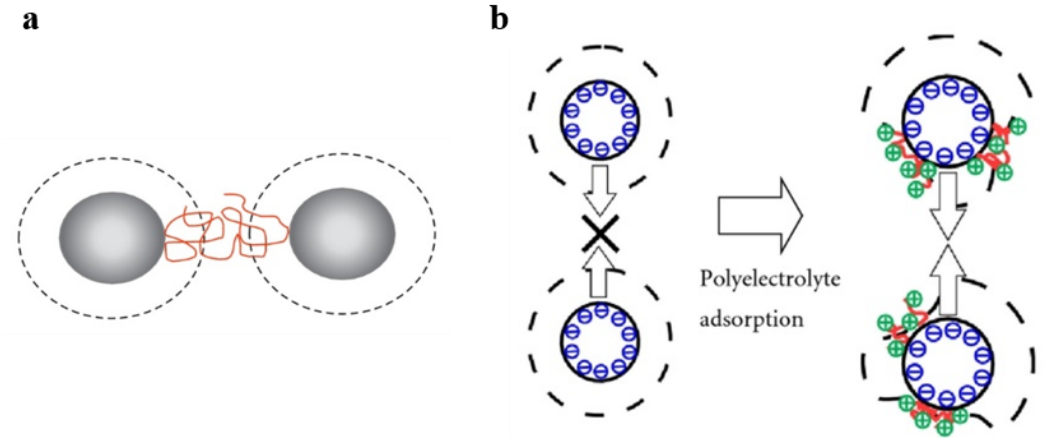

Figure 2.3. Particle aggregation mechanisms through (a) polymer bridging (b) charge patching.[41]

The conformation of adsorbed polymer on solid surfaces is equally important in flocculation.[40] Depending on the polymer characteristics, different adsorbed polymer configurations are possible, as shown in Figure 2.4.[42] Strong attraction (e.g. highly-charged polymers) results in multiple site attachments to the solid surface (C and F), and conversely, weak attraction (e.g. non-ionic polymers) leads to polymer tails extending away from its adsorbed sites (A). High molecular weight polymers are more likely to be randomly coiled (D). For hydrophilic polymers with strong water affinity (e.g. PAM), the polymer chains maximize contact area with water to form polymer brushes (A, B, and D), which can lead to formation of open structure flocs. On the other hand, hydrophobic polymers minimize its contact area with water, forming mushroom-like configuration (F). Inorganic-organic hybrid polymers with star-like structure are likely to adsorb with non-uniform segment distribution (E).[42]

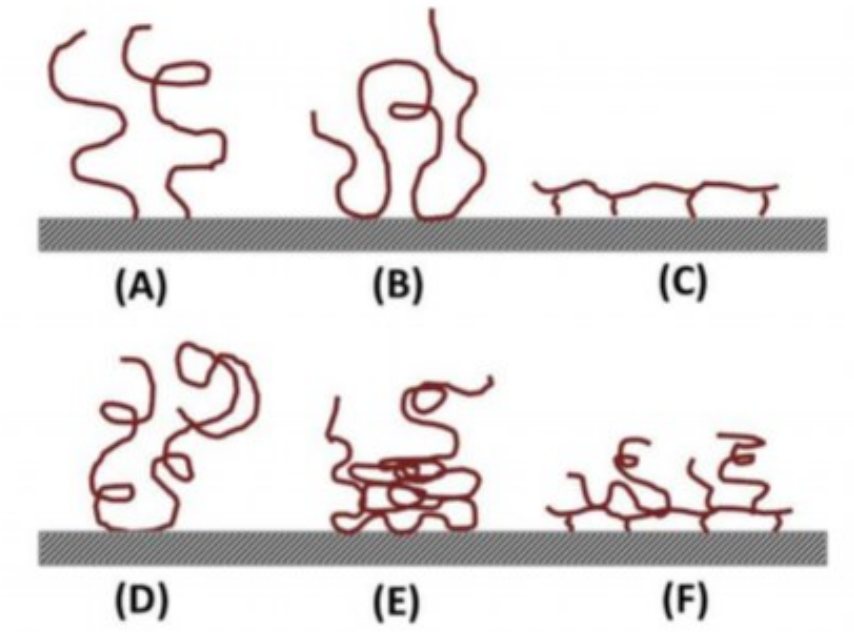

Figure 2.4. Possible configurations of polymeric flocculant adsorbed at solid/water interface.[42]

2.3 Thermoresponsive Polymers

Stimuli-responsive polymers can have a broad range of applications in numerous industries, such as chemical, coatings, food and biomedical.[43] In solid-liquid separation, the use of stimuli-responsive polymers as flocculants has also been considered to improve settling and consolidation of stable suspension.[44-47] The distinctive chemistry of stimuli-responsive polymers enables rapid changes in their properties under the influence of external stimuli, such as temperature, pH and photosensitivity. Among the available suites of stimuli responses, thermal response is arguably the most extensively studied due to its practicality in many applications. For instance, in a typical oil sands mining process, there exist various temperature changes with opportunities for heat integration. Polymers that exhibit a phase transition behavior in response to a change in temperature are commonly known as thermoresponsive polymers. Figure 2.5 shows the schematic phase diagram for thermoresponsive polymer solutions.[48] Depending on the miscibility gap, the minimum of the phase diagram is referred to as lower critical solution temperature

(LCST) or the maximum of the phase diagram is referred to as upper critical solution temperature (UCST).[48-49] Specifically, the LCST and UCST are the respective temperature below and above in which the polymer and the solvent are miscible at any given concentration. Phase separation is entropy driven for LCST polymers and enthalpy driven for UCST polymers.[48]

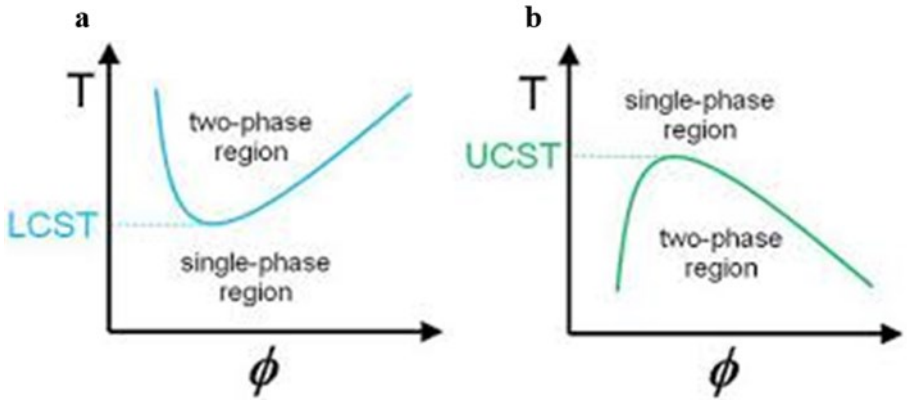

Figure 2.5. Schematic phase diagram of (a) LCST and (b) UCST polymers.[48]

In literature, the most well-known thermoresponsive polymer is poly(NIPAM), which shows a sharp phase transition at the LCST of ~32°C that is almost independent of polymer concentration or molecular weight.[49-50] Upon cycling the temperature above the LCST, poly(NIPAM) undergoes a coil-globule transition, where the polymer molecules transform from extended coils (hydrophilic) to collapsed globules (hydrophobic). Such phase behavior can be explained by the competition between the intermolecular and intramolecular hydrogen bonding below and above the LCST, as illustrated in Figure 2.6a.[51] Below the LCST, the amide functional group in poly(NIPAM) binds with water molecules through intermolecular hydrogen bonding, thus poly(NIPAM) stays hydrated and extended in aqueous solution. Above the LCST, the hydrogen bonds are disrupted in favor of intramolecular bonds between the C=O and N–H groups, causing the poly(NIPAM) molecules to coil up in collapsed conformation. As a result, the poly(NIPAM) minimize the contact area with water, as demonstrated by the change in water contact angle on poly(NIPAM) film from 63.5° (25°C) to 93.2° (40°C) (Figure 2.6b).

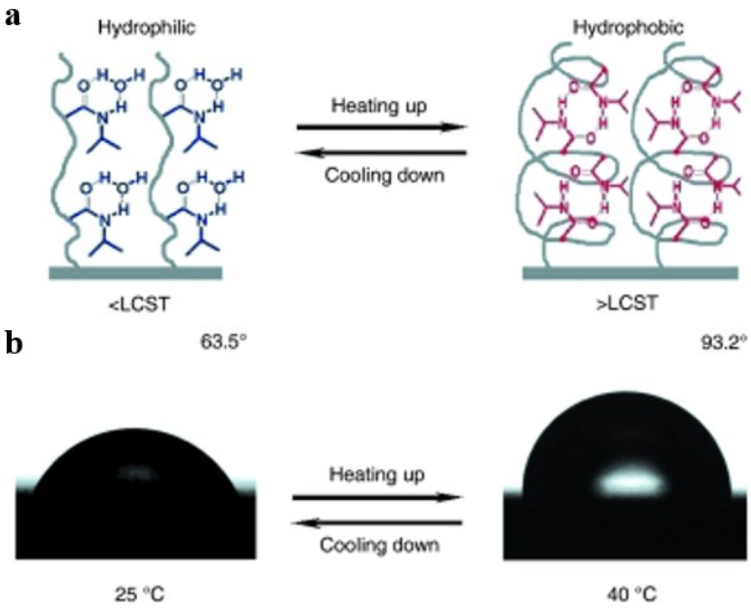

Figure 2.6. Wettability for a flat poly(NIPAM)-modified surface. (a) schematic of the molecular mechanism of coil-globule transition and (b) change of water drop profile with temperature.[51]

The coil-globule transition of poly(NIPAM) allows some exciting applications as a flocculant in separation of suspended solids. The concept has been first described by Guillet and Heskin[44] in their patent in 1985. The standard flocculation protocol typically involves mixing the polymers and suspended particles below the LCST, where poly(NIPAM) adsorbs on particle surfaces and flocculates via polymer bridging. Similar to PAM, poly(NIPAM) flocculants with higher molecular weights are more favorable in flocculation.[52] By triggering the thermal switch of poly(NIPAM), the coil-globule transition pulls the primary particles closer together within the flocculated network, resulting in more tightly-packed flocs. Above the LCST, flocculation using poly(NIPAM) occurs not only by polymer bridging, but also by interparticle attraction forces due to increased polymer hydrophobicity.[35, 53] Using AFM, Li et al.[27] measured the adhesion force between kaolinite clays covered with poly(NIPAM). The measured adhesion force was low (0.07 mN/m) after the addition of 50 ppm poly(NIPAM) at room temperature but increased considerably to 3.5 mN/m with much weaker long-range repulsion at 40°C,

confirming the role of hydrophobic force in particle aggregation above the LCST. Several studies directly compared poly(NIPAM) and PAM in flocculation, citing the coil-globule transition and hydrophobic interaction of poly(NIPAM) leads to superior settling and consolidation than PAM-based flocculants in various model suspension (kaolinite, silica and TiO_2) and MFT.[24, 28, 54-55]

However, adsorption of non-ionic poly(NIPAM) on highly-charged particle surfaces can be limited.[55] Incorporation of cationic or anionic charged functional groups to poly(NIPAM) via copolymerization has been used to promote electrostatic interactions. Cationic poly(NIPAM) copolymers are appropriate to induce aggregation of most negatively-charged suspension because of strong adsorption on mineral surfaces, as in the case of cationic PAM.[44] Deng and Pelton[45] showed that cationic copolymer of diallyldimethylammonium chloride and NIPAM induced TiO_2 flocculation even above the LCST due to formation of cationic colloidal particles. Franks and coworkers[56] incorporated dimethylaminoethylacrylate quaternary ammonium (DQA) into their poly(NIPAM) copolymer to flocculate silica particles with enhanced settling rates via electrostatic interactions. Using a cationic copolymer of NIPAM and *N*-dimethylaminopropylacrylamide (DMAPAA), Sakohara et al.[55, 57] showed that the LCST increased substantially with higher DMAPAA content with pH dependence, suggesting the influence of comonomer content and solution pH on LCST for ionic copolymers. On the other hand, anionic copolymers can be made by the copolymerization of NIPAM with acrylic acid, sodium acrylate and methacrylic acid to treat positively-charged suspension.[44, 56]. Generally, the main disadvantage to industrial application of LCST polymers can be associated with the energy requirement, which becomes a major barrier given the large scale of oil sands tailings treatment. Though there are opportunities to lessen energy inputs through heat optimization within the process, for example, mixing warm tailings with already-cooled tailings to bring the mixture to the desired temperature,[26] the phase transition temperature of the LCST polymers must be reasonably low to minimize energy cost.

2.4 Inorganic-organic Hybrid Polymers

In wastewater and mineral tailings treatment, multi-step coagulation-flocculation processes have been widely used to improve the flocculation of suspended fine particles.[40] The sequential process typically involves addition of coagulants to neutralize the surface charges of fine particles followed by addition of high molecular weight polymeric flocculants to bridge the primary particles into large flocs. For oil sands tailings, Yuan et al. showed that the sequential chemical addition flocculated fine solids better than the single use of coagulant or flocculant.[58]

Recent research has also explored the concept of combining coagulation and flocculation in one-step using a single polymer composite that constituted of inorganic material and organic polymer (i.e. inorganic-organic hybrid polymer).[59] Hybrid polymers are attractive in many applications due to synergetic structural properties that often outperform their individual counterparts. As such, hybrid materials represent one of the fastest growing research areas in current polymer science.[59] A review on the fundamental development and characterization of hybrid materials for wastewater treatment applications is summarized by Lee et al.[60] In the flocculation of kaolinite suspension, Yang et al. showed that $Al(OH)_3$-polyacrylamide (Al-PAM) hybrid outperformed its corresponding PAM flocculant and blend of PAM/$AlCl_3$.[29] Similarly, Wang et al. demonstrated that Al-PAM flocculated the ultrafine solids in high fines tailings (40 wt.% fines) more effectively than a commercial HPAM (Magnafloc 1011), significantly reducing the turbidity of the supernatant.[22] The authors attributed the enhanced performance of Al-PAM to the synergism between the inorganic and organic components, promoting strong electrostatic interactions between the cationic $Al(OH)_3$-cores and the negatively-charged particles as well as the adsorption-bridging effect. Using AFM and single molecular force spectroscopy, Sun et al.[61] revealed the star-like structure of Al-PAM, with $Al(OH)_3$-cores connected to PAM polymer chains through ionic bonds, as illustrated in Figure 2.7. Such structure is expected to bridge fine clay particles closer together, forming pellet-like flocs that are denser, larger

and more spherical than PAM-induced flocs. Due to pellet flocculation, Al-PAM polymers were also tested as polymer aids for filtration of high fines tailings and MFT suspension.[22-23] Results showed Al-PAM-assisted filtration can produce dry stackable filter cakes, thus offering a viable solution to treat existing FFT/MFT inventories. The molecular weight and metal content of hybrid polymers have been found to influence settling and filtration performance, where Al-PAM with higher molecular weight and Al content performs better.[62] Other hybrid polymers such as $Fe(OH)_3$-PAM and $CaCl_2$-PAM have also been demonstrated to be effective flocculants.[63-64]

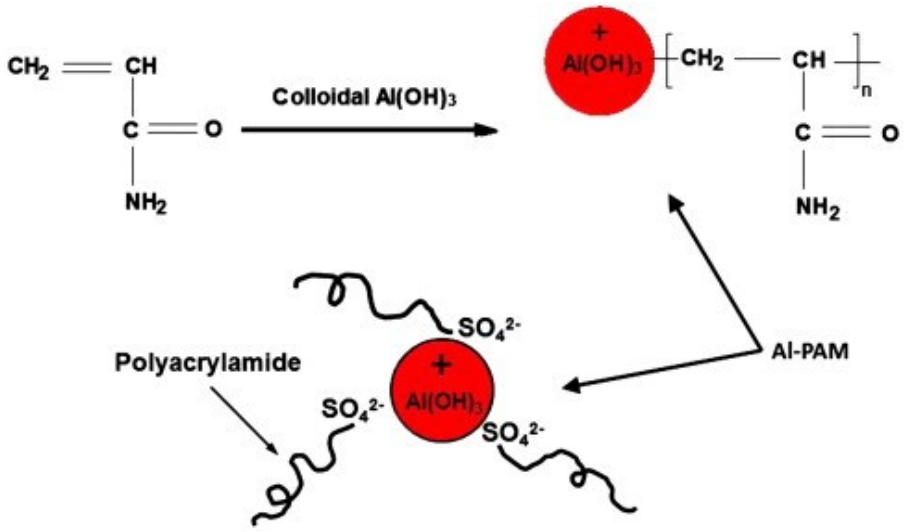

Figure 2.7. Schematic representation of Al-PAM.[23]

As discussed in Section 2.3, stimuli-responsive polymers react to environmental changes. Recent advances in polymer science have led to novel hybrid materials that combine inorganic components with responsive organic polymers.[43, 65-66] These advanced materials can potentially have a wide range of emerging applications (e.g. drug delivery, sensing, separations, etc.). An example of stimuli-responsive hybrid polymers can be represented by the core-shell particle structure in Figure 2.8, where responsive organic polymers are attached on the surfaces of inorganic particles.[43] When external stimuli are applied, the polymer molecules undergo conformational changes, thus exhibiting interesting properties both in solution and possibly at the interface. Inorganic particles with specific properties

can be chosen depending on the application. For instance, inorganic metal hydroxides (e.g. $Al(OH)_3$ and $Fe(OH)_3$) with strong clay affinity are appropriate for flocculation of fine clays in FFT/MFT. Chan et al.[67-68] first synthesized an $Al(OH)_3$-poly(NIPAM-*co*-DMAPMA) cationic copolymer for the settling and filtration of kaolinite suspension, demonstrating the hybrid's (Al-CP) exceptional flocculation and dewatering potential and stimuli-responsive properties.

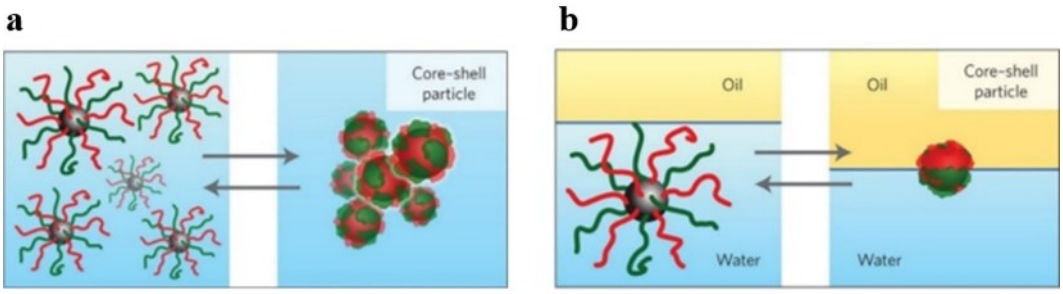

Figure 2.8. Schematic designs of stimuli-responsive hybrid materials (a) in suspension and (b) at the interface.[43]

As thermoresponsive polymers and inorganic-organic hybrid polymers have been demonstrated to be promising alternative flocculants to conventional PAM-based flocculants, their individual benefits in flocculation provide a scientific background for development of new polymeric flocculants. In this study, a thermoresponsive inorganic-organic hybrid polymer (Al-NIPAM) has been synthesized by integrating $Al(OH)_3$ colloidal particles into poly(NIPAM) molecules. The most obvious advantage of such modification is that the individual properties of the inorganic and organic components can be combined in a multifunctional polymer composite. The flocculation potential and alternative benefits of thermoresponsive hybrid polymer will be discussed in the subsequent chapters.

Chapter 3: Materials and Methods

3.1 Materials

Deionized (DI) water with resistivity of 18.2 MΩ.cm, prepared by an Elix 5 followed by a Millipore-UV plus water purification system (Millipore Inc., Canada) was used wherever applicable throughout this study. Laboratory grade HCl and NaOH, purchased from Fisher Scientific, were used to adjust solution pH when necessary.

3.1.1 Polymer Solutions

The dry polymer was dissolved in either DI water or oil sands process water (OSPW) (see Section 3.1.3) to the desired concentration one day prior to use to allow complete dissolution and relaxation of the polymer chains. For effective flocculation, flocculant dilution is an important step to facilitate mixing of the flocculants and the suspension to be treated. For PAM-based flocculants, stock polymer solution is generally diluted to very low concentration due to the highly viscous nature of PAM molecules, which can lead to handling and preparation problems. On the other hand, poly(NIPAM) has a much lower intrinsic viscosity than PAM at equivalent molecular weight (see Figure A.4). Therefore, the stock polymer solution of poly(NIPAM)-based flocculants can be more concentrated. In this study, the stock polymer solution was prepared at 2000 ppm, unless otherwise specified.

3.1.2 Mature Fine Tailings

The MFT samples were supplied by Horizon Oil Sands operation (CNRL, Fort McMurray AB). The solids content of the as-supplied MFT was calculated to be 29.4 wt.% solids, as determined by dividing the mass of dry solids (obtained via oven drying) by the mass of the wet MFT sample. Using laser diffraction, the particle size distribution was determined by the Mastersizer 3000 particle size analyzer (Malvern Instruments, UK), as shown in Figure 3.1 (courtesy of Chen Wang). The as-supplied MFT had a d_{50} and d_{90} of 5 and 17 μm respectively,

indicating nearly all solids smaller than the < 44 μm fines fraction with a considerable < 2 μm clay fraction.

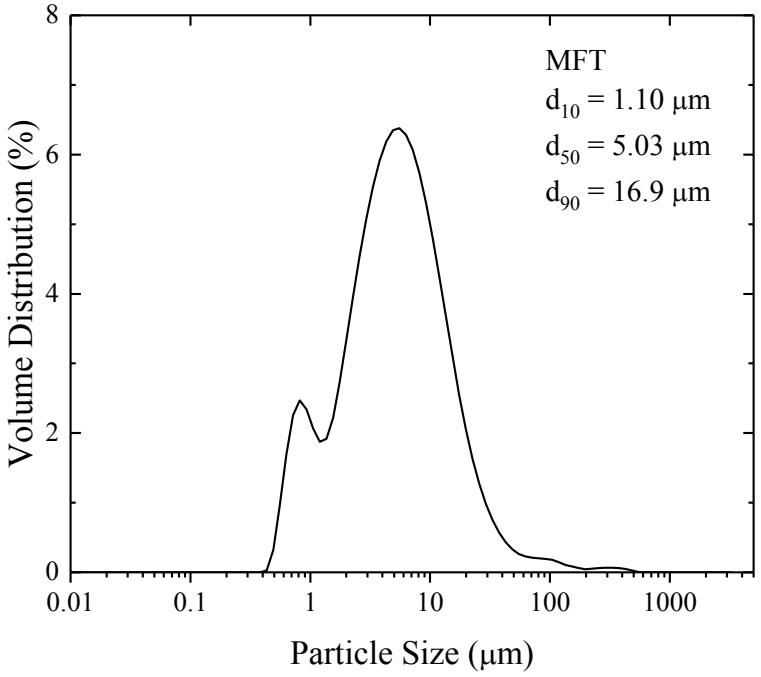

Figure 3.1. Particle size distribution of MFT sample.

3.1.3 Oil Sands Process Water

The oil sands process water (OSPW) was supplied by Syncrude Canada from the Aurora operation (Fort McMurray AB) with a pH ~8. The major ion composition was analyzed using ion chromatography (Table 3.1) (courtesy of Jie Ru). The OSPW was filtered to remove fine solids prior to its uses.

Table 3.1. Major ion composition in oil sands process water.

Major Ions	**Ca^{2+}**	**Mg^{2+}**	**Na^{+}**	**K^{+}**	**Cl^{-}**
Concentration (ppm)	83	19	691	21	444

3.1.4 Oil Sands Ore

The frozen oil sands ores samples (SUNP210) were supplied by Suncor Energy Inc. with composition shown in Table 3.2. Prior to liberation experiment, the ore sample was thawed at room temperature overnight.

Table 3.2. Composition of oil sands ore sample.

Ore Composition	Bitumen	Water	Solids	Fines
By weight (wt.%)	10.6	2.6	86.8	25.0

3.2 Flocculation Experiments

Flocculation depends on sub-processes such as mixing of the polymer with the suspension, adsorption of polymer on the particle surfaces as well as floc formation and growth (i.e. particle aggregation).[40] Zeta potential and QCM-D measurements were used to study the adsorption interactions between charged surfaces and polymer molecules. Settling tests and FBRM experiments were used to determine the optimal flocculation condition for each synthesized polymeric flocculant.

3.2.1 Zeta Potential Measurement

The zeta potential of fine solids in tailings was measured using the Zetasizer Nano ZS analyzer (Malvern Instruments, UK). To understand the interactions between tailings particles and polymeric flocculants, the zeta potentials of 0.1 wt.% solids MFT in OSPW were measured with and without polymer addition. The diluted MFT was mixed at 500 rpm for 30 min to fully disperse the solids. For each experiment, polymer was added at a specific concentration to the suspension (ppm), and the mixture was conditioned in an ultrasonic bath (Fisher Scientific, USA) for 15 min. The top of the sample was removed for zeta potential measurement. Each condition was repeated three times and the average value was reported along with error.

3.2.2 QCM-D

At the micro-scale, the adsorption interactions between polymers and charged surfaces were studied by quartz crystal microbalance with dissipation monitoring (QCM-D) using Q-Sense E4 (Q-Sense, Sweden). A QCM-D sensor is made of thin quartz disk that is placed between a pair of electrodes.[69] Due to the piezoelectric properties of quartz, the application of AC voltage causes the quartz crystal to oscillate at its resonance frequency. Upon removal of the voltage, the crystal resonance decreases exponentially. The QCM-D instrument measures these changes in the resonance frequency of the sensors and dissipation caused by the adsorption of polymer on the sensor surface. By analyzing the oscillation (frequency) and the decay (dissipation), the polymer adsorption and conformation behaviors can be determined.

In this study, Q-Sense quartz crystal sensors coated with silica (SiO_2, QSX 303) and alumina (Al_2O_3, QSX 309) were purchased from Biolin Scientific. Prior to each experiment, the sensor and QCM-D flow module were cleaned with 2 wt.% sodium dodecyl sulfate (SDS) solution, rinsed with water, and blow-dried with N_2. To remove organic contaminants, the sensor was placed under UV-light for 20 min. At the start of experiment, DI water was pumped into the flow module (with mounted sensor) at rate of 0.15 mL/min using peristaltic pump (Ismatec, Switzerland). To more closely resemble real tailings conditions, OSPW was used as the background solution, allowing the ions in OSPW to adsorb on the sensor to an equilibrium. Once a horizontal baseline (i.e. constant signals) was established, the flow was switched to polymer solution (100 ppm), and the frequency and dissipation changes were recorded. After reaching stable adsorption, the background solution was re-introduced. The conformational change of thermoresponsive polymer can be studied using QCM-D with stepwise increase in temperature.[70-71] Two parallel flow modules (with mounted silica sensors) were used, where the first sensor was covered with a stable layer of adsorbed polymer at 25°C while the other sensor was used as a control to account for the influence temperature on physical properties of water (e.g. viscosity, density). Then, the QCM-D cell temperature was increased in

step-wise increments of 5°C to 40°C and the corresponding shifts in frequency (-Δf) and dissipation (ΔD) signals were recorded, as illustrated in Figure 3.2.[70] By subtracting the frequency and dissipation changes in the control sensor (i.e. $-\Delta f_{water}$ and ΔD_{water}) from the first sensor (i.e. adsorbed layer), the changes caused solely by the adsorbed polymer layer ($-\Delta f_{polymer}$ and $\Delta D_{polymer}$) with temperature can be calculated.

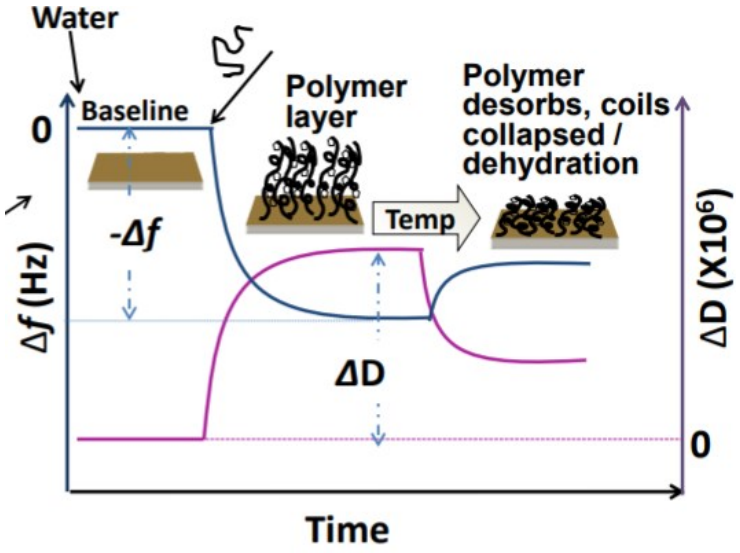

Figure 3.2. Schematic of QCM-D response with temperature ramp-up.[70]

3.2.3 Settling Test

For each setting test, 100 g of 5 wt.% MFT in OSPW was prepared in a 250-mL beaker fitted with four stainless steel baffles walls (6.5 mm width). To ensure homogeneous distribution of solids, the suspension was mixed at 500 rpm using an overhead mechanical stirrer (IKA, Germany) attached to a 4-bladed 45° pitched axial-flow impeller attachment with 3 cm diameter and 1 cm clearance. Following the pre-mixing, the mixing speed was adjusted to the optimal (see Section 6.1.1), and the stock polymer solution was added at a rate of 0.1 mL/s with a micropipette. The dosage is expressed in units of kg of dry flocculant per tonne of dry solids in MFT (kg/t). For consistency, mixing was stopped immediately after flocculant addition. Two settling temperatures were investigated: room temperature (21°C) and elevated temperature (40°C). For room temperature settling, the sample was

gently transferred into a 100-mL graduated cylinder and inverted 3 times before placing on the lab bench for settling measurement. During settling, the position of the interface between the supernatant and the settling solids (i.e. mudline) was recorded as a function of time, as illustrated in Figure 3.3. The initial settling rate (ISR) refers to the linear portion of the normalized mudline height-time plot. Examples of normalized mudline height-time plots (see Figure B.7 and B.8) can be found in Appendix B.

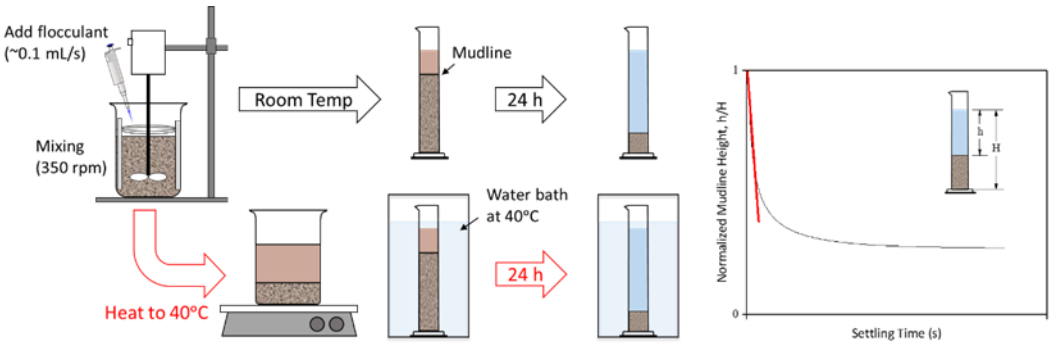

Figure 3.3. Schematic of settling test procedure and a typical settling curve.

For the elevated temperature protocol, the flocculated sample was heated to the target settling temperature (40°C) using a hot plate before transferring to a graduated cylinder. The graduated cylinder was inverted three times and then settled in a large clear container with heated water circulation using the RTE 7 bath circulator (Thermo Neslab, USA) at 40°C.

The primary parameters that are indicative of solid-liquid separation are the ISR and concentration of fine solids in suspension.[40] Both fast settling and clear supernatant result from strong interparticle attraction forces, which also determines the size of the formed flocs. One of the best technique to quantify the concentration of fine solids in suspension is nephelometry since the suspended particles can scatter the incident light beam. At specific times, about 20 mL of supernatant was carefully decanted from the settling cylinder and measured by the Micro 100 laboratory turbidimeter (HF Scientific, USA) to assess the water quality. Prior to measurement, the turbidimeter was calibrated by standard samples with turbidities

of 0.02 NTU, 10.0 NTU and 1000 NTU. In this study, the ISR and supernatant clarity (15 min) were used to evaluate the flocculation potential of the polymeric flocculants.

Consolidation performance can be evaluated based on the solids concentration of the formed sediment bed. After 24 h of settling, the remaining supernatant was removed from the consolidated wet sediment. The weights of the wet sediment and dry solids were measured. To obtain dry solids, the wet sediment was dried overnight using an oven set at 100°C. The solids content of the sediment was calculated by dividing the mass of the dry solids by the mass of the wet sediment. Solids mass balances (> 95%) were obtained, indicating minimal solid losses during handling and sample transfer. For repeatability, each settling test condition was repeated three times and the average data was reported with the corresponding standard errors.

3.2.4 In-situ Flocculation using FBRM

Focused beam reflectance measurement (FBRM) technology was used to assess the in-situ flocculation performance by tracking the macroscopic changes in a flocculated particle system in real time.[72] The measurement is based on a focused laser beam reflected from particles passing across a sapphire window, which provides particle chord lengths over the range from 0.5 to 1000 μm in diameter. The chord length is calculated by the time period of backscatter from one edge of particle to the opposite edge multiplied by the scan speed. Detailed principles about FBRM can be found elsewhere.[72]

For each experiment, 50 g of 5 wt.% MFT in OSPW was placed in a 100-mL beaker. The beaker was placed on a fixed beaker stand provided by Lasentec with the Lasentec S400 FBRM probe (Mettler Toledo, USA) and dual-bladed axial flow impeller. To disperse the fine solids in tailings, the suspension was conditioned for 5 min at 400 rpm, establishing a stable chord length baseline. Following addition of stock polymer solution at specific dosage (kg/t), the changes in the chord length were recorded at a scan speed of 3 m/s. The mixing speed was kept constant at 400

rpm for the 30 min experimental duration, sufficiently keeping any flocculated particles from settling to the bottom of the beaker. To investigate the effect of temperature, a temperature-controlled FBRM setup was used with heating supplied by a water jacket, as illustrated in Figure 3.4. Using the RTE 7 bath circulator (Thermo Neslab, USA), heating medium (water) maintained at 60°C was circulated to transfer heat into the sample. To monitor the slurry temperature, a temperature probe was inserted, but was placed as far away from the FBRM probe as possible to minimize the effect of flow disturbance. For data analysis, a moving average (10 steps) on the chord length was applied.

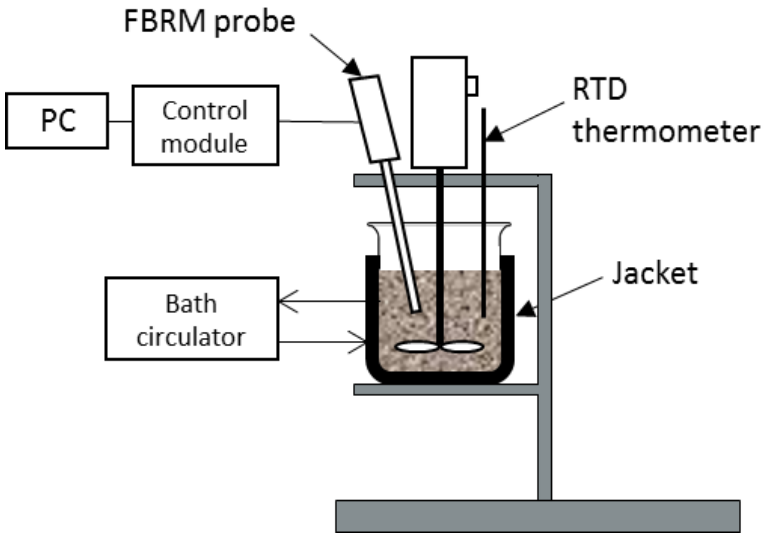

Figure 3.4. Schematic of modified FBRM setup with temperature control.

3.3 Extraction Experiments

3.3.1 Interfacial Tension by Du Noüy Ring Method

The surface tension or interfacial tension is defined as the work required to create unit area of surface or interface.[73] Using the Du Noüy ring method, the K12 force tensiometer (Krüss, Germany) was used to measure the force acting on an optimally wettable ring (platinum) resulting from the tension of the withdrawn liquid lamella. The interfacial tension (γ) can be related to the force required to pull the ring (F) and the wetted length of the ring (sum of inner and outer circumference) by

Equation 3.1. The interfacial tension between polymer solution (10 to 100 ppm in DI water) and ACS-grade toluene was measured at temperatures between 20°C to 50°C ± 0.5°C.

$$\gamma = \frac{F}{2\pi(r_i + r_o)} \tag{3.1}$$

3.3.2 Bitumen Liberation by Stereo Microscope

The bitumen liberation process was visualized using the stereo microscope (Olympus SZX10, Japan). The oil sands ore sample was thawed under room temperature overnight. Around 1 g of sample was packed into a metal sample holder and flattened using a metal rod. The sample holder was then placed on a portable heating plate set to 50°C. The polymer was dissolved in process water and pre-heated to 50 °C. At the start of each experiment, polymer solution (50 ppm in OSPW) was introduced onto the surface of the sample and images at corresponding liberation time were taken using CCD camera over the next 10 min. For data analysis, the recorded color image was converted to 'Gray Scale 8' format using an image analysis software (Image-Pro), as shown in Figure 3.5. Each pixel in the gray-scale image has a specific value that ranges from 0 (pure black) to 255 (pure white). A threshold value of 80 was applied for the ore sample studied, where pixels below 80 were converted to black (unliberated area) and pixels above 80 were converted to white (liberated area).[74] The degree of bitumen liberation (DBL) can be calculated using Equation 3.2:

$$DBL(\%) = \frac{A_0 - A_t}{A_0} \times 100\% \tag{3.2}$$

where A_0 is the area of black pixels at time zero (start of liberation) and A_t is the area of black pixels at a specific liberation time. As bitumen liberates from the sand grains, the area of black pixels decreases and DBL increases. Each condition was completed 5 times with good repeatability. For clarity, only one representative set of data was shown in the results.

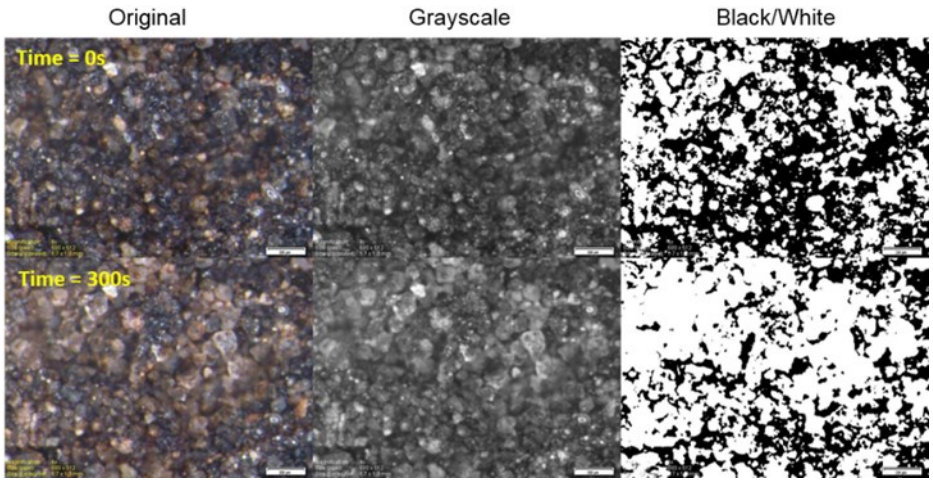

Figure 3.5. Example of image analysis process for DBL

3.3.3 Bitumen Aeration by Induction Timer

An in-house built induction timer was used to determine the bitumen-air attachment time under different solution environments, thus the effect of the polymers on the aeration process of bitumen can be studied.[75] The induction time of bitumen-air bubble attachment is defined as the contact time (50% probability) required of an air bubble in contact with the bitumen surface for attachment. A schematic of the induction timer apparatus is shown in Figure 3.6a.

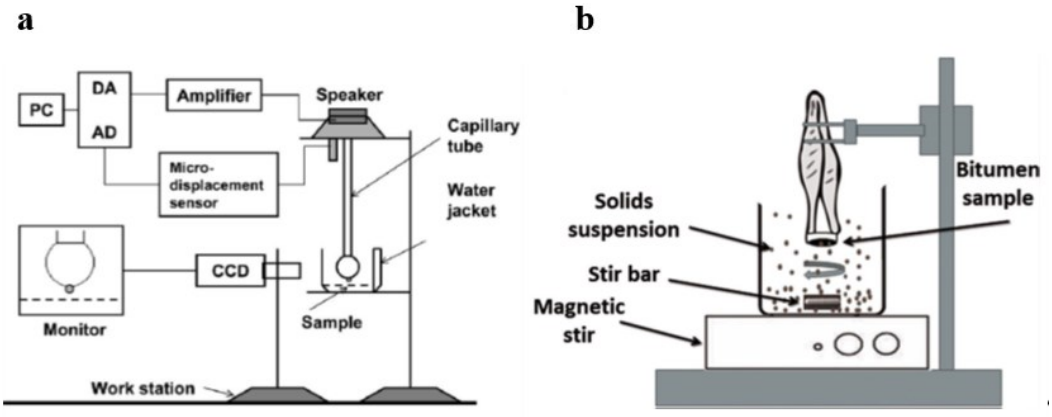

Figure 3.6. Setup of induction timer experiment. (a) schematic of in-house built induction timer and (b) preparation of fines-coated bitumen.[75-76]

Syncrude vacuum distillate feed (VDU) bitumen was placed into a half-sphere Teflon disk and the surface was flattened using a razor blade. The sample was set for 30 min until a flat bitumen surface was obtained. To more closely resemble the presence of fines in floatation process, oil sands fines provided by Teck Limited were used to condition the bitumen surface. The mineralogy and composition of the fines, as determined by X-ray diffractions (XRD), can be found in Table B.1. The largest clay fractions were kaolinite and illite. The solids were sieved using a Mesh 325 sieve that retained particles smaller than 45 μm. Since the suspension becomes extremely turbid with fines addition, it is problematic to view the bitumen-air attachment process in a suspension containing fines solids. To overcome this problem, the bitumen sample was first coated with fines following the procedures developed by our research group previously, as shown in Figure 3.6b.[76] The bitumen surface on the Teflon disk was held upside down by a pair of tweezers and immersed in the fine suspension (0.5 wt.%) with slow agitation for 15 minutes. The bitumen surface was conditioned with OSPW or polymer addition (50 ppm) to the fines suspension, allowing the bitumen to interact with fines under different solution conditions.

The fine-coated bitumen was then placed into the cubic glass cell with clear testing solution, already heated to 50°C, for the induction time measurement. Using a micro-syringe, air bubbles with a diameter of 1.5 mm were generated through the capillary tube. The initial gap between air bubble and bitumen surface was set as 0.25 mm. The displacement, approach/retract speed and contact time of the capillary tube at the set displacement was adjusted by a speaker that was controlled through a charge amplifier and computer interface. The approach/retract speed of the air bubble to the bitumen surface was set at 40 mm/s. Different contact times between air bubble and bitumen surface were varied and the approach-contact-retract cycle were recorded by a CCD camera equipped with a macro lens. For each contact time, the approach-contact-retract cycle was repeated at least 20 times and the percentage of attachment upon contact was calculated. The curve was fitted with the Boltzmann function with the induction time defined as the probability of 50% attachment.

Chapter 4: Polymer Synthesis and Characterization

4.1 Materials

Monomer *N*-isopropylacrylamide (NIPAM, 99%) was purchased from Fisher Scientific. Initiator ammonium persulfate (APS, > 98%), accelerator *N*, *N*, *N*', *N*'-tetramethylethylenediamine (TEMED, > 99%), aluminum chloride (99%) and ammonium carbonate (> 99%) were purchased from Sigma-Aldrich and used without further purification.

4.2 Polymer Synthesis

The non-ionic poly(NIPAM) was synthesized in-house by conventional free radical polymerization based on the procedures described by Sakohara and Nishikawa.[28] NIPAM monomer was dissolved in DI water (0.88 M) with N_2 purging (1 h). APS and TEMED were used as the redox (reduction-oxidation) initiator pair, where APS acted as strong oxidizing agent and TEMED catalyzed the polymerization reaction. The pair produced free radicals at room temperature. The molar concentration of APS and TEMED were 2 and 6 mM respectively.[28] The polymerization reaction proceeded for 12 h at 25°C. The poly(NIPAM) gel was purified using heated filtration at 60°C and dried using a vacuum oven.

4.2.1 Preparation of Aluminum Hydroxide Colloids

To synthesize the aluminum-based hybrid polymer, $Al(OH)_3$ colloids were prepared by adding ammonium carbonate solution into excess aluminum chloride solution under vigorous mixing, as shown by the chemical reaction (Equation 4.1). The aluminum speciation depends on the pH of solution. Between pH of 5.0 and 6.2, a mixture of Al^{3+}, $Al(OH)^{2+}$, $Al(OH)_2^{+}$, and colloidal $Al(OH)_3$ species exists.[77]

$$2\mathrm{Al}Cl_{3(aq)} + 3(NH_4)_2CO_{3(aq)} + H_2O_{(l)} \rightarrow 2\mathrm{Al}(OH)_{3(aq)} + 6NH_4Cl_{(aq)} + 3CO_{2(g)} \quad (4.1)$$

25 g $AlCl_3$ solution (0.1M) was prepared in a 250-mL beaker with baffles. Similarly, 50 g $(NH_4)_2CO_3$ solution (0.1M) was prepared in a separate 250-mL beaker. As the reaction is sensitive to dust, Parafilm was used to cover both beakers. The $(NH_4)_2CO_3$ solution was added to the $AlCl_3$ solution at a rate of 0.5-0.6 g/min using a peristaltic pump (MasterFlex, USA), while the mixture was stirred at 500 rpm with an overhead mechanical stirrer. The amount of $(NH_4)_2CO_3$ added was monitored by an electronic balance. A total of 35.5g of $(NH_4)_2CO_3$ was added, corresponding to a molar ratio of 1:1.43. The mixture was stirred at 300 rpm for an additional hour to complete the reaction. The pH of the $Al(OH)_3$ solution was recorded with pH meter (Fisher Scientific), and the particle size and zeta potential were measured by the Zetasizer Nano ZS, as given in Table 4.1. As the colloid size changes over time, freshly-prepared solution was used for polymer synthesis.

Table 4.1. Physical properties of $Al(OH)_3$ colloids used for polymer synthesis.

Physical Properties of Colloids	
pH	5.60
Size (nm)	27.7
Zeta Potential (mV)	+36.7

4.2.2 Synthesis of Thermoresponsive Hybrid Polymer

The synthesis of the thermoresponsive hybrid polymer (Al-NIPAM) followed the same procedure as poly(NIPAM), except the monomers were dissolved in the prepared $Al(OH)_3$ solution instead of DI water. Total of 5 g NIPAM monomers were dissolved in 50 mL of $Al(OH)_3$ colloidal suspension in a 100-mL 3-necked glass flask immersed in a water bath at 25°C. The reactor flask was sealed and purged with N_2 through a stainless steel needle, while the mixture was stirred at 250 rpm using a magnetic stir bar. N_2 purging prevents undesirable reactions with air molecules (i.e. oxidization) that inhibit polymerization. The reactor was also

wrapped up with aluminum foil to prevent light exposure to the reactants. After 1 h of N_2 purging, 45 µL of TEMED was added as the accelerator and then 2.3 mL of APS solution (10 g/L) was added to the mixture at ~0.5 mL/min. Gelation (i.e. increase in molecular weight) occurred shortly after initiator addition, but the polymerization reaction was allowed to proceed for much longer (12 h) to ensure maximum monomer conversion. The obtained polymer gel was dissolved in 1 L of water and the solution was heated to 60°C, where polymer precipitates formed. The precipitates were removed and the remaining solution was filtered using a heated filtration setup. This purification process was repeated three times to remove unreacted monomers and residual initiators. The purified polymer gel was vacuum-dried at 60°C on a Teflon dish to obtain the final polymer product.

Figure 4.1 shows the molecular representation of Al-NIPAM. The presence of the $Al(OH)_3$ colloids changes the structure of the polymer molecule and its charge density. Since $Al(OH)_3$ colloidal particles are positively-charged, it can form a stable electrical double layer in solution. As such, the negatively-charged persulfate ions in APS can move to the surface of the $Al(OH)_3$ particles. As sulfate free radicals ($SO_4^{\bullet -}$) are produced using APS/TEMED, the free radical polymerization is expected to initiate at the positively-charged surface of $Al(OH)_3$ colloidal particles. As such, the thermoresponsive hybrid Al-NIPAM is intuitively expected to exhibit a star-like structure with polymer chains connected to the cationic core through ionic bonds, as previously reported for hybrid Al-PAM.[29, 61]

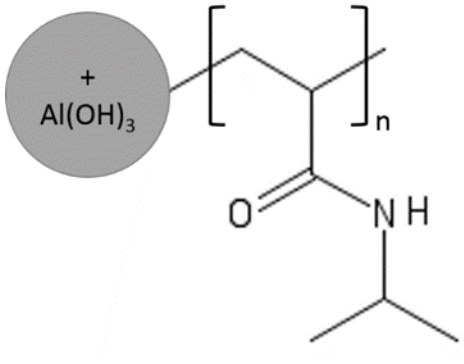

Figure 4.1. Molecular representation of Al-NIPAM.

4.3 Polymer Characterization

4.3.1 Molecular Weight

The molecular weight and intrinsic viscosity of polymer are important flocculant characteristics. It is well known that the viscosity-average molecular weight ($\bar{M}_v$) can be related to the intrinsic viscosity ($[\eta]$) of the polymer by the Mark-Houwink equation (Equation 4.2).[78-79]

$$[\eta] = K\bar{M}_v{}^{a} \tag{4.2}$$

where a and K are constants for a specific polymer-solvent system. The intrinsic viscosities of poly(NIPAM) and Al-NIPAM were measured in tetrahydrofuran (THF, > 99%) solution at 27°C with respect to polymer concentration using the Ubbelohde viscometer (CANNON Instrument Company, USA).[78] On the other hand, the mixture blend was prepared by dissolving poly(NIPAM) in dilute $Al(OH)_3$ colloidal suspension and its intrinsic viscosity was measured at 20°C.[79] Detailed intrinsic viscosity calculations can be found in Appendix A. The molecular weight of the polymers was estimated using the corresponding Mark-Houwink parameters (Table 4.2). The molecular weights of the synthesized polymers ranged from 2.2 to 2.5 MDa, which can be generally classified as low molecular weight flocculants. It is worth noting that the molecular weight of the polymer can be varied by adjusting the initiator concentration during polymerization.

Table 4.2. Molecular weight of polymers determined by Mark-Houwink equation.

Polymer	**Solvent**	K **(10^{-3})**	**a**	$[\eta]$ **(mL/g)**	$\bar{M}_v$ **(MDa)**
poly(NIPAM)	THF at 27°C[78]	9.59	0.65	138	2.5
poly(NIPAM)+Al	Water at 20°C[79]	14.5	0.50	230	2.5
Al-NIPAM	THF at 27°C[78]	9.59	0.65	127	2.2

4.3.2 Aluminum Content

The aluminum (Al) content of Al-NIPAM was measured by the SpectrAA 220FS atomic absorption spectrophotometer (AAS) (Varian, Australia), which can determine the concentration of specific elements in a sample.[80] Free atoms generated in an atomizer absorb light at specific wavelength (one for each element). The amount of light absorbed is proportional to the concentration of the absorbing atoms. With known standards between amount of light absorption and analyte concentration, the concentration of the element can be determined by measuring the amount of light absorbed. The polymer samples were prepared as 1000 ppm Al-NIPAM dissolved in DI water. Blank solution (1000 ppm poly(NIPAM)) was used for the instrument calibration. The concentration of elemental Al in the sample was measured at 1.1 ± 0.05 ppm, corresponding to an Al content of 0.11 ± 0.005 wt.%.

To understand the role of the $Al(OH)_3$-core structure in the hybrid polymer in flocculation, the hybrid polymer was compared to poly(NIPAM) dissolved in diluted $Al(OH)_3$ solution (0.11 wt.%), referred to as poly(NIPAM)+Al. The mixture blend was prepared one day prior to use with $Al(OH)_3$ colloids of sizes between 20 to 50 nm, zeta potential greater than +30 mV, and pH range between 5.5 to 6.0.

4.3.3 Solution Properties of Polymers

The LCST of thermoresponsive polymers in aqueous solution is a complex interaction taking place over a temperature range, which can depend on polymer concentration, molecular weight, nature of the end groups, structural architecture, comonomer content and distribution along the chains.[48-50] Experimentally, the LCST phase separation can be determined by turbidimetry (i.e. cloud point).

The synthesized polymers were dissolved in DI water (2000 ppm) and the solution pH was adjusted to pH ~8. The turbidities of the polymer solutions were measured at temperatures between 20 and 50°C using the Micro 100 laboratory turbidimeter, where the LCST is defined as the inflection point of the transition zone in the turbidity-temperature plot, see Figure 4.2 and Table 4.3. At low temperatures (< 30°C), the aqueous solution of thermoresponsive polymers was transparent,

indicating that the polymers are hydrophilic and extended in solution. As the temperature increased, the solution turned turbid (i.e. milky) because the polymer molecules became hydrophobic and separated out of solution. All synthesized polymers and mixture blend showed distinct responsiveness to temperature within narrow temperature ranges. For poly(NIPAM), a sharp reversible LCST around 32.5°C was observed, which is in good agreement with the literature value of 32°C.[50] The mixture blend of poly(NIPAM) and $Al(OH)_3$ solution showed a similar transition curve with poly(NIPAM), signifying that the presence of $Al(OH)_3$ particles has a negligible influence on the solution behavior of poly(NIPAM). For the hybrid Al-NIPAM, the LCST was slightly higher (34°C) than poly(NIPAM), along with the transition from transparent to opaque also more gradual than poly(NIPAM). As the LCST is dependent on the hydrogen bonding between the water molecules and the functional groups of poly(NIPAM), it can be influenced by structural parameters of polymers such as the hydrophilic/hydrophobic balance and polymer architecture.[49]

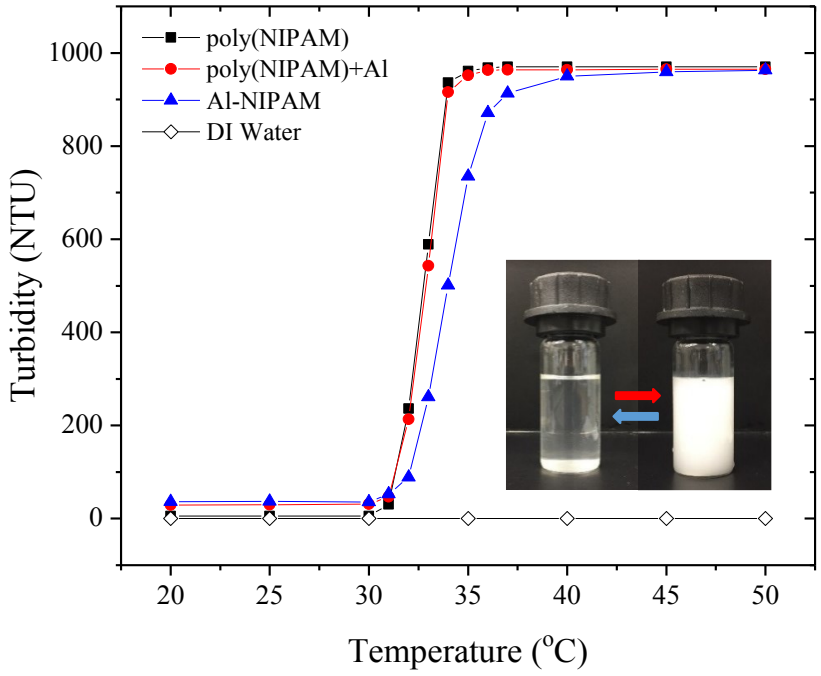

Figure 4.2. LCST of synthesized thermoresponsive polymers at pH 8.

In general, incorporation of hydrophilic groups increases the LCST whereas incorporation of hydrophobic groups decreases the LCST. Hence, the observed increase in $LCST_{Al\text{-}NIPAM}$ can be attributed to the inclusion of hydrophilic $Al(OH)_3$-core in the hybrid structure, leading to a polymer molecule with increased hydrophilicity. Copolymerization of poly(NIPAM) with cationic monomers has been shown to significantly affect the LCST of the copolymer, increasing the LCST as the copolymerization ratio increases.[53, 55] Hence, hybrid modification of poly(NIPAM) can be an alternative approach to copolymerization with cationic monomers to incorporate cationic charge into poly(NIPAM).

4.3.4 Zeta Potential of Polymer Solutions

The zeta potential distribution of the polymer species in DI water (100 ppm) was measured at 25°C using the Zetasizer Nano ZS, see Figure B.2-4. The measured zeta potential for poly(NIPAM) was close to zero, which is to be expected due to the neutral charge characteristics of poly(NIPAM). For poly(NIPAM)+Al, two distinct peaks were observed in the zeta potential distribution, corresponding to poly(NIPAM) (0 mV) and $Al(OH)_3$ colloids (> +30 mV). On the other hand, the zeta potential of Al-NIPAM polymer solution was slightly positive (+0.7 mV). Also, there is only one zeta potential peak, confirming the hybrid polymer is not simply a blend of poly(NIPAM) and $Al(OH)_3$ particles. The physical properties of the hybrid polymer differ from the individual polymer, as shown in Table 4.3. Also, the conductivity of hybrid polymer can change compared to the homopolymer,[60] see Figure B.6.

Table 4.3. Physical properties of polymeric flocculants studied.

Polymer	**Type**	$\bar{M}_v$ **(MDa)**	**LCST (°C)**	**Al (wt.%)**	**ζ (mV)**
poly(NIPAM)	Non-ionic	2.5	32.5	-	0 ± 0.3
poly(NIPAM)+Al	Mixture blend	2.5	32.5	0.11	-
Al-NIPAM	Cationic Hybrid	2.2	~34	0.11	+0.7 ± 0.1

Chapter 5: Polymer Adsorption Mechanisms

5.1 Zeta Potential of MFT and Polymer-MFT Mixtures

To study the interaction of synthesized polymers with fine solids in MFT, the zeta potentials of the MFT suspension were measured as a function of polymer concentration (Zetasizer Nano ZS), as shown in Figure 5.1. The measurements were performed using ~0.1 wt.% MFT suspension in OSPW without any electrolyte. In the absence of polymer, the zeta potential of the fine solids in MFT was highly negative (-32 mV, see Figure B.5), which is consistent to the strong colloidal stability of the MFT suspension. With polymer addition, the surface charge of the fine solids in tailings became less negative, thus indicating polymer-particle interactions. Higher polymer concentration also led to greater polymer adsorption on fine solids and further reduced the surface charge of tailings particles, but it did not result in charge reversal.

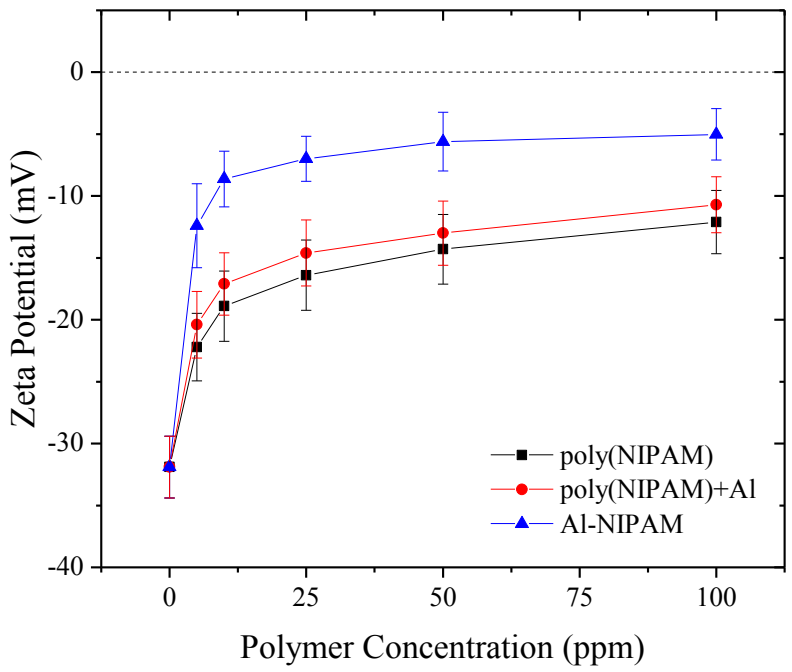

Figure 5.1. Effect of polymer addition on zeta potential of fine solids in MFT.

For non-ionic poly(NIPAM), the reduced electronegativity of the solids can be attributed to surface coverage of polymers on the fine solids, subsequently blocking the negatively-charged sites on the particle surfaces. On the other hand, the positively-charged $Al(OH)_3$ colloids in poly(NIPAM)+Al and Al-NIPAM are expected to reduce the surface charge of fine clays in tailings via electrostatic driving forces.[40] Specifically, Al-NIPAM reduced the electrostatic repulsion between the fine solids by charge neutralization. Based on these results, flocculation of MFT suspension is expected following the addition of these synthesized flocculants.

5.2 Adsorption Studies with QCM-D

5.2.1 Polymer Adsorption on Silica and Alumina Surfaces

Polymer adsorption on particle surfaces is crucial in flocculation. QCM-D can be used to study the adsorption and conformation of polymers at the solid-liquid interface.[81] Kaolinite, a major clay component in oil sands, has complex surface chemistry, consisting of tetrahedral silica and octahedral alumina basal planes with distinct edge surfaces of a combination of silica-alumina surface chemistry (see Section 2.1.1). In this study, silica- and alumina-coated QCM-D sensors were used to model the basal planes of kaolinite. OSPW was used as the background solution with a pH of 8. At this pH condition, silica surface is negatively-charged due to the deprotonation of surface hydroxyl groups whereas alumina surface has a slightly positive charge due to surface hydrolysis and dihydroxylation.[30, 81]

The adsorption kinetic of Al-NIPAM on silica and alumina surfaces at 24°C is shown in Figure 5.2. The background solution was used to establish a horizontal baseline, followed by the introduction of polymer solution (100 ppm) until a new equilibrium was reached. The hybrid polymer adsorbed on silica and alumina surfaces at an equilibrium of ~5.7 and ~2 mg/m^2 respectively. The higher adsorption mass of Al-NIPAM on the silica-coated surface arises from strong electrostatic attraction between the $Al(OH)_3$-cores and negatively-charged sites (deprotonated silanol groups) on the silica surface as well as hydrogen bonding.[81]

It is worth noting that $Al(OH)_3$-core in the hybrid polymer has a high surface potential of +36.7 mV (Table 4.1), which provides strong binding sites. In contrast, adsorption of cationic Al-NIPAM on positively-charged alumina surface can be hindered by electrostatic repulsion, thus limiting active sites for adsorption via hydrogen bonding interactions,[40] As such, there was considerably less polymer adsorbed on alumina. The observed differences in polymer adsorption behavior on the model basal surfaces confirm the charge selective adsorption nature of the cationic Al-NIPAM hybrid polymer, which is in good agreement with another QCM-D study using hybrid Al-PAM.[81] The adsorption of HPAM has been previously found to occur only on alumina basal planes, whereas inorganic-organic hybrid polymer Al-PAM can adsorb on both silica (strongly) and alumina (weakly) basal planes. Such adsorption behavior can lead to improved flocculation of clay particles.

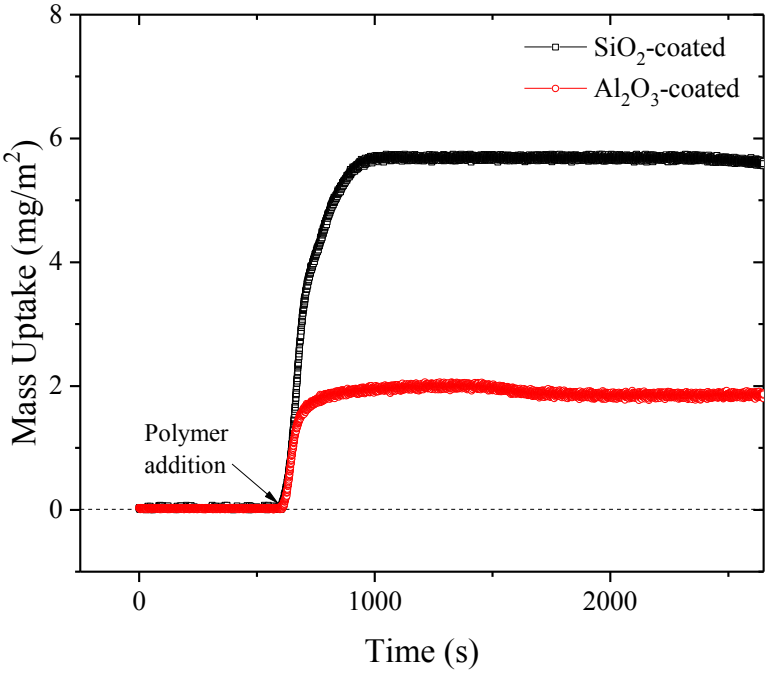

Figure 5.2. Adsorption of Al-NIPAM on silica and alumina surfaces at 24°C and pH 8.

5.2.2 Polymer Conformation Change with Temperature

The use of QCM-D to investigate the thermoresponsive behavior of LCST polymers has been demonstrated by several studies measuring the changes in the frequency and dissipation from the adsorbed layer as a function of temperature.[71, 82] In this study, two parallel silica-coated QCM-D sensors were mounted onto the flow modules and the cell temperature was increased from 25 to 40°C in a stepwise manner (5°C). A stable layer of adsorbed polymer covered the first sensor, while the second sensor acted as control to account for the influence of temperature on the physical properties of the background solution. Figure 5.3 and 5.4 show the frequency and dissipation measured by the sensor with adsorbed polymer and the control with temperature respectively. For the first sensor, polymer solution was introduced at 25°C to an equilibrium, followed by a background solution rinse to form a stable polymer layer on the surface. As the cell temperature was increased, measurable shifts in frequency and dissipation were recorded by the QCM-D sensors, which can be caused by a combination of changes in polymer conformation and water properties with temperature.

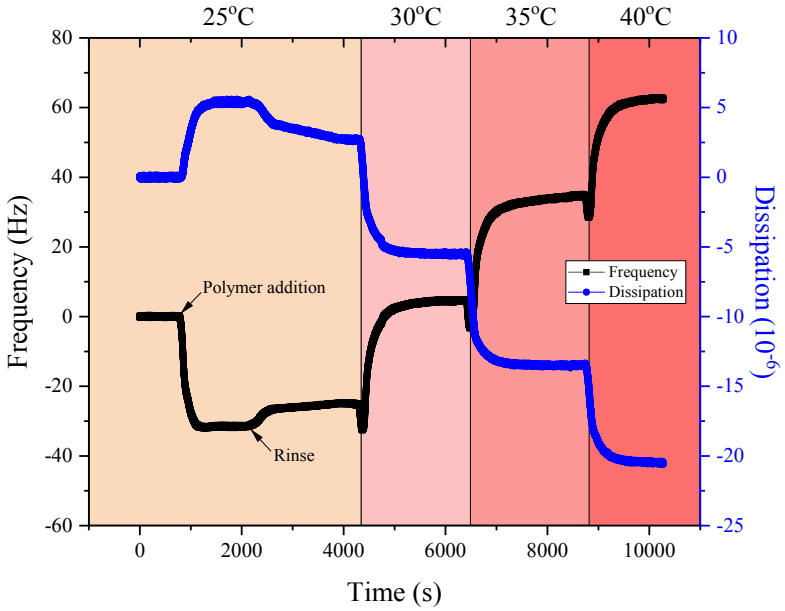

Figure 5.3. Frequency and dissipation response of silica-coated sensor as a function of temperature (with adsorbed Al-NIPAM polymer layer).

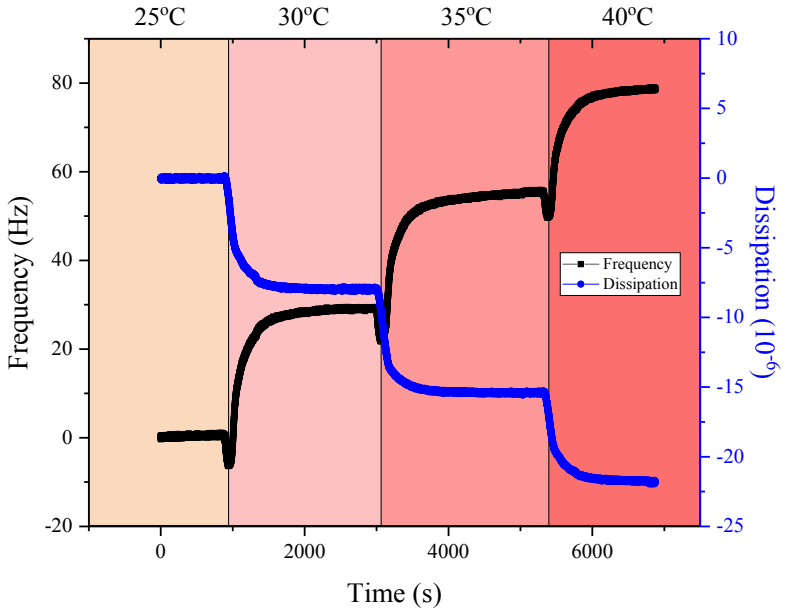

Figure 5.4. Frequency and dissipation response of silica sensor as a function of temperature (control).

Therefore, the difference between the frequency ($-\Delta f$) and dissipation (ΔD) shifts measured by the two parallel sensors can be associated with the conformational changes in the adsorbed polymer layer (see Section 3.2.2). Figure 5.5 and 5.6 show the $-\Delta f$ and ΔD shifts caused by the adsorbed Al-NIPAM layer respectively, as a function of temperature. Each data point in these figures represents the equilibrium $-\Delta f$ and ΔD value at the given temperature. At 25°C (below LCST), the frequency and dissipation signals were highest, indicating that the adsorbed layer is in its most elastic and hydrated conformation. From 30 to 40°C, significant decreases in frequency and dissipation occurred as the temperature exceeded the LCST. The decrease in $-\Delta f$ implies mass loss from the adsorbed layer, which can be attributed to either polymer dehydration or detachment. On the other hand, the decrease in ΔD suggests an increased rigidity of the adsorbed polymer layer. It is likely that these changes are mostly caused by the increased polymer hydrophobicity above the LCST, leading to dehydration of the polymer (i.e. forces out bounded water) and polymer conformation change (i.e. collapsed polymer chains) simultaneously.

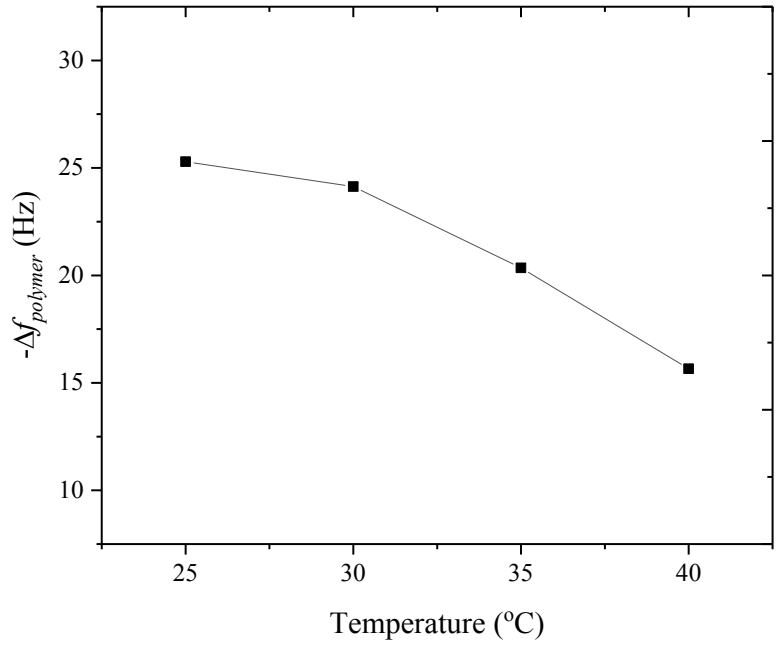

Figure 5.5. -Δ*f* of adsorbed Al-NIPAM layer as a function of temperature.

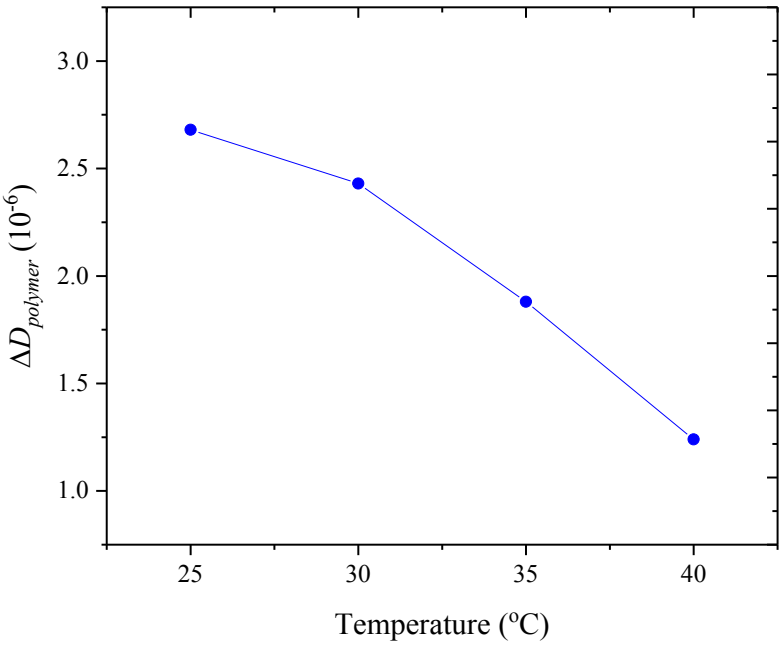

Figure 5.6. Δ*D* of adsorbed Al-NIPAM layer as a function of temperature.

In this chapter, the polymer adsorption mechanisms were explored by zeta potential measurements and QCM-D. Zeta potential measurements showed that the polymers interacted with the fine solids in MFT, reducing the electronegativity of the fine solids. Based on QCM-D adsorption studies, the hybrid polymer was more selective towards negatively-charged silica-coated surfaces and adopted a collapsed conformation above the LCST. Results obtained from the adsorption and conformational experiments provide some insight on the working mechanisms behind the use of hybrid Al-NIPAM in flocculation. The following flocculation mechanism using the hybrid polymer Al-NIPAM is proposed, as illustrated in Figure 5.7.

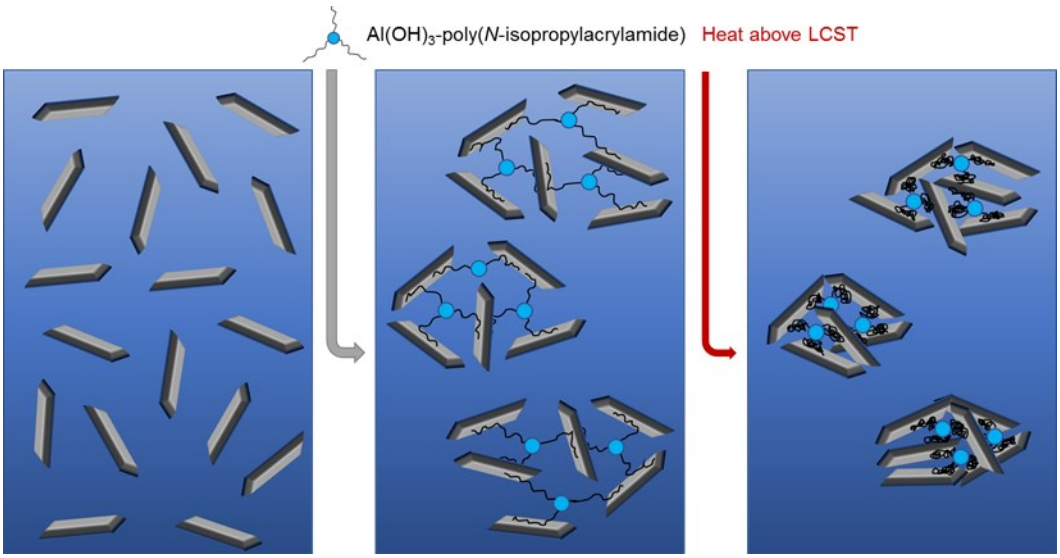

Figure 5.7. Schematic representation of the interactions between Al-NIPAM and fine clays in MFT.

As the clays suspended in tailings carry a net negative charge, flocculation using the cationic hybrid can occur through a synergetic combination of bridging and charge neutralization. Below the LCST, Al-NIPAM polymer chains are in its most elastic and hydrated conformation. As such, the hybrid polymer is to be added to the fine tailings at temperatures below the LCST so that maximum binding of polymer chains to suspended particles at different sites occurs via non-covalent interactions such as hydrogen bonding and van der Waals forces.[40] Furthermore,

the exposed cationic $Al(OH)_3$-cores strongly attract and bind fine clays within the extended poly(NIPAM) chains, providing a dual coagulation and flocculation effect to maximize polymer-particle interactions. The formed flocs are expected to be compact due to strong electrostatic attractions between the fine solids and the hybrid polymer molecules. Star-like polymer structure revealed in cationic Al-PAM is also expected to form with Al-NIPAM due to the similarities in the initiation step of polymerization.[22, 61] Such structure has been shown to form large and dense spherical flocs due to induced pelleting flocculation, although the thermal switch of Al-NIPAM can further increase floc densification. When the temperature exceeds the LCST, the thermoresponsive polymer chains in the hybrid undergo the coil-globule transition, forcing retained water away from the flocculated network while pulling the particles closer together simultaneously.[27] As such, the formed flocs become more tightly-packed (i.e. increase in floc density).

Based on the proposed flocculation mechanism, the flocculation and consolidation performances using Al-NIPAM are anticipated to be superior compared to poly(NIPAM) and its coagulant/flocculant mixture blend, while increasing the temperature above the LCST following flocculation should enhance floc densification. The flocculation and consolidation performance of MFT suspension using the synthesized polymeric flocculants will be discussed in the following chapter.

Chapter 6: Flocculation and Consolidation Performance on MFT Suspension

6.1 Initial Settling Rate

6.1.1 Effect of Mixing

The performance of flocculants can be significantly affected by the hydrodynamic conditions during treatment related to polymer adsorption and floc growth/breakage. For each polymeric flocculant, an equivalent polymer dose was added under different mixing speeds and the optimum mixing speed was determined by the highest initial settling rate (ISR). Such dependence on mixing speed has been frequently reported and relates to the size of the particle flocs being limited by particle collision and floc breakage.[83] Figure 6.1 shows the effect of the mixing speed during flocculant addition on the ISR.

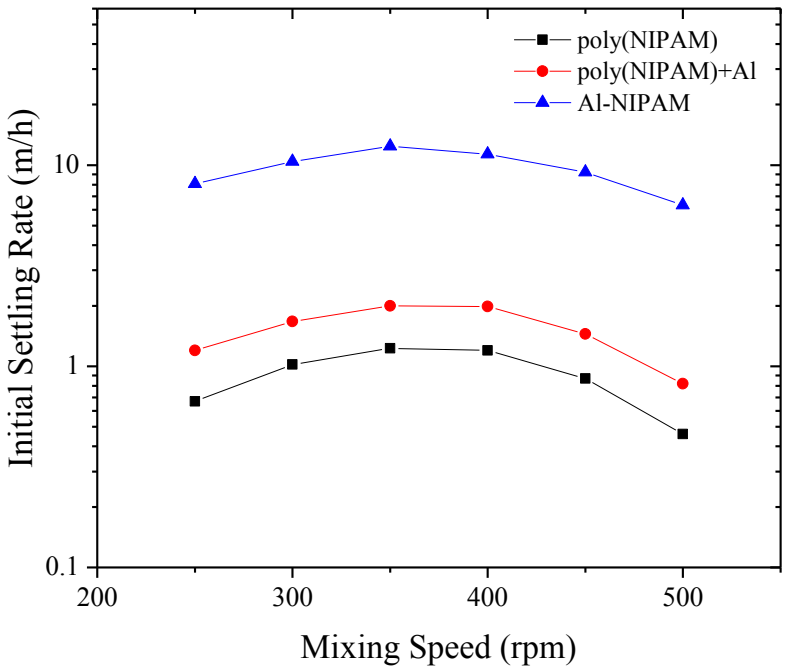

Figure 6.1. Effect of mixing speed on the ISR of MFT treated with flocculants.

At low shear, the suspended particles often fail to join with the polymeric flocculants to form aggregates, which can lead to low settling rate. An increase in shear ensures the flocculants being well-mixed in the suspension for improved polymer adsorption and increases the probability of particle collisions for floc growth. However, floc breakage also happens at high shear, which can deteriorate the settling performance due to the irreversible aggregate breakage into smaller particles. For poly(NIPAM) and poly(NIPAM)+Al, the optimum mixing occurred in the range between 350 to 400 rpm. For Al-NIPAM, the optimum was near 350 rpm. For consistency, all subsequent settling tests were conducted at a mixing speed of 350 rpm during the flocculant addition stage.

6.1.2 Comparison of Polymers as Flocculants

To compare the flocculation performance between the polymers, the ISRs of non-ionic poly(NIPAM), coagulant/flocculant mixture blend poly(NIPAM)+Al and cationic hybrid Al-NIPAM were measured. For consistency, the polymers were synthesized with comparable molecular weights due to the known influence of polymer molecular weight on flocculation performance.[40, 52] Furthermore, two settling temperatures, 21°C (below LCST) and 40°C (above LCST), were investigated to study the effects of temperature on settling performance.

The ISR of 5 wt.% MFT treated with poly(NIPAM) is shown in Figure 6.2. In the absence of polymer, the MFT suspension showed an extremely slow ISR (~0 m/h), with virtually no settling regardless of the settling temperature. At poly(NIPAM) dosages less than 5 kg/t, the ISRs remained low, likely due to insufficient bridging links between the polymer chains and the fines/clays in MFT. Since poly(NIPAM) is a non-ionic polymer, the adsorption capability on charged particles can be limited.[55] Higher polymer dosage allows more surface coverage for solids attachment, reducing the electronegativity of the solids and facilitating polymer bridging.[40] As such, the ISR increased with polymer dosage up to 8 kg/t. It is generally accepted that the settling rate increases with flocculant addition until an optimum dosage is reached, corresponding to the optimal surface coverage for attachment. Further polymer addition resulted in slight decreases in ISR, possibly

due to polymer overdose. Excess polymer coverage on particle surfaces can prevent contact with vacant sites on another particle and lead to re-stabilization of the particles.[40] The high dosage requirement flocculating with poly(NIPAM) has also been reported in other fine particle flocculation studies using poly(NIPAM) as flocculants.[25, 27]

The settling temperature significantly affected the ISR. Elevated temperature settling (40°C) improved the settling rates for poly(NIPAM), highlighting the benefit of flocculating with thermoresponsive polymers. At the optimum dosage, the ISR increased from 1.1 to 2.1 m/h due to the thermal switch of poly(NIPAM). The driving force for the enhanced flocculation above the LCST can be attributed to floc densification and particle aggregation via hydrophobic interaction.[27, 53-54] Sun et al. previously reported a transition for a poly(NIPAM)-coated surface from completely hydrophilic at 29°C to highly hydrophobic at 40°C.[51] Hence, hydrophobic flocs can be formed with poly(NIPAM) above the LCST.

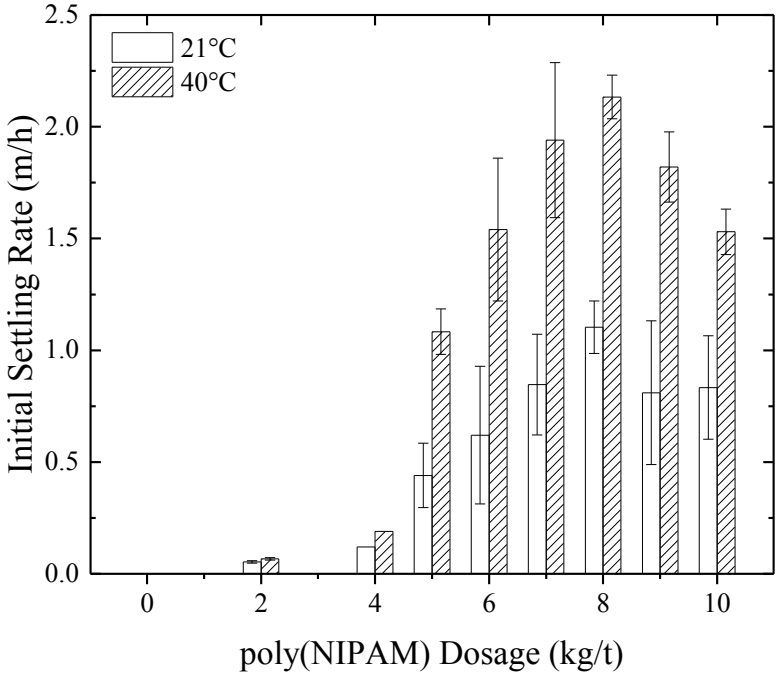

Figure 6.2. Initial settling rate of 5 wt.% MFT treated with poly(NIPAM).

The coagulant/flocculant mixture blend poly(NIPAM)+Al was prepared such that it had the same Al content (0.11 wt.%) as Al-NIPAM. The mixture blend offered a marked improvement in the settling rates over the poly(NIPAM) at comparable dosages, as shown in Figure 6.3. This can be attributed to the combination of inorganic coagulant and organic flocculant that improves suspension destabilization. The unbounded aluminum species in the mixture blend likely reduce the surface charge of the suspended particles, potentially facilitating the formation of micro-flocs. Simultaneously, the organic poly(NIPAM) chains bridge the micro-flocs together into larger flocs that settled faster. The dosage range for poly(NIPAM) and poly(NIPAM)+Al did not vary substantially, which is expected due to their equivalent molecular weight and structure. At high dosage, overdose can be caused by excess polymer coverage on the particle surfaces and possibly excess coagulants. Similar to poly(NIPAM), elevated temperature settling yielded significantly higher ISR compared to room temperature settling.

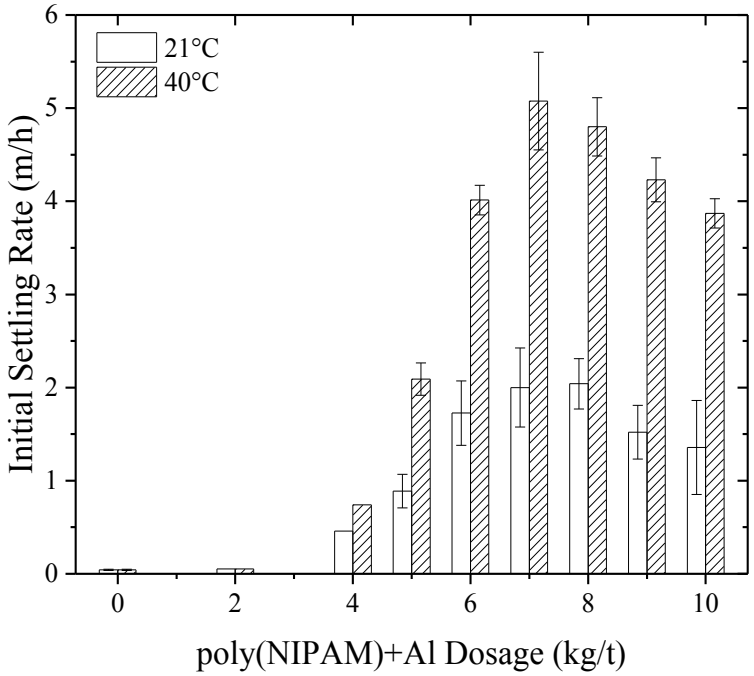

Figure 6.3. Initial settling rate of 5 wt.% MFT treated with poly(NIPAM)+Al.

Although both poly(NIPAM) and poly(NIPAM)+Al induced settling of MFT, the high polymer dosage becomes impractical due to costly polymeric flocculants. Figure 6.4 shows the ISR of flocculated MFT at different Al-NIPAM dosages. While poly(NIPAM) and poly(NIPAM)+Al flocculated within a similar dosage range, the hybrid polymer induced flocculation at much lower dosages. At low polymer dosage (< 1 kg/t), the ISR remained low, signifying polymer underdose. Increased Al-NIPAM dosage resulted in higher settling rates, before the maximum ISR measured at a dosage of 2.5 kg/t. At room temperature settling, the maximum ISR was 14.7 m/h, which is a significant increase over the ISR obtained with poly(NIPAM) (1.10 m/h, 8 kg/t). Although poly(NIPAM)+Al (2.04 m/h, 8 kg/t) offered an improvement over poly(NIPAM), the performance was still substantially inferior to the hybrid polymer. Hence, a simple mixture blend of poly(NIPAM) and $Al(OH)_3$ particles does not produce a synergistic improvement in flocculation. The better performance of the hybrid over the individual coagulants and flocculants can be attributed to the synergy in the hybrid structure.[29]

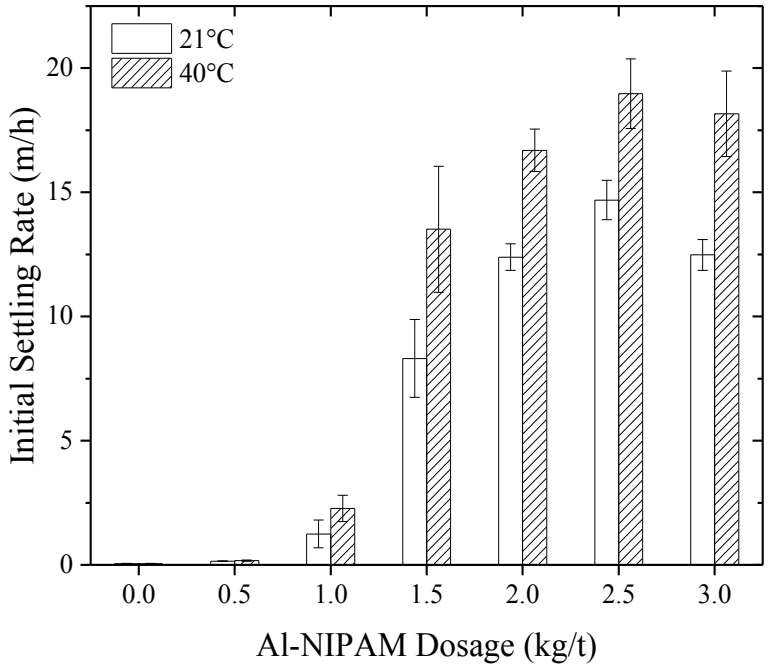

Figure 6.4. Initial settling rate of 5 wt.% MFT treated with Al-NIPAM.

At 40°C, the thermal switch of Al-NIPAM also produced faster settling flocs, increasing the ISR from 14.7 to 19.0 m/h (2.5 kg/t). The coil-globule transition offered by the hybrid polymer provides the best processing solution for flocculation in this study. At room temperature, the polymer is fully extended. The exposed cationic $Al(OH)_3$-core attracts negatively-charged fine clays in tailings and maximizes the number of adsorption sites for optimal interaction. However, this extended state is not the optimum conformation for settling and the flocculated network can be further densified by increasing the temperature above the LCST.[27] The extended polymer structure then recoils towards the inorganic core, squeezing retained water from the floc. The effective increase in floc density promotes the observed high settling rates at 40°C. Figure 6.5 shows a comparison of the sediment height of 5 wt.% MFT with and without polymer treatment after 10 min of settling at room temperature. For the diluted MFT (5 wt.%), the suspension remained extremely stable and showed virtually no settling. With flocculant additions, various extents of flocculation were observed, where Al-NIPAM outperformed the mixture blend and linear poly(NIPAM), see Figure B.7 and B.8 for the normalized mudline settling curves.

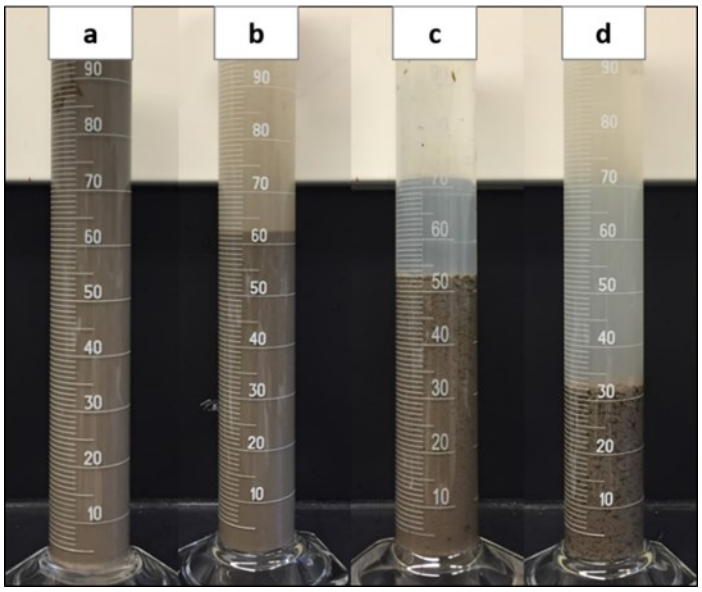

Figure 6.5. Comparison of settling tests for a) 5 wt.% MFT and MFT treated with b) poly(NIPAM) c) poly(NIPAM)+Al and d) Al-NIPAM (21°C, 10 min settling).

6.2 Supernatant Turbidity

Following 15 min of settling, the released supernatant was decanted for turbidity measurement, which gives an indication of the concentration of suspended fine solids in suspension. The supernatant turbidity of 5 wt.% MFT treated with poly(NIPAM) as a function of polymer dosage is shown in Figure 6.6. The supernatant turbidity at low poly(NIPAM) dosages (< 5 kg/t) were not measured as there was insufficient volume of supernatant released due to poor settling. At room temperature settling, the collected supernatant from MFT treated with poly(NIPAM) were highly turbid (> 500 NTU), as the non-ionic poly(NIPAM) failed to neutralize and reduce the surface charge of the suspended fine solids. Furthermore, the poly(NIPAM) flocculants used in this study may have large polydispersity due to synthesis via conventional free radical polymerization. Some of the adsorbed non-ionic poly(NIPAM) with low molecular weights may lead to steric repulsion between the particles and thus poor supernatant clarity.[6, 25]

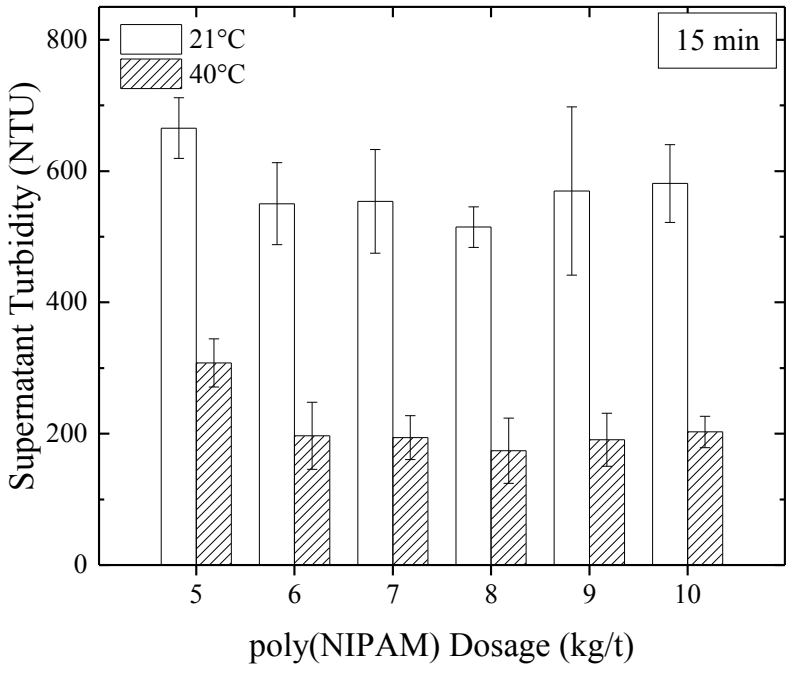

Figure 6.6. Supernatant turbidity of 5 wt.% MFT treated with poly(NIPAM).

When the sample settled at 40°C, the supernatant turbidity decreased significantly, indicating better flocculation of fine solids at elevated temperature. The improvement may be due to the aggregation and settling of residual poly(NIPAM)-adsorbed fine solids caused by hydrophobic interaction above the LCST, as reported in other studies using thermoresponsive polymers as flocculants.[24, 84]

The supernatant turbidity of 5 wt.% MFT treated with poly(NIPAM)+Al is shown in Figure 6.7. At room temperature settling, the produced supernatants were clearer (~300 NTU) than poly(NIPAM). The unbounded aluminum species in the mixture blend are effective in reducing or neutralizing the surface charges of fine solids, thus leading to destabilization of the fine solids and better supernatant clarity. Aluminum-based coagulants has been well understood to improve water clarity in wastewater treatment through charge neutralization.[40] Similar to poly(NIPAM), settling temperature enhanced flocculation of fine solids, where lower supernatant turbidities were measured at 40°C settling.

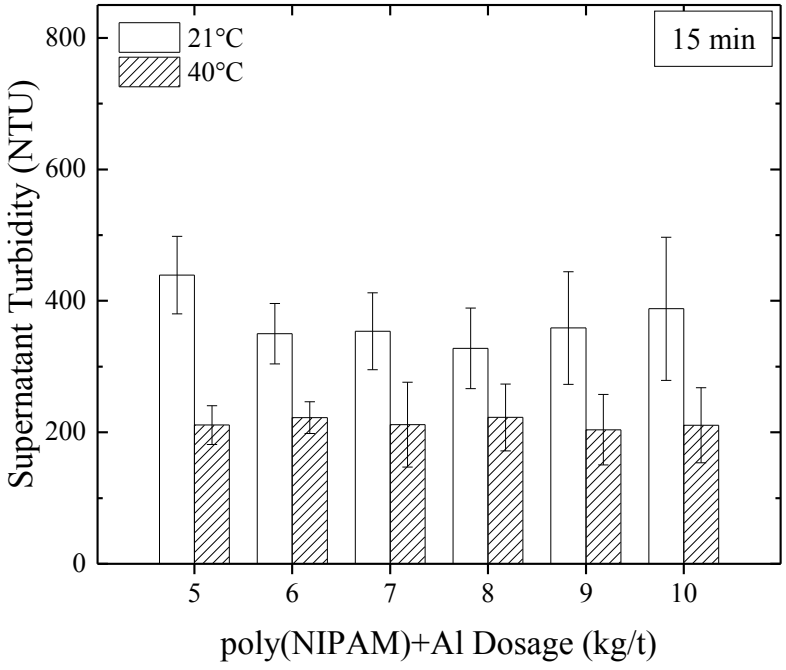

Figure 6.7. Supernatant turbidity of 5 wt.% MFT treated with poly(NIPAM)+Al.

Figure 6.8 shows the supernatant turbidity of 5 wt.% MFT treated with Al-NIPAM. Compared to poly(NIPAM) and poly(NIPAM)+Al, the enhanced performance of the hybrid polymer was once again evidenced, producing the lowest supernatant turbidities (< 200 NTU) at room temperature. The high charge potential $Al(OH)_3$-core in the hybrid structure attracts and captures the fine solids within the branched polymer chains. This effectively neutralizes their surface charges and reduces the repulsion between the fine solids, providing a dual coagulation and flocculation effect.

At elevated temperature settling, the turbidity of the supernatant was reduced to < 150 NTU at 2.5 kg/t, eventually decreasing to ~33 NTU after 24 h settling. It is worth noting that the heat-induced improvement in the supernatant turbidity for Al-NIPAM was less noticeable than in the cases of poly(NIPAM) and poly(NIPAM)+Al.

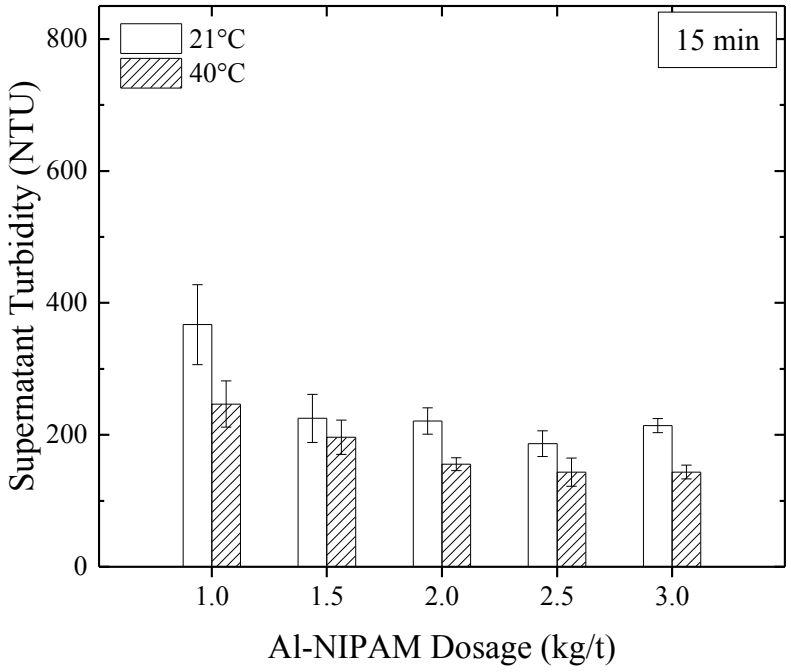

Figure 6.8. Supernatant turbidity of 5 wt.% MFT treated with Al-NIPAM

6.3 Sediment Solids Content

Following 24 h of settling, the flocculated MFT suspension consolidated to a final sediment state with solids content shown in Figure 6.9, 6.10 and 6.11. At room temperature, the final solids contents did not vary much between poly(NIPAM) and poly(NIPAM)+Al (17 to 18 wt.%), as these polymers were unable to produce large flocs. On the other hand, Al-NIPAM produced sediments with higher solids content (~20 wt.%). Due to the strong electrostatic attraction between the fine solids and the hybrid polymer molecules, the pellet-like flocs produced by the hybrid polymer were larger and more compact, contributing to improved consolidation over poly(NIPAM) and poly(NIPAM)+Al. At 40°C settling, the sediments consolidated more than room temperature settling, as evidenced by the higher sediment solids contents obtained for all polymers. For poly(NIPAM) and poly(NIPAM)+Al, the solids contents increased to ~20 wt.%. Likewise, Al-NIPAM enhanced sediment consolidation, producing sediments with the highest solids content at ~22 wt.%.

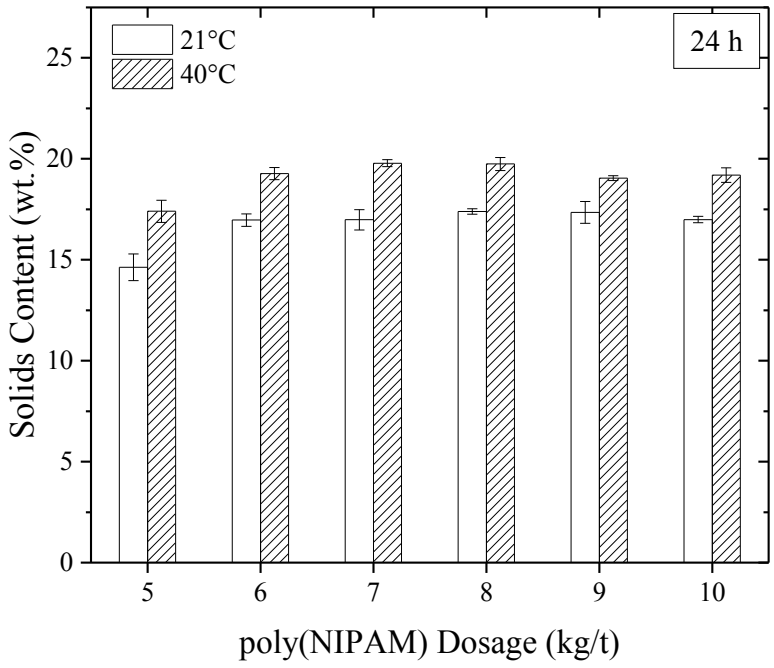

Figure 6.9. Solids content of sediments formed with poly(NIPAM).

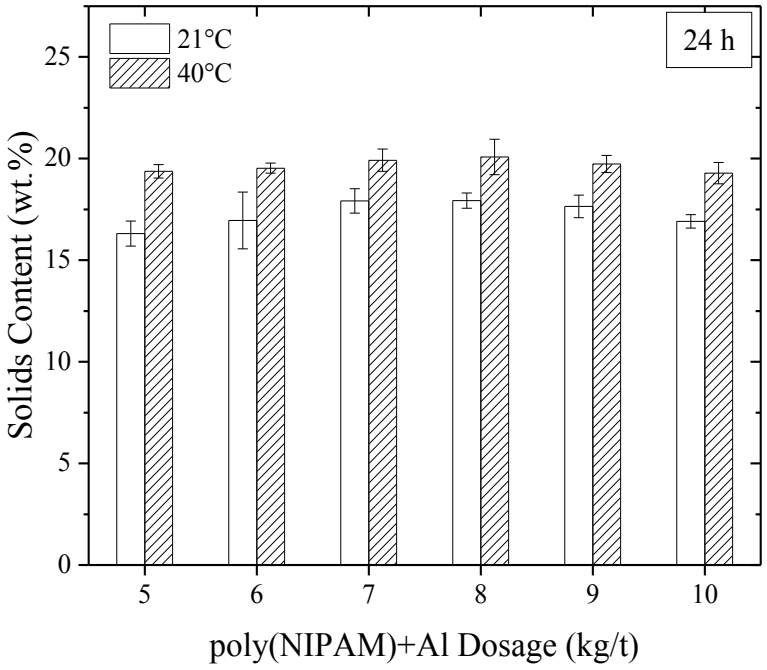

Figure 6.10. Solids content of sediments formed with poly(NIPAM)+Al.

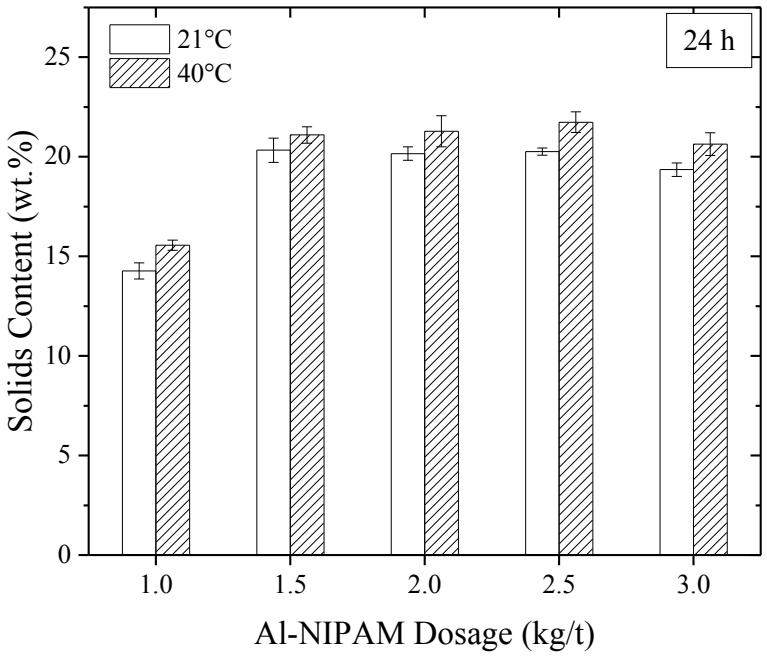

Figure 6.11. Solids content of sediments formed with Al-NIPAM.

Clearly, the coil-globule transition of thermoresponsive polymers can be advantageous in sediment consolidation due to formation of dense hydrophobic flocs with improved dewatering characteristics, resulting in less water retention within the sediment.[25, 27] Several studies have demonstrated that sediments formed with poly(NIPAM) consolidated better than PAM in the flocculation of silica and MFT suspension with better dewatering characteristics.[24, 52] Furthermore, poly(NIPAM)-treated MFT has been shown to evaporate faster than PAM-treated MFT under natural drying, which can be a useful flocculant characteristic in evaporative technologies. Hence, the hybrid modification of poly(NIPAM) represents a viable approach to enhance the functionality of the homopolymer.

Even though polymer addition assisted the MFT suspension to reach its sediment state much faster, it had negligible effect on net water release from MFT. This is in agreement with other reports using polymeric flocculants, as the high clay fractions of MFT makes it very difficult to dewater by gravity sedimentation alone. To further release water from the sediments, dewatering technologies with applied external forces (e.g. filtration, centrifugation) are often necessary. Filtration studies using Al-PAM[23] and Al-CP[67] have demonstrated the effectiveness of hybrid polymers as filtration aids due to the benefits of pellet flocculation in producing porous filter cakes. As Al-NIPAM shares structural similarities with Al-PAM and Al-CP, it is intuitive that the hybrid Al-NIPAM can also be an effective filtration aid for dewatering of MFT, with the added benefit of thermal switchable properties.

Table 6.1 shows the performance overview of poly(NIPAM), poly(NIPAM)+Al and Al-NIPAM at the optimal flocculation condition. Settling at 40°C was the best processing solution, reaping the benefits of flocculating with thermoresponsive polymers. Results also showed that Al-NIPAM was best in all performance indicators (dosage, ISR, turbidity and sediment solids content). The enhanced performance of the hybrid polymer over its respective inorganic and organic components suggests that the synergetic hybrid structure (dual coagulation and flocculation) plays a significant role in flocculation and consolidation.

Table 6.1. Optimal flocculation performance for each polymeric flocculant.

Polymer	Optimal Dosage (kg/t)	ISR (m/h)		Turbidity (NTU)		Solids (wt.%)	
		21°C	40°C	21°C	40°C	21°C	40°C
poly(NIPAM)	8	1.1	2.1	515	174	17.4	19.7
poly(NIPAM)+Al	8	2.0	4.8	328	227	17.9	20.1
Al-NIPAM	2.5	14.7	19.0	187	143	20.2	21.7

6.4 In-situ Floc Characteristics

To understand the in-situ aggregation behavior of a flocculated particle system, FBRM technology was used to measure the floc size, expressed in chord length, under constant shear (400 rpm). Figure 6.12 shows the square-weighted mean chord length of the fine solids in MFT during the conditioning and flocculation stages at room temperature under optimal polymer dosages for each synthesized flocculants.

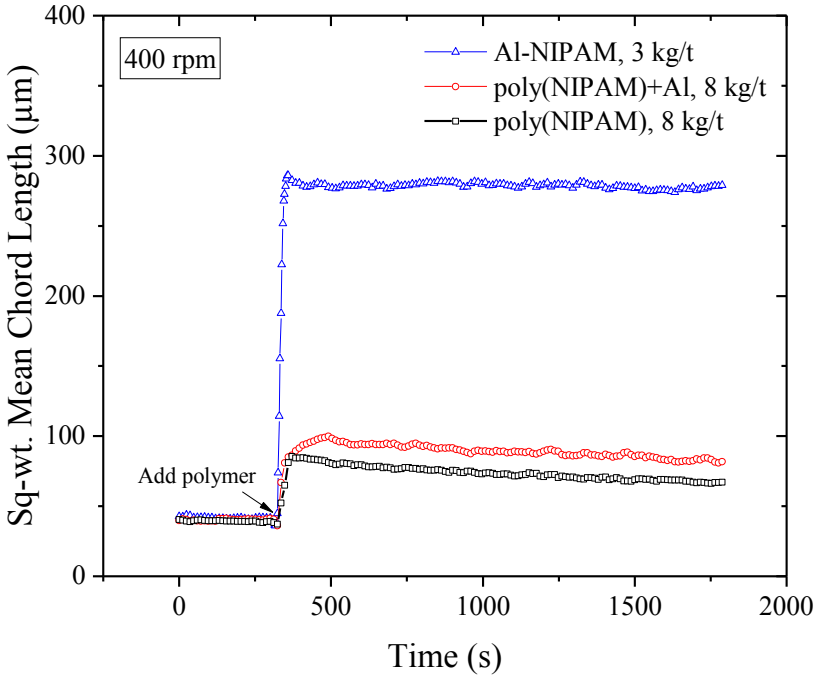

Figure 6.12. Sq-wt. mean chord length of 5 wt.% MFT with flocculant additions.

Although the chord length distribution is not identical to particle size distribution, the square-weighted mean chord length has been reported to closely resemble mean particle diameter obtained using conventional sizing method.[85] The suspension was initially mixed for 5 min to establish a stable horizontal baseline. Following polymer addition, the square-weighted mean chord length increased rapidly, indicating floc formation and growth. The maximum size of flocs induced by Al-NIPAM (~280 μm) was significantly larger than those obtained with poly(NIPAM) (~85 μm) and poly(NIPAM)+Al (~100 μm), confirming the effectiveness of the cationic $Al(OH)_3$-core to attract and flocculate fine solids and clays. The large floc size induced by Al-NIPAM is in good agreement with the highest obtained ISR, as the square-weighted mean chord length can be related to the settling rate.[21] Even though agitation promotes particle-particle collision necessary for floc formation and growth, it can also result in floc fragmentation and breakage. After reaching the plateau (i.e. max floc sizes), the size of the flocs formed with poly(NIPAM) and poly(NIPAM)+Al decreased with extended period of agitation, eventually decreasing to ~65 μm and ~80 μm respectively at the end of the experiment. This is likely attributed to either restructuring or fragmentation of the flocs. On the other hand, the flocs formed with Al-NIPAM were relatively stable, as indicated by the steady floc sizes throughout the experimental duration. Clearly, the larger and more shear-resistant flocs produced by Al-NIPAM are more desirable floc characteristics. Similar studies have also reported that flocs produced by hybrid polymers (e.g. Al-PAM and $Fe(OH)_3$-PAM) are able to resist breakage under comparable mixing conditions.[86]

Figure 6.13 shows the cumulative square-weighted chord length distribution of 5 wt.% MFT suspension as a function of Al-NIPAM dosages at 400 rpm. In the absence of flocculant addition, the chord lengths of the fine solids in MFT were small. As anticipated, polymer dosage significantly affected floc size, where higher dosage led to greater counts of larger flocs (i.e. shifting distribution to the right). Higher polymer concentration in suspension allowed greater chance of interparticle bridging, although a diminishing improvement with dosages was observed. The

limiting maximum floc size was measured at a dosage of 3 kg/t, which is in good agreement to the optimal dosage as previously determined based of ISR.

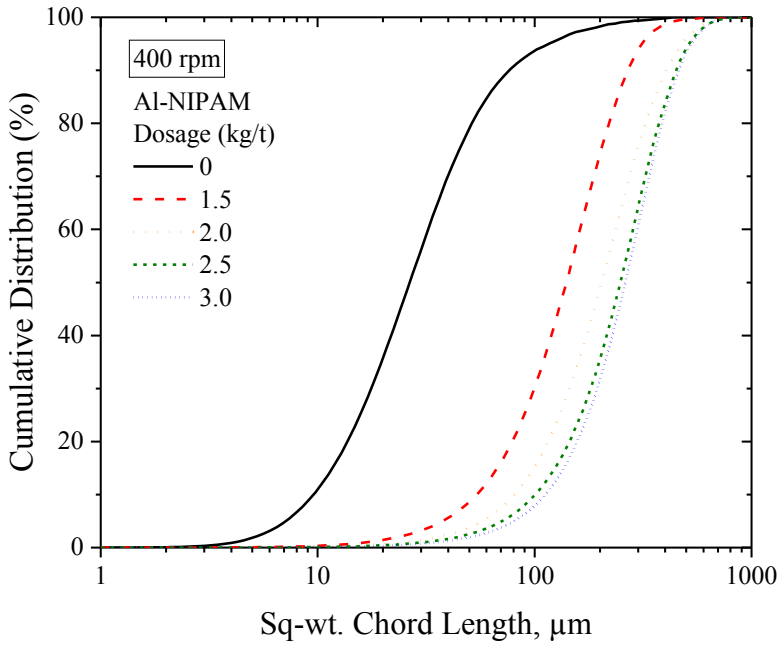

Figure 6.13. Cumulative sq-wt. chord length distribution of 5 wt.% MFT at different Al-NIPAM dosages.

To evaluate the effect of temperature on the size of the formed flocs, the flocculated slurry was heated and the changes in the floc size were recorded as a function of temperature using a temperature-controlled FBRM setup (see Figure 3.4). Figure 6.14 shows the floc sizes (Al-NIPAM) as a function of temperature. The flocs formed with Al-NIPAM were stable without any heating (see insert), providing a baseline for comparison purposes (control). For the other case (heat), heating was introduced to increase the slurry temperature while the continuous agitation (400 rpm) ensured temperature homogeneity in the slurry. Below the LCST of the hybrid Al-NIPAM (34°C), there were negligible changes in the size of the formed flocs. However, when the slurry temperature exceeded the $LCST_{Al\text{-}NIPAM}$, an obvious decreasing trend in the chord length with increasing temperature was observed. Such changes can be attributed to the coil-globule transition of the polymer that

contributes to a densified flocculated network, as the hydrophobic polymer pulls the flocculated particles closer together and simultaneously forces retained water away from the floc structure. This effective increase in floc density results in the observed enhancement in the settling of MFT suspension using the elevated temperature settling protocol, as shown previously in Figure 6.4. At elevated temperatures, it is also plausible that some fine solids may detach from the polymer-particle aggregate due to strong hydrophobic forces.

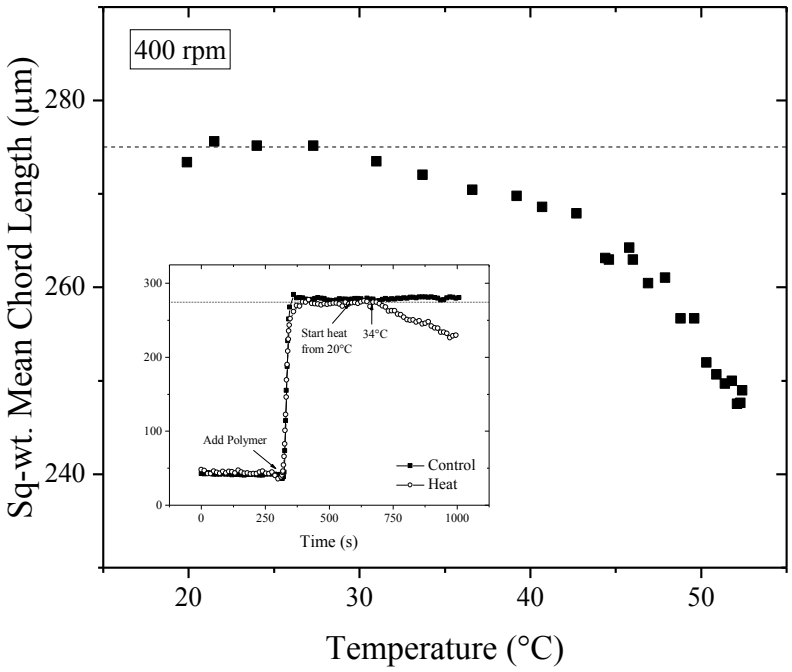

Figure 6.14. Sq-wt. mean chord lengths of 5 wt.% MFT treated with Al-NIPAM (3 kg/t) as a function of suspension temperature.

Chapter 7: Integration with Bitumen Extraction

Process aids are often used to improve bitumen recovery for processing of low-grade oil sands ores with high fines content in CHWE processes.[6] Caustics are widely used due to its effectiveness and robustness. While caustics addition is beneficial for bitumen extraction, it leads to poor tailings settling. As such, several studies have investigated polymeric flocculants as process aids to provide a holistic improvement in bitumen extraction and tailings settling.[22, 87-88]

Long et al.[88] tested poly(NIPAM) as a process aid in bitumen extraction in a laboratory hydrotransport extraction system (LHES). When the extraction was carried out at 40°C (above $LCST_{poly(NIPAM)}$), poly(NIPAM) addition was shown to improve bitumen recovery and tailings settling, although the bitumen froth quality deteriorated. The higher bitumen recovery was attributed to the changes in polymer conformation from extended coils to collapsed globules, forming dense flocs that settle from the slurry faster. Other researchers also demonstrated that poly(NIPAM)-based block copolymers enhanced bitumen recovery due to their ability to reduce the bitumen-water interfacial tension.[89-90] These block copolymers have well-defined segments that allow the formation of ordered structures. On the other hand, hybrid Al-PAM has also been studied for processing of low-grade oil sands ores. Using the LHES, Li et al.[87] showed that Al-PAM improved bitumen froth quality and tailings settling, forming dense spherical flocs of fine solids that are not easily brought to the bitumen froth during flotation. However, Al-PAM caused strong bitumen-bitumen attraction interactions and thus resulted in formation of large bitumen lumps that deteriorated bitumen recovery. The authors resolved the bitumen coalescence problem by using a dual-polymer system (Al-PAM and HPAM).

In this chapter, the potential effects of thermoresponsive hybrid polymer (Al-NIPAM) in bitumen extraction were investigated. The interfacial properties of the thermoresponsive polymers at a model oil-water interface were determined, and the effects of the polymers in bitumen liberation and aeration processes were studied.

7.1 Interfacial Properties of Polymer Solutions

To investigate the interfacial properties of the polymer solutions, the Du Noüy Ring method was used to measure the interfacial tension of a model toluene-DI water interface. Figure 7.1 shows the interfacial tension as a function of polymer concentration at room temperature. Above 10 ppm concentration, the interfacial tension was significantly reduced. Compared to poly(NIPAM), the interfacial tension of the Al-NIPAM solution was slightly higher, possibly due to the hydrophilic $Al(OH)_3$-cores in the hybrid molecules. Since the interfacial tension remained unchanged beyond 50 ppm, the subsequent extraction experiments were conducted using a polymer concentration of 50 ppm.

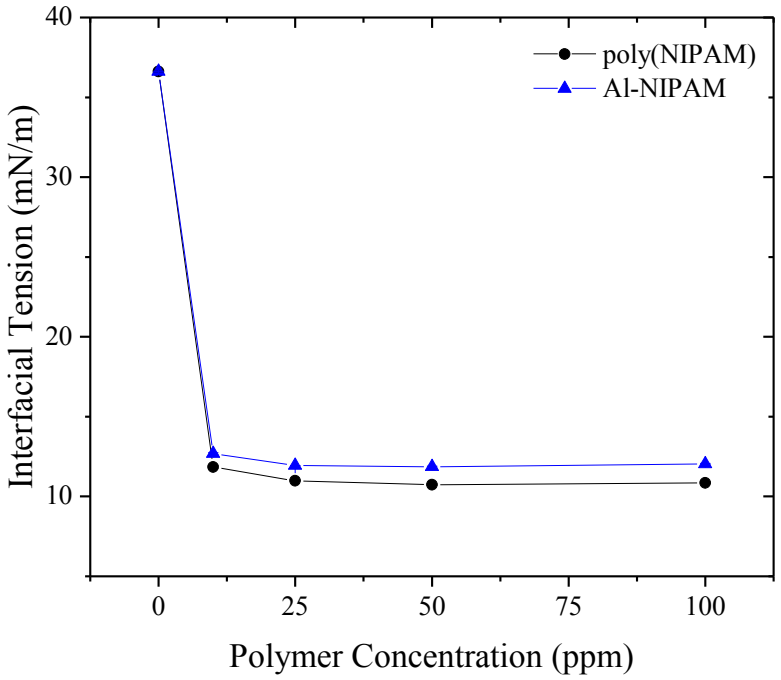

Figure 7.1. Interfacial tension at toluene-water interface as a function of polymer concentration at 20°C.

Figure 7.2 shows the interfacial tension for DI water, 50 ppm poly(NIPAM) and 50 ppm Al-NIPAM at the toluene-water interface as a function of temperature. The temperature dependence of toluene-water interfacial tension is in good agreement

to literature values.[91] Both poly(NIPAM) and Al-NIPAM showed exceptional interfacial activity due to adsorption at the oil-water interface, with strong temperature dependences. This may be due to the heat-induced change in the polymer hydrophobicity. For poly(NIPAM), two distinct regimes existed, where the interfacial tension decreased with temperatures until a minimum was reached (close to the $LCST_{poly(NIPAM)}$) and increased afterwards. Similar behavior has been reported for poly(NIPAM) at the n-dodecane-water and n-heptane-water interfaces.[92-93] Both poly(NIPAM) and Al-NIPAM exhibited similar interfacial properties and showed interfacial minimums near the LCST. It is worth noting that the measured interfacial tension of Al-NIPAM was slightly lower than poly(NIPAM) beyond 35°C. For Al-NIPAM, a hydrophilic $Al(OH)_3$-core integrated with poly(NIPAM) chains may contribute to a more amphiphilic polymer structure at elevated temperature.

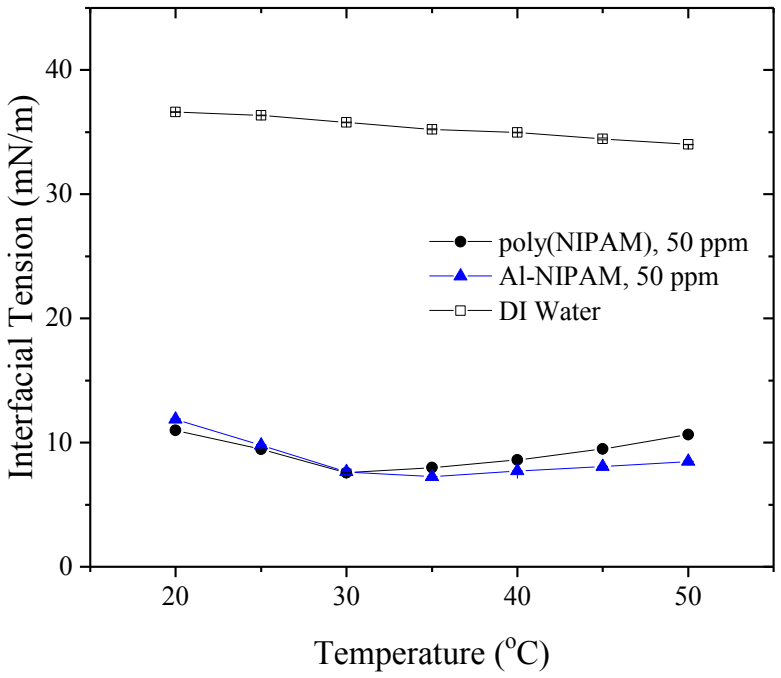

Figure 7.2. Interfacial tension for DI water, 50 ppm poly(NIPAM) and 50 ppm Al-NIPAM at the toluene-water interface as a function of temperature.

7.2 Bitumen Liberation

Bitumen liberation is a sub-process in bitumen extraction involving the separation of bitumen from sand grains. It can be influenced by process conditions (temperature and pH), interfacial properties, mechanical agitation and chemical additives.[6] A stereo microscope was used to visualize the liberation process of an oil sands ore sample with 25.0 wt.% fines content under different solution environments. Due to the high fines content, the ore can be considered to be low-grade. The solution was prepared with or without polymer addition in filtered OSPW (pH 8). To understand effects of temperature in bitumen liberation, two different liberation temperatures were conducted: room temperature (21°C) and elevated temperature (50°C). The elevated temperature of 50°C closely resembles the typical extraction temperature in oil sands commercial operations.

Figure 7.3 and 7.4 show the degree of bitumen liberation as a function of time at 21 and 50°C respectively. For the control (OSPW), the degree of bitumen liberation and liberation rate were low, which is to be expected due to the high viscosity of bitumen at room temperature. With the addition of poly(NIPAM) and Al-NIPAM (50 ppm), the bitumen liberation was slightly higher. However, the improvement was not obvious as the high viscosity of bitumen remained the dominant barrier for liberation. Compared to 21°C, the liberation performance was significantly improved at 50°C, highlighting the importance of temperature in the bitumen liberation process.[6, 18] At elevated temperature, the reduced viscosity of the bitumen favored bitumen liberation from the sand grains. More importantly, the addition of 50 ppm poly(NIPAM) and 50 ppm Al-NIPAM solution increased the degree of bitumen liberation and the liberation rate with a marked improvement over the control, showing comparable liberation profiles. As discussed in Section 7.1, poly(NIPAM) and Al-NIPAM were able to reduce the interfacial tension at the toluene-water interface. It is very likely these amphiphilic polymers can also lead to the reduction in the interfacial tensions between bitumen and water, thus facilitating the bitumen liberation process.[6]

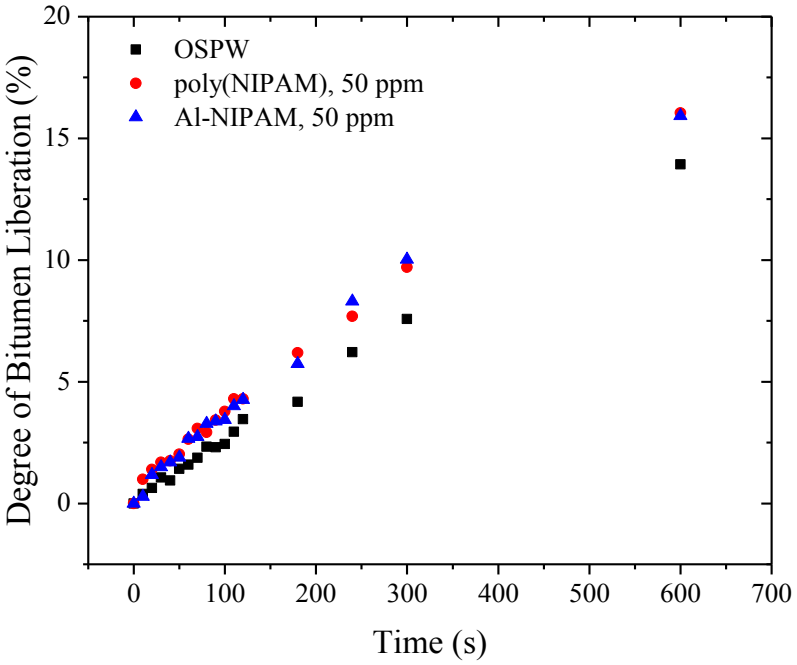

Figure 7.3. Bitumen liberation of oil sands ore conducted at 21°C.

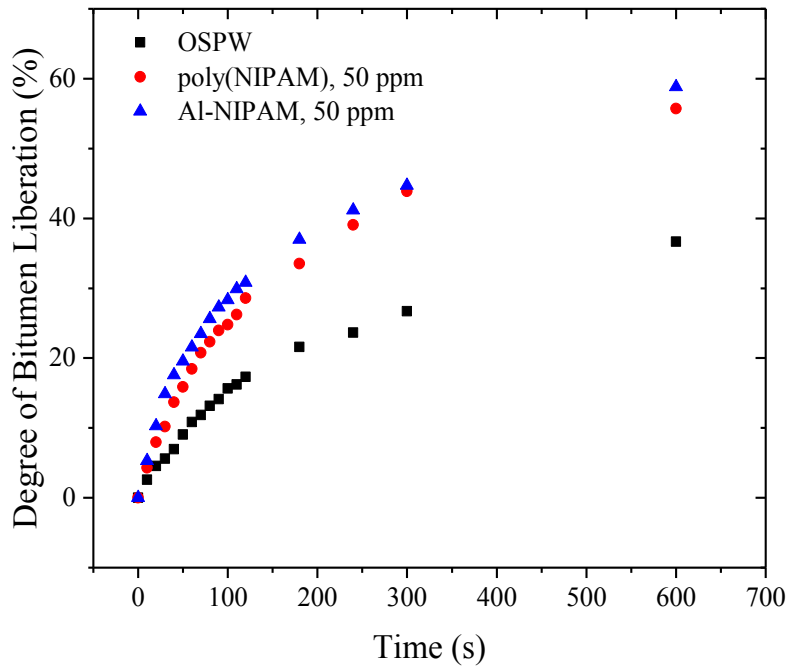

Figure 7.4. Bitumen liberation of oil sands ore conducted at 50°C.

7.3 Bitumen Aeration

Bitumen aeration is the process of attachment between liberated bitumen and air bubbles.[6] The aerated bitumen floats to the surface as froth due to the lower density. An induction timer was used to study the bitumen aeration process at 50°C and the induction time was defined as the contact time leading to 50% probability for an air bubble in contact with bitumen to attach.[6, 76] As fines are present during the floatation process, the effect of fines on the induction time is shown in Figure 7.5. The fines-covered bitumen surface was prepared by a conditioning step in a solids suspension containing 0.5 wt.% fines (see Section 3.3.3). The induction time for the fines-covered bitumen was ~1600 ms, much higher than the clean bitumen surface (~600 ms). The higher induction time for fines-covered bitumen can be attributed to the interactions between divalent cations in OSPW (see Table 3.1) and fines, promoting hetero-coagulation between bitumen and fines (slime coating).[6, 18-19] Fines deposited on bitumen alter the wettability of the bitumen surface to more water-wet, which becomes less favorable for bitumen-bubble attachment.

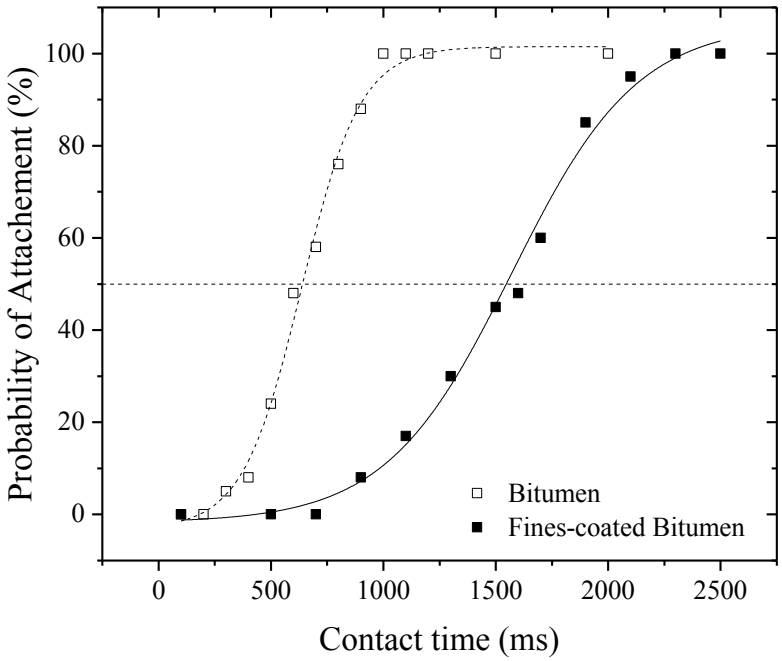

Figure 7.5. Effect of fines on probability of air bubble attachment with bitumen.

To study the effect of polymers on bitumen aeration process, the bitumen surface was conditioned in the fines suspension (0.5 wt.%) with polymer addition. Hence, the bitumen can interact with fines prior to induction time under different polymer solution environments. Figure 7.6 shows the effect of the polymers on the induction time. Compared to the control (OSPW), 50 ppm poly(NIPAM) increased the induction time, suggesting a worsening effect of slime coating. From a previous study, results of interaction forces between bitumen and fines suggested that poly(NIPAM) potentially induced slime coating of fine solids on bitumen.[88] On the other hand, 50 ppm Al-NIPAM lowered the induction time to ~1050 ms, showing an improvement over the control. This improvement is likely driven by the selective flocculation of fines using Al-NIPAM, resulting in less fines deposition onto the bitumen surface. As such, the extent and tendency of slime coating were reduced.

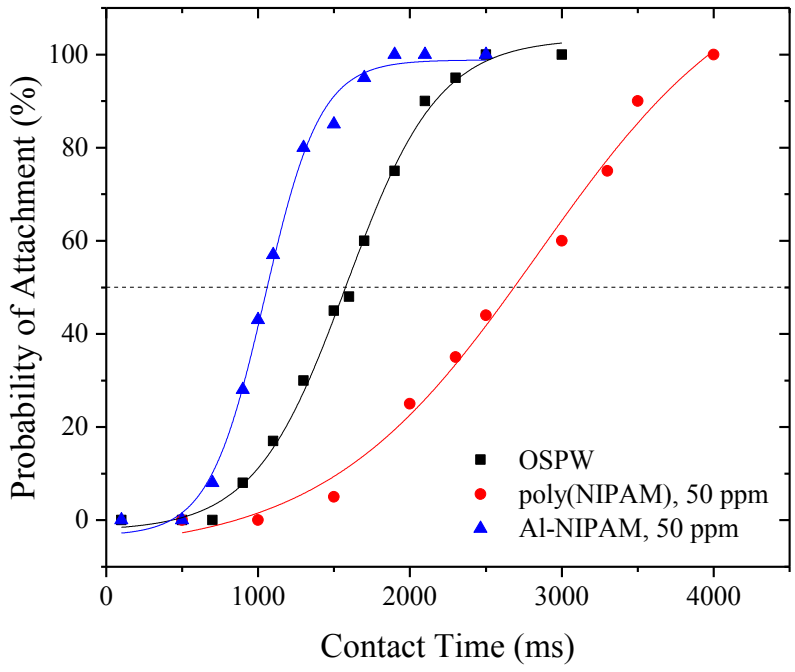

Figure 7.6. Probability of air bubble attachment with fines-coated bitumen under polymer solutions at 50°C.

In a previous flotation study, the use of poly(NIPAM) to process a low-grade oil sands ore was shown to improve bitumen recovery and tailings settling at elevated temperature.[88] Based on the qualitative liberation results, it is plausible that Al-NIPAM can improve bitumen recovery to a certain degree. Although both poly(NIPAM) and Al-NIPAM were able to improve the liberation of bitumen from the tested ore, poly(NIPAM) detrimentally affects bitumen-bubble attachment due to potential slime coating of fine solids on bitumen. Based on the induction time results, Al-NIPAM should be a better polymer aid for bitumen recovery compared to poly(NIPAM) due to its ability to flocculate fine solids and form dense flocs. However, it is worth noting that quantitative recovery experiments (e.g. Denver Cell, Batch Extraction Unit and LHES) are necessary to evaluate the extraction performance using these thermoresponsive polymers. Preliminary results showed that the hybrid polymer may have benefits in the bitumen extraction for its ability to reduce bitumen-water interfacial tension and flocculate fine clays.

In oil sands mining, integration of bitumen extraction and tailings management can be highly desirable. The potential of thermoresponsive hybrid polymer, as a polymer aid for bitumen extraction and tailings settling, makes it an attractive polymer for further studies.

Chapter 8: Conclusions

In this study, three kinds of thermoresponsive polymeric flocculants were synthesized and evaluated based on their performance on the flocculation and consolidation of mature fine tailings (MFT) suspension. Specifically, the flocculants included non-ionic poly(*N*-isopropylacrylamide) (poly(NIPAM)), cationic hybrid $Al(OH)_3$-poly(*N*-isopropylacrylamide) (Al-NIPAM) and coagulant/flocculant mixture blend of $Al(OH)_3$ colloids and poly(NIPAM) (poly(NIPAM)+Al). All synthesized polymers showed a lower critical solution temperature (LCST), confirming the heat-induced conformational transition from hydrophilic extended coils to hydrophobic collapsed globules.

Various methods were used to understand the adsorption and conformational behavior of the thermoresponsive hybrid polymer and its implications on flocculation. Zeta potential measurements showed that the surface charge of fine solids in MFT reduced with polymer addition, thus indicating polymer-particle interactions. QCM-D measurements showed that Al-NIPAM preferentially adsorbed on negatively-charged surface through electrostatic driving force. Upon heating, the adsorbed polymer layer was shown to become dehydrated and more compact simultaneously.

For the laboratory settling tests, the initial settling rate, supernatant turbidity and sediment solids content were used as performance indicators to evaluate each polymeric flocculants. Two temperature settling protocols were also used to assess the role of temperature in flocculation: room temperature (21°C) and elevated temperature (40°C). Compared to poly(NIPAM) and poly(NIPAM)+Al, the hybrid Al-NIPAM demonstrated superior settling and consolidation of MFT suspension. The $Al(OH)_3$-core in Al-NIPAM effectively destabilized the negatively-charged fine clays in MFT through charge neutralization, while the hybrid structure enhanced flocculation via the synergy between the inorganic coagulant and organic flocculant. All synthesized flocculants performed better when settled at 40°C, highlighting the benefit of flocculating with thermoresponsive polymers. When

dosed with 2.5 kg/t Al-NIPAM, the settling rate of the flocculated MFT reached 19 m/h, releasing a supernatant with turbidity < 150 NTU after 15 min. In-situ flocculation experiments using FBRM also confirmed that Al-NIPAM produced the largest and most shear resistant flocs, which was further densified when heated above the LCST.

The potential effects of the polymers in bitumen extraction were also studied. Due to the amphiphilic nature of poly(NIPAM), the thermoresponsive polymers were interfacially-active at the toluene-water interface. Preliminary liberation results showed that the synthesized polymers increased the degree of bitumen liberated from the ores at elevated temperature, likely due to reduction in the bitumen-water interfacial tension. Preliminary induction time results also showed that Al-NIPAM improved bitumen-bubble attachment in the presence of fines, likely reducing slime coating of fines on bitumen surface. Overall, the concept of using thermoresponsive hybrid polymer, as a potential polymer aid in tailings treatment and bitumen extraction, makes it an interesting polymer for further studies.

8.1 Original Contributions

Some of the original contributions are listed as follows:

- Applied thermoresponsive hybrid polymer for settling and consolidation of MFT suspension and showed the benefits of hybrid modification of poly(NIPAM).
- Studied the adsorption selectivity and conformation behavior of thermoresponsive hybrid polymer with respect to temperature using QCM-D.
- Demonstrated the in-situ densification of flocs (coil-globule transition) with a temperature-controlled FBRM setup.
- Investigated the interfacial properties of thermoresponsive hybrid polymer and its implications on the bitumen liberation and aeration processes.

Chapter 9: Future Works

The current study applied an $Al(OH)_3$-poly(*N*-isopropylacrylamide) hybrid polymer as a flocculant for oil sands tailings treatment and as a process aid for bitumen extraction. However, the results are limited to laboratory-scale testing and the working mechanisms need to be further explored. The following future works are recommended:

1. The thermoresponsive hybrid polymer should be systematically synthesized to evaluate the effect of molecular weight and aluminum content on flocculation and consolidation performance. As the molecular weight of hybrid polymers is generally lower than the comparable organic polymers, synthesis procedures to increase molecular weight and aluminum content of hybrid polymers should be considered to improve its applicability in industrial applications.

2. The residual polymer in supernatants after tailings treatment should be determined, and the recyclability of polymers should be explored.

3. The interaction forces between clays, fines and bitumen in polymer solution should be measured to better understand the mechanisms behind flocculation and extraction using the thermoresponsive hybrid polymer.

4. Bitumen extraction experiments (Denver Cell, Batch Extraction Unit) should be conducted for different oil sands ores to quantify the effect of thermoresponsive hybrid polymer in oil sands extraction.

5. Selection of inorganic and organic components should be optimized to improve the applicability of stimuli-responsive hybrid polymer in oil sands tailings treatment.

The synergetic combination of inorganic particles and organic stimuli-responsive polymer molecules will undoubtedly have many emerging applications in the coming years.

References

[1] Alberta Energy, Oil Sands. http://www.energy.alberta.ca/OS/, 2017 (accessed 2 April 2017).

[2] Oil Sands Magazine, Oil Sands 101: Process Overview. http://www.oilsandsmagazine.com/technical/oilsands-101/, 2016 (accessed 2 April 2017).

[3] Alberta Energy Regulator, ST98: 2018 Alberta's Energy Reserves & Supply/Demand Outlook. https://www.aer.ca/, 2018 (accessed 14 February 2018).

[4] Canadian Manufacturers & Exporters, Oil Sands Manufacturing. http://www.cme-mec.ca/download.php?file=hoh8olat.pdf/, 2013 (accessed 30 June 2017).

[5] Natural Resources Canada, Oil Sands: Tailings Management. http://www.nrcan.gc.ca/energy/publications/, 2015 (accessed 2 April 2017).

[6] J. H. Masliyah, J. Czarnecki, Z. Xu, Handbook on Theory and Practice of Bitumen Recovery from Athabasca Oil Sands: Theoretical Basis, volume 1, Kingsley Knowledge Publishing, Canada, 2011.

[7] J. R. McDougall (Alberta Research Council), Sustainable Development of Oil Sands – Challenges in Recovery and Use. http://www.arc.ab.ca/, 2006 (accessed 5 May 2017).

[8] R. Simmon, J. Allen (NASA), Mining Canada's Oil Sands. https://svs.gsfc.nasa.gov/10838/, 2011 (accessed 5 May 2017).

[9] Imperial Oil Ltd., Oil sands and Environment. http://www.imperialoil.ca/en-ca/company/environment/, 2017 (accessed 13 October 2017).

[10] N. Beier, M. Alostaz, D. Sego, Natural Dewatering Strategies for Oil Sands Fine Tailings, in *Tailings and Mine Waste 2009 Conference*, Banff Canada, 2009.

[11] J. Czarnecki, J. H. Masliyah, Z. Xu, M. Dabros, Handbook on Theory and Practice of Bitumen Recovery from Athabasca Oil Sands: Industrial Practice, volume 2, Kingsley Knowledge Publishing, Canada, 2013.

[12] Alberta Energy Regulator, Directive 085: Fluid Tailings Management for Oil Sands Mining Projects. https://www.aer.ca/documents/directives/Directive 085.pdf/ , 2017 (accessed 13 October 2017).

[13] Canada's Oil Sands Innovation Alliance, Tailings. http://www.cosia.ca/initiatives/tailings/, 2016 (accessed 2 April 2017).

[14] Natural Resources Canada, Oil Sands: Water Management. http://www.nrcan.gc.ca/energy/publications/, 2015 (accessed 5 May 2017).

[15] Alberta Innovates - Energy and Environment Solutions, Oil Sands Tailings Technology Deployment Roadmap, http://www.cosia.ca/, 2012 (accessed 30 June 2017).

[16] BGC Engineering Inc., Oil Sands Tailings Technology Review. http://www.infomine.com/library/publications/docs/BGCEngineering2010.pdf/, 2010 (accessed 30 June 2017).

[17] R. J. Chalaturnyk, J. D. Scott, B. Özüm, Management of Oil Sands Tailings, *Pet. Sci. Technol.* 20 (2002) 1025–1046.

[18] J. H. Masliyah, Z. Zhou, Z. Xu, J. Czarnecki, H. Hamza, Understanding water-based bitumen extraction from Athabasca oil sands, *Can. J. Chem. Eng.* 82 (2004) 628–654.

[19] T. Kasongo, Z. Zhou, Z. Xu, J. H. Masliyah, Effect of clays and calcium ions on bitumen extraction from Athabasca oil sands using flotation, *Can. J. Chem. Eng.* 78 (200) 674–681.

[20] G. M. Moody, Polymeric Flocculants, in: P. A. Williams (Ed.), Handbook of Industrial Water Soluble Polymers, Blackwell Publishing Ltd, Oxford UK, 2007, pp. 134–173.

[21] P. Fawell, Solid-Liquid separation of Clay Tailings, in: M. Gräfe, C. Klauber, A. J. McFarlane, D. J. Robinson (Eds.), Clays in the Minerals Processing Value Chain, first edition, Cambridge University Press, Perth Australia, 2017, pp.327–380.

[22] X. Wang, X. Feng, Z. Xu, J. H. Masliyah, Polymer aids for settling and filtration of oil sands tailings, *Can. J. Chem. Eng.* 88 (2010) 403–410.

[23] A. Alamgir, D. Harbottle, J. Masliyah, Z. Xu, Al-PAM assisted filtration system for abatement of mature fine tailings, *Chem. Eng. Sci.* 80 (2012) 91–99.

[24] H. Li, J. Zhou, R. Chow, A. Adegoroye, A. Najafi, Enhancing treatment and geotechnical stability of oil sands fine tailings using thermo-sensitive poly(*n*-isopropyl acrylamide), *Can. J. Chem. Eng.* 93 (2015) 1780–1786.

[25] D. Zhang, T. Thundat, R. Narain, Flocculation and Dewatering of Mature Fine Tailings Using Temperature-Responsive Cationic Polymers, *Langmuir* 33 (2017) 5900–5909.

[26] D. Vedoy, J. B. P. Soares, Water-soluble polymers for oil sands tailings treatment: a review, *Can. J. Chem. Eng.* 93 (2015) 888–904.

[27] H. Li, J. Long, Z. Xu, J. H. Masliyah, Flocculation of kaolinite clay suspension using a temperature–sensitive polymer, *AlChE J.* 53 (2007) 479–488.

[28] S. Sakohara, K. Nishikawa, Flocculation and compaction of highly concentrated suspension by using thermosensitive polymers, *Kagaku Kogaku Ronbun.* 26 (2000) 298–304.

[29] W. Y. Yang, J. W. Quan, Z. Q. Shen, A novel flocculant of $Al(OH)_3$-polyacrylamide ionic hybrid, *J. Colloid Interface Sci.* 273 (2004) 400–405.

[30] R. J. Hunter, Foundations of Colloid Science, second ed., Oxford University Press, New York USA, 2001.

[31] D. J. Shaw, Electrophoresis, first ed., Academic Press Inc, London / New York, 1969.

[32] D. Grasso, K. Subramaniam, M. Butkus, K. Strevett, J. Bergendahl, A review of non-DLVO interactions in environmental colloidal systems, *Rev. Environ. Sci. Biotechnol.* 1 (2002) 17–38.

[33] R. Pashley, P. McGuiggan, B. Ninham, D. Evans, Attractive Forces between Uncharged Hydrophobic Surfaces: Direct Measurements in Aqueous Solution, *Science* 229 (1985) 1088–1089.

[34] E. Meyer, K. Rosenberg, J. Israelachvili, Recent progress in understanding hydrophobic interactions, *Proc. Natl. Acad. Sci. U.S.A.* 103 (2006) 15739–15746.

[35] G. V. Franks, E. Forbes, H. Li, J.-P. O'Shea, Mechanism Responsible for Flocculation in Poly-(*N*-Isopropylacrylamide) Temperature Responsive Dewatering - Attractive Interaction Forces Induced by Surface Hydrophobicity, in *XXV International Mineral Processing Congress*, Brisbane Australia, 2010.

[36] J. Liu, Z. Xu, J. H. Masliyah, Interaction forces in bitumen extraction from oil sands, *J. Colloid Interface Sci.* 287 (2005) 507–520.

[37] W. J. Rankin, Minerals, Metals and Sustainability: Meeting Future Material Needs, first ed., CSIRO Publishing, Melbourne Australia, 2011.

[38] J. Duan, J. Gregory, Coagulation by hydrolysing metal salts, *Adv. Colloid Interface Sci.* 100–102 (2003) 475–502.

[39] H.-J. Butt, M. Kappl, Surface and Interfacial Forces, first ed., Wiley-VCH Verlag GmbH & Co. KGaA, Weinheim Germany, 2010.

[40] R. Hogg, Flocculation and Dewatering of Fine-Particle Suspension, in: B. Dobias, H. Stechmesser (Eds.), Coagulation and Flocculation, second ed., CRC Press, Boca Raton USA, 2005, pp. 805–850.

[41] Y. Adachi, A. Kobayashi, M. Kobayashi, Structure of Colloidal Flocs in relation to the Dynamic Properties of Unstable Suspension, *Int. J. Polym. Sci.* 2012 (2012) 1–14.

[42] L. Alagha, S. Wang, L. Yan, Z. Xu, J. H. Masliyah, Probing Adsorption of Polyacrylamide–Based Polymers on Anisotropic Basal Planes of Kaolinite Using Quartz Crystal Microbalance, *Langmuir* 29 (2013) 3989–3998.

[43] M. A. Stuart, W. T. Huck, J. Genzer, M. Müller, C. Ober, M. Stamm, G. B. Sukhorukov, I. Szleifer, V. V. Tsukruk, M. Urban, F. Winnik, S. Zauscher, I. Luzinov, S. Minko, Emerging applications of stimul-responsive polymer materials, *Nat. Mater. 9* (2010) 101–113.

[44] J. E. Guillet, M. Heskins, D. G. Murray, Polymeric flocculants, U.S. patent 4536294, 20 August 1985.

[45] Y. Deng, H. Xiao, R. Pelton, Temperature–sensitive flocculants based on poly(*N*-isopropylacrylamide-co-diallyldimethylammonium chloride), *J. Colloid Interface Sci.* 179 (1996) 188–193.

[46] G. V. Franks, C. V. Sepulveda, G. J. Jameson, pH-sensitive flocculation: Settling rates and sediment densities, *AlChE. J.* 52 (2006) 2774–2782.

[47] G. V. Franks, G. J. Jameson, Y. Y. Yan, S. R. Biggs, Stimulant sensitive flocculation and consolidation, U.S. patent 9174860B2, 3 November 2015.

[48] M. A. Ward, T. K. Georgious, Thermoresponsive polymers for biomedical applications, *Polymers* 3 (2011) 1215–1242.

[49] A. Gandhi, A. Paul, S. O. Sen, K. K. Sen, Studies on thermoresponsive polymers: Phase behaviour, drug delivery and biomedical applications, *Asian J. Pharm. Sci.* 10 (2015) 99–107.

[50] H. G. Schild, Poly(*N*-isopropylacrylamide: experiment, theory and application, *Prog. Polym. Sci.* 17 (1992) 163–249.

[51] T. Sun, G. Wang, L. Feng, B. Liu, Y. Ma, L. Jiang, D. Zhu, Reversible switching between superhydrophilicity and superhydrophobicity, *Angew. Chem. Int. Edit.* 43 (2004) 357–360.

[52] H. Li, J.-P. O'Shea, G. V. Franks, Effect of molecular weight of poly(*N*-isopropyl acrylamide) temperature-sensitive flocculants on dewatering, *AIChE J.* 55 (2009) 2070–2080.

[53] S. Sakohara, T. Kimura, K. Nishikawa, Flocculation Mechanism of Suspended Particles Using the Hydrophilic/Hydrophobic Transition of a Thermosensitive Polymer, *KONA* 20 (2002) 246–250.

[54] G. V. Franks, J.-P. O'Shea, E. Forbes, Improved solid-liquid separations with temperature responsive flocculants: a review," in *Chemeca 2012*, Wellington New Zealand, 2012.

[55] S. Sakohara, K. Nishikawa, Compaction of TiO_2 suspension utilizing hydrophilic/hydrophobic transition of cationic thermosensitive polymers, *J. Colloid Interface Sci.* 278 (2004) 304–309.

[56] J.-P. O'Shea, G. G. Qiao, G. V. Franks, Temperature responsive flocculation and solid–liquid separations with charged random copolymers of poly(*N*-isopropyl acrylamide), *J. Colloid Interface Sci.* 360 (2011) 61–70.

[57] S. Sakohara, E. Ochiai, T. Kusaka, Dewatering of activated sludge by thermosensitive polymers, *Sep. Purif. Technol.* 56 (2007) 296–302.

[58] X. S. Yuan, W. Shaw, Novel Processes for Treatment of Syncrude Fine Transition and Marine Ore Tailings, *Can. Metall. Quart. Eng.* 46 (2007) 265–272.

[59] M. R. Bockstaller, Progress in polymer hybrid materials, *Prog. Polym. Sci.* 40 (2015) 1–2.

[60] K. E. Lee, N. Morad, T. T. Teng, B. T. Poh, Development, characterization and the application of hybrid materials in coagulation/flocculation of wastewater: A review, *Chem. Eng. J.* 203 (2012) 370–386.

[61] W. Sun, J. Long, Z. Xu, J. H. Masliyah, Study of $Al(OH)_3$-Polyacrylamide-Induced Pelleting Flocculation by Single Molecule Force Spectroscopy, *Langmuir* 24 (2008) 14015–14021.

[62] G. Guo, Understanding Al-PAM Assisted Oil Sands Tailings Treatment, MSc thesis, University of Alberta, Edmonton, 2012.

[63] H. L. Wang, J. Y. Cui, W. F. Jiang, Synthesis, characterization and flocculation activity of novel $Fe(OH)_3$-polyacrylamide hybrid polymer, *Mater. Chem. Phys.* 130 (2011) 993–999.

[64] K. E. Lee, T. T. Teng, N. Morad, B. T. Poh, Y. F. Hong, Flocculation of kaolin in water using novel calcium chloride-polyacrylamide ($CaCl_3$-PAM) hybrid polymer, *Sep. Purif. Technol.* 75 (2010) 346–351.

[65] D. Roy, J. N. Cambre, B. S. Sumerlin, Future perspectives and recent advances in stimuli-responsive materials, *Prog. Polym. Sci.* 35 (2010) 278–301.

[66] T. Ogoshi, Y. Chujo, Organic-inorganic polymer hybrids prepared by the sol-gel method, *Compos. Interfaces* 11 (2005) 8–9.

[67] M. C. W. Chan, A Novel Flocculant for Enhanced Dewatering of Oil Sands Extraction Tailings, MSc thesis, University of Alberta, Edmonton, 2011.

[68] Q. Liu, D. Yeung, Z. Xu, R. Gupta, J. H. Masliyah, Temperature switchable polymers for fine coal dewatering, U.S patent 20130228525A1, 5 September 2013.

[69] Biolin Scientific, Measurements: QCM–D, http://www.biolinscientific.com/measurements/qcm–d/, 2017 (accessed 9 September 2017).

[70] S. Wang, Adsorption and Conformational Transition of Thermal-sensitive Polymers CP05 and Al-CP05 on Solid Surfaces. http://www.xumaster.com/, 2012 (accessed 18 December 2017).

[71] G. Zhang, C. Wu, Quartz Crystal Microbalance Studies on Conformational Change of Polymer Chains at Interface, *Macromol. Rapid Commun.* 30 (2008) 328–335.

[72] Mettler Toledo, FBRM Method of Measurement. https://www.mt.com/ca/en/home/library/videos/automated-reactors/Lasentec-FBRM-Method-of-Measurement.html/, 2017 (accessed 9 September 2017).

[73] Krüss, Du Noüy ring method. https://www.kruss-scientific.com/services/education-theory/glossary/du-nouey-ring-method/, 2017 (accessed 9 September 2017).

[74] L. He, Y. Zhang, F. Lin, Z. Xu, X. Li, H. Sui, Image analysis of heavy oil liberation from host rocks/sands, *Can. J. Chem. Eng.* 93 (2015) 1126–1137.

[75] G. Gu, Z. Xu, K. Nandakumar, J. H. Masliyah, Effects of physical environment on induction time of air-bitumen attachment, *Int. J. Miner. Process.* 69 (2003) 235–250.

[76] T. Chen, F. Lin, B. Primkulov, L. He, Z. Xu, Impact of salinity on warm water-based mineable oil sands processing, *Can. J. Chem. Eng.* 95 (2017) 281–289.

[77] R. Milačič, Speciation of Aluminum, in: R. Cornelis, J. Caruso, H. Crews, K. Heumann (Eds.), Handbook of Elemental Speciation - Species in the Environment, Food, Medicine and Occupational Health, volume 2, John Wiley & Sons, Chichester, 2005, pp. 7–19.

[78] S. Fujishige, Intrinsic viscosity-molecular weight relationships for poly(*N*-isopropylacrylamide) solutions, *Polym. J.* 19 (1987) 297–300.

[79] K. Kubota, S. Fujishige, I. Ando, Solution Properties of Poly(*N*-isopropylacrylamide) in Water, *Polym. J.* 22 (1990) 15–20.

[80] Varian Australia Pty Ltd., Atomic Spectroscopy. http://www.ufjf.br/baccan/files/2011/05/AAS-Varian1.pdf/, 1997 (accessed 9 September 2017).

[81] L. Alagha, S. Wang, Z. Xu, J. H. Masliyah, Adsorption Kinetics of a Novel Organic–Inorganic Hybrid Polymer on Silica and Alumina Studied by Quartz Crystal Microbalance, *J. Phys. Chem.* 115 (2011) 15390–15402.

[82] J.-P. O'Shea, G. G. Qiao, G. V. Franks, Solid-liquid separations with a temperature–responsive polymeric flocculant: effect of temperature and molecular weight on polymer adsorption and deposition, *J. Colloids Interface Sci.* 348 (2010) 9–23.

[83] P. Javis, B. Jefferson, J. Gregory, S. Parsons, A review of floc strength and breakage, *Water Res.* 39 (2005) 3121–3137.

[84] Q. Lu, Understanding Two–step Polymer Flocculation, MSc thesis, University of Alberta, Edmonton, 2016.

[85] A. R. Heath, P. D. Fawell, P. A. Bahri, J. D. Swift, Estimating Average Particle Size by Focused Beam Reflectance Measurement (FBRM), *Part. Part. Syst. Charact.* 19 (2002) 84–95.

[86] S. Wang, L. Alagha, Z. Xu, Adsorption of organic–inorganic hybrid polymers on kaolin from aqueous solutions, *Colloids Surf. A.*, 453 (2014) 13–20.

[87] H. Li, J. Long, Z. Xu, J. H. Masliyah, Novel polymer aids for low-grade oil sand ore processing, *Can. J. Chem. Eng.* 86 (2008) 168–176.

[88] J. Long, H. Li, Z. Xu, J. H. Masliyah, Improving oil sands processability using a temperature-sensitive polymer, *Energy Fuels* 25 (2011) 701–707.

[89] B. Yang, J. Duhamel, Extraction of Oil from Oil Sands Using Thermoresponsive Polymeric Surfactants, *ACS Appl. Mater. Interfaces* 7 (2015) 5879–5889.

[90] C. Han, Design and Synthesis of Temperature Switchable Non-ionic Block Copolymers for Application to Oil Sands Extraction, MSc thesis, University of Alberta, Edmonton, 2016.

[91] J. Saien, S. Akbari, Interfacial Tension of Toluene + Water + Sodium Dodecyl Sulfate from (20 to 50) °C and pH between 4 and 9, *J. Chem. Eng. Data* 51 (2006) 1832–1835.

[92] C. Monteux, C. Marlière, P. Paris, N. Pantoustier, N. Sanson, P. Perrin, Poly(*N*-isopropylacrylamide) microgels at the oil-water interface: interfacial properties as a function of temperature, *Langmuir* 26 (2010) 13839–13846.

[93] Z. Li, W. Richtering, T. Ngai, Poly(*N*-isopropylacrylamide) microgels at the oil-water interface: temperature effect, *Soft Matter* 10 (2014) 6182–6191.

[94] R. J. Young, P. A. Lovell, Introduction to Polymers, second ed., Chapman and Hall, London UK, 1991.

[95] P. Munk, T. M. Aminabhavi, P. Williams, D. E. Hoffman, M. Chmelir, Some Solution Properties of Polyacrylamide, *Macromolecules* 13 (1980) 871–876.

Appendix A: Molecular Weight of Polymer by Intrinsic Viscosity

The intrinsic viscosity $[\eta]$ of polymer solution is the viscosity of solution without interacting polymer coils and can be defined by Equation A.1:[94]

$$[\eta] = \lim_{c \to 0} \left(\frac{\eta_{sp}}{c} \right), \qquad \eta_{sp} = \frac{\eta - \eta_o}{\eta_o} \tag{A.1}$$

where η_{sp} is the specific viscosity, η_o is the viscosity in the absence of any polymer and c is the concentration of polymer in solution. The reduced viscosity (η_{red}) and inherent viscosity (η_{inh}) can be related to the concentration of polymer in solution by the Huggins (Equation A.2) and Kraemer equation (Equation A.3), where k' and k'' are the Huggins and Kramer coefficient respectively. The Kraemer equation is an empirical equation expressing the reduced viscosity of a polymer in dilute solution. The intrinsic viscosity can be determined by extrapolation to zero concentration on the plot of reduced and inherent viscosities.

$$\eta_{red} = \frac{\eta_{sp}}{c} = \mathrm{k}'[\eta]^2 c + [\eta] \tag{A.2}$$

$$\eta_{inh} = \frac{\ln(\eta/\eta_o)}{c} = \mathrm{k}''[\eta]^2 c + [\eta] \tag{A.3}$$

To measure the viscosity of polymer solution, the solution of known concentration was prepared and the flow of solution through a capillary of the Ubbelohde viscometer was timed. The viscosity measurement was measured at five different concentrations, ranging from 1 to 5 g/L. The η_{red} and η_{inh} were plotted against concentration (Dual Huggins-Kraemer plot). Figure A.1-3 show the dual Huggins-Kraemer plots for poly(NIPAM), poly(NIPAM)+Al and Al-NIPAM respectively. By data extrapolation, the average of the y-intercepts corresponded to the intrinsic viscosity of the polymer. The viscosity-average molecular weight can then be calculated with the intrinsic viscosity using the Mark-Houwink equation, as discussed in Section 4.3.1. It is worth noting that the molecular weight determined from the Mark-Houwink equation is an approximation approach.

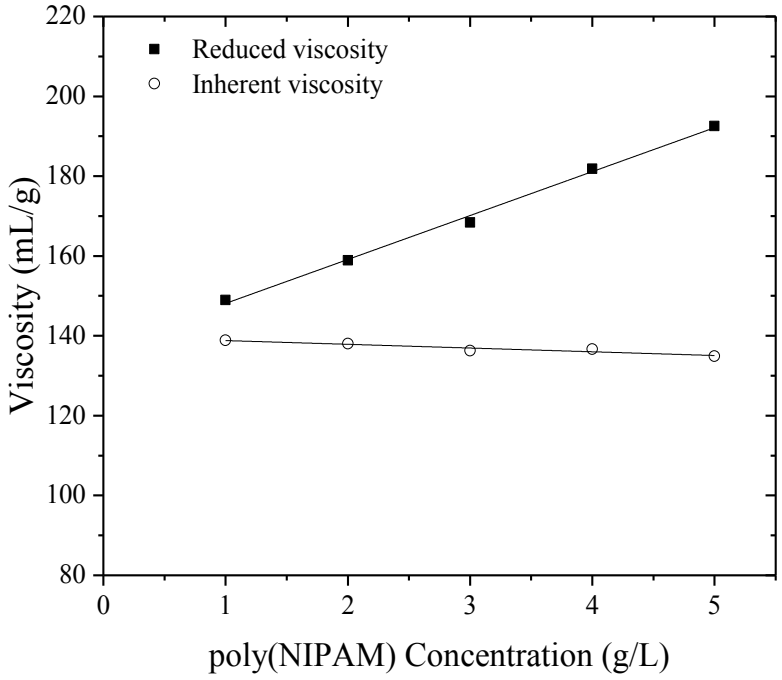

Figure A.1. Dual Huggins-Kraemer plot for poly(NIPAM) in THF.

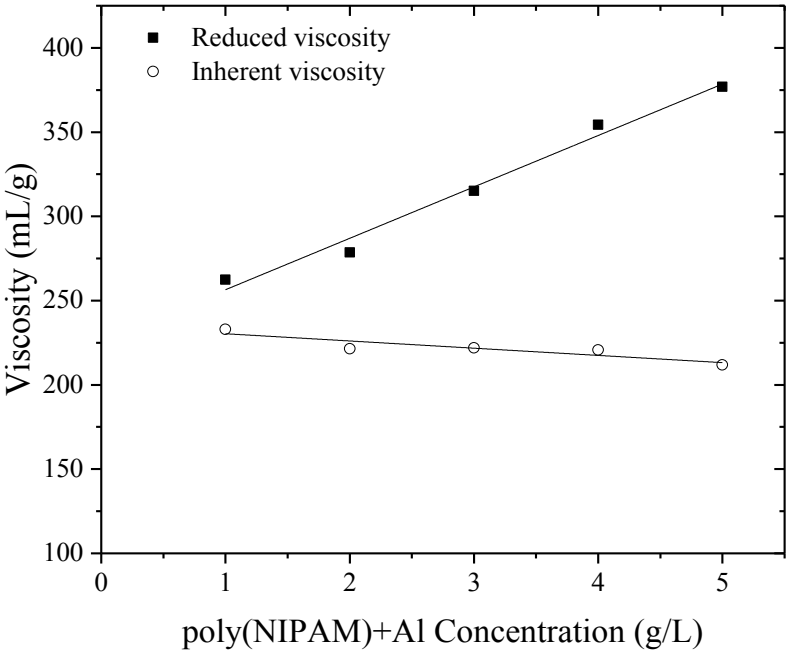

Figure A.2. Dual Huggins-Kraemer plot for poly(NIPAM)+Al in water.

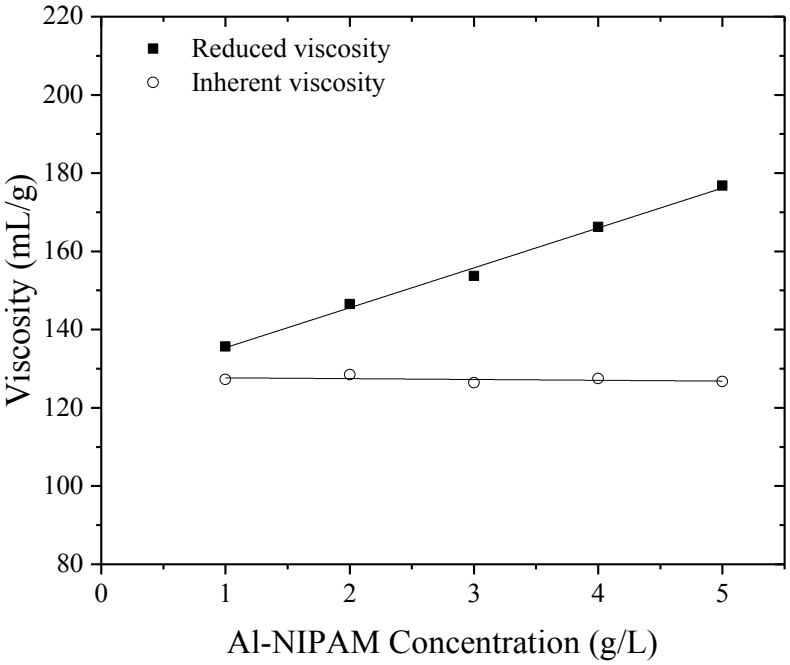

Figure A.3. Dual Huggins-Kraemer plot for Al-NIPAM in THF.

Table A.1 shows the Mark-Houwink constants for PAM and poly(NIPAM) in water.[79, 95] As shown in Figure A.4, the intrinsic viscosity of poly(NIPAM) was much lower than PAM at any given molecular weight of the polymer. Due to the viscous nature of PAM molecules, the polymer solution must be considerably diluted, which can lead to handling and preparation problems. As poly(NIPAM) has a significantly lower intrinsic viscosity than PAM, the stock poly(NIPAM) polymer solution can be prepared at higher concentration.

Table A.1. Mark-Houwink constants for PAM and poly(NIPAM).

Polymer	**Solvent**	K **(10^{-3})**	**a**	$\bar{M}_v$ **Range**
PAM	Water at 20°C[95]	3.02	0.68	$13.8 – 910 \times 10^4$
poly(NIPAM)	Water at 20°C[79]	14.5	0.50	$25.0 – 300 \times 10^4$

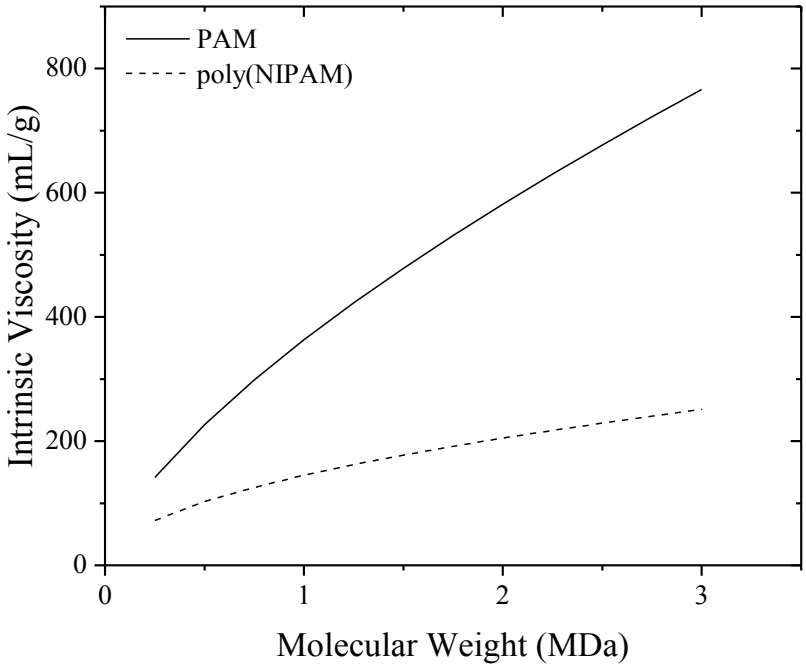

Figure A.4. Comparison of intrinsic viscosities of PAM and poly(NIPAM) using the Mark-Houwink equation.

Appendix B: Sample Supplementary Data

Size Distribution

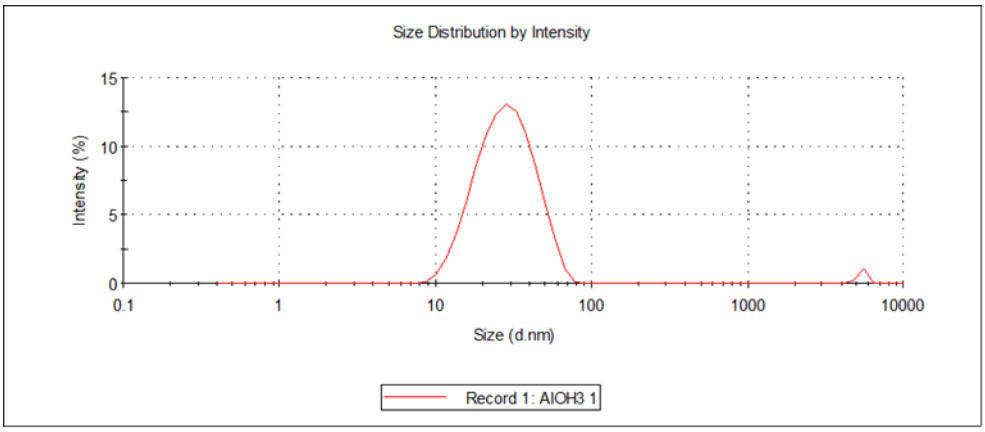

Figure B.1. Size distribution of $Al(OH)_3$ nanoparticles by intensity.

Zeta Potential Distribution

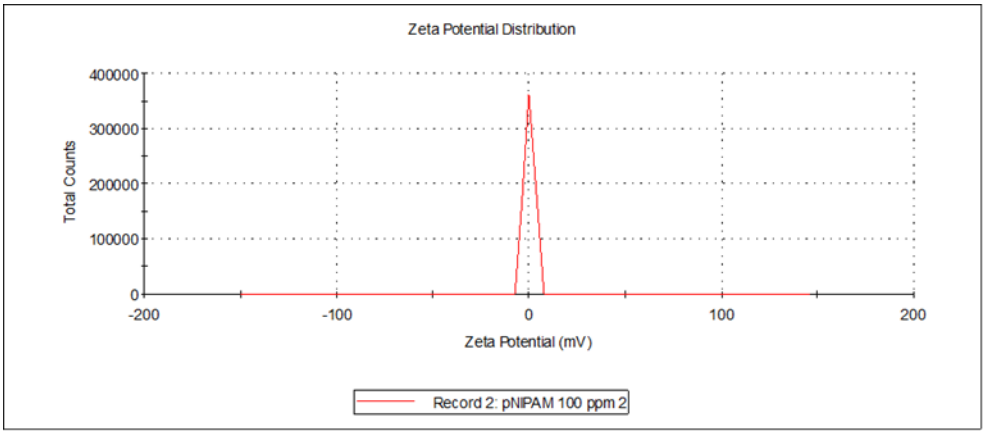

Figure B.2. Zeta potential distribution of poly(NIPAM) solution.

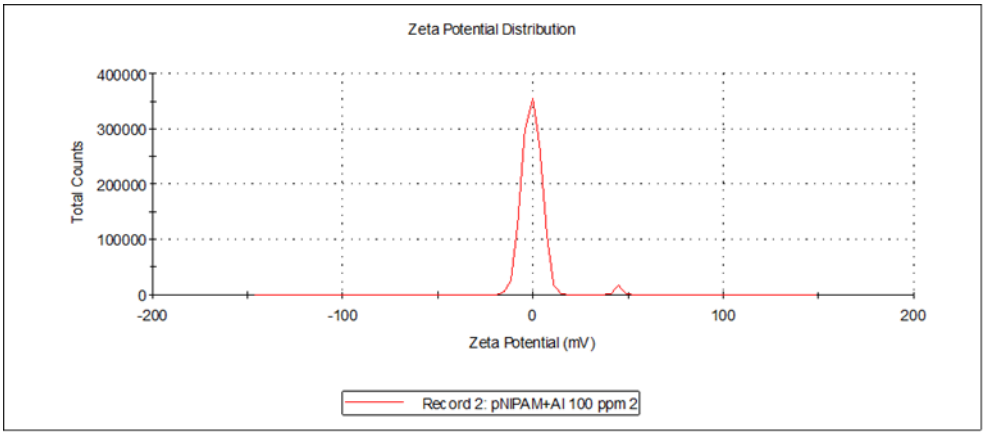

Figure B.3. Zeta potential distribution of poly(NIPAM)+Al mixture blend.

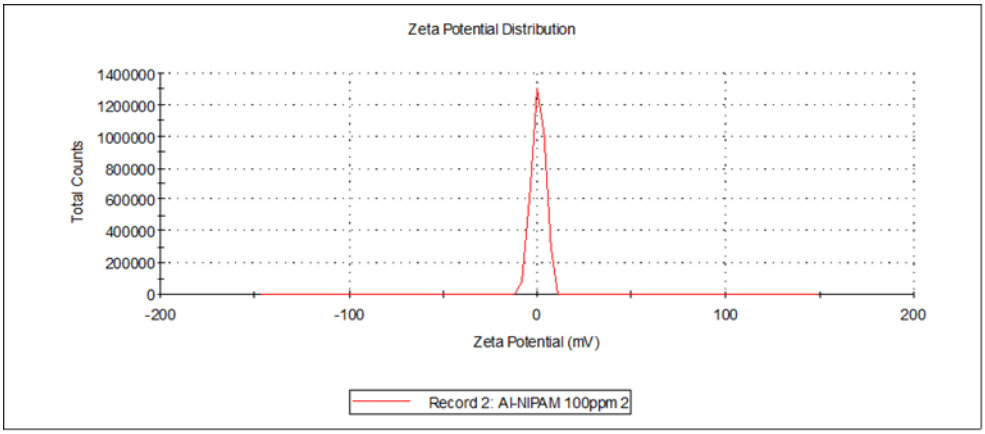

Figure B.4. Zeta potential distribution of Al-NIPAM solution.

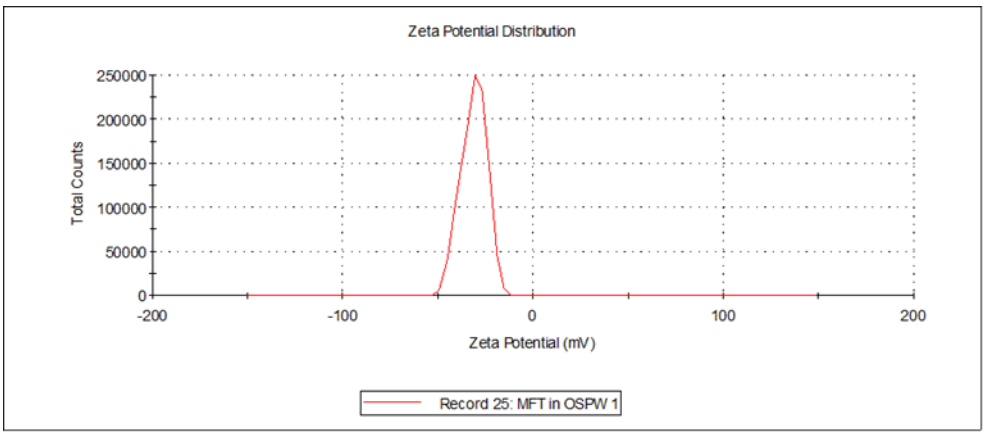

Figure B.5. Zeta potential distribution of 0.1 wt.% MFT in OSPW.

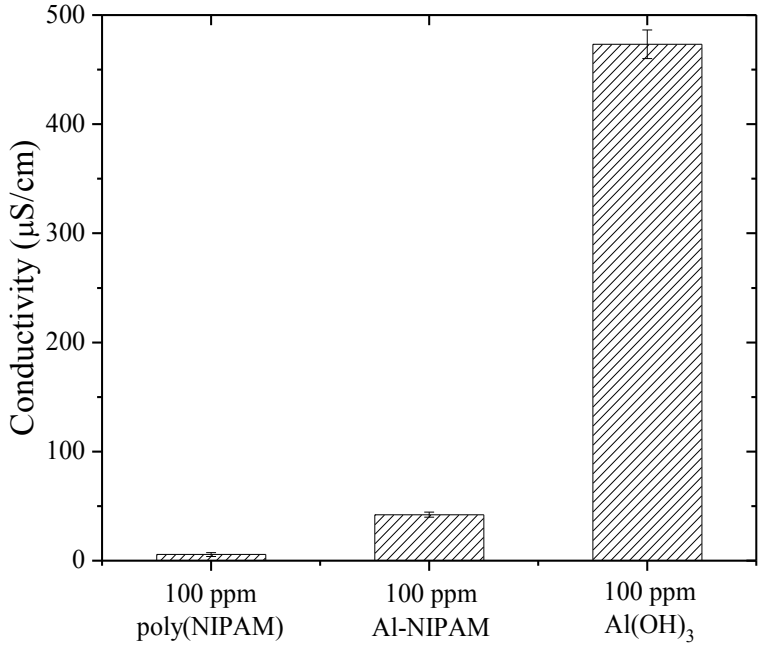

Figure B.6. Conductivities of poly(NIPAM), Al-NIPAM and $Al(OH)_3$ in water.

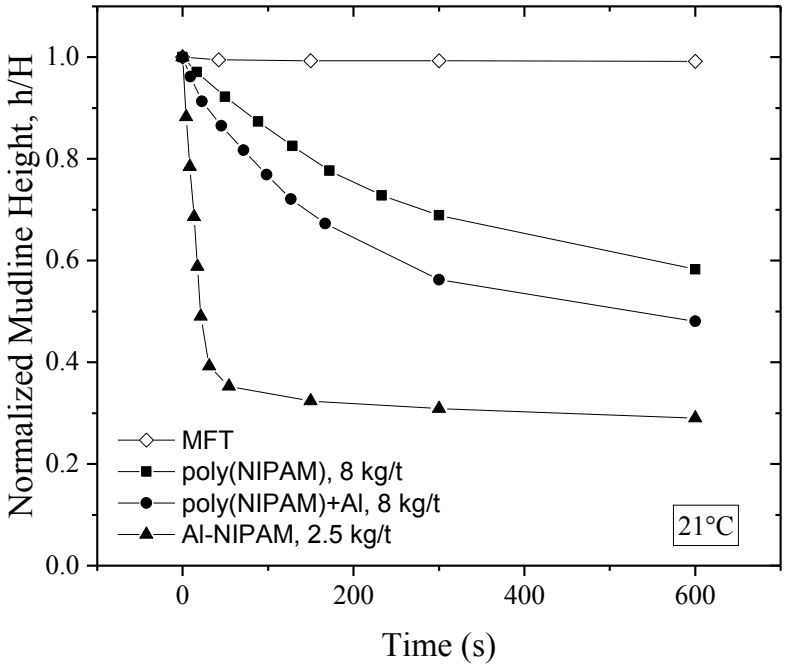

Figure B.7. Settling curves of 5 wt.% MFT and flocculated MFT at 21°C.

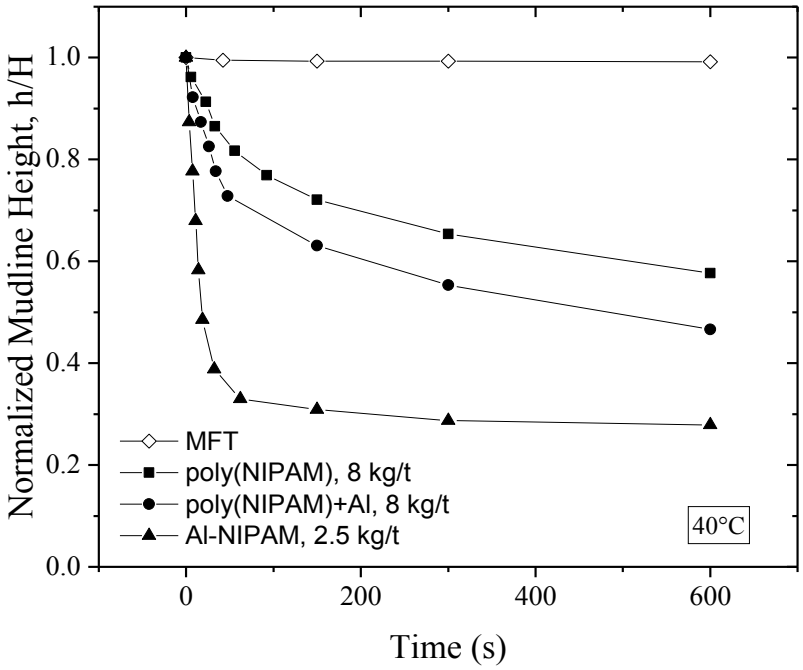

Figure B.8. Settling curves of 5 wt.% MFT and flocculated MFT at 40°C.

Table B.1. Mineralogy and composition of fines by XRD.

Composition (Sample BHF0073P2)	**Bulk fraction (wt.%)**	**Clay fraction (wt.%)**	**Overall (wt.%)**
Total Solids	59.86 ± 6.63	40.14 ± 6.63	100 ± 0.00
Total Clays	19.40 ± 5.47	88.97 ± 5.41	47.33 ± 1.08
Quartz	77.00 ± 5.67	11.03 ± 5.41	50.51 ± 1.26
K-feldspar	1.14 ± 0.81	-	0.67 ± 0.43
Plagioclase	0.41 ± 0.08	-	0.25 ± 0.08
Calcite	0.54 ± 0.20	-	0.33 ± 0.16
Dolomite	0.31 ± 0.12	-	0.19 ± 0.10
Siderite	0.73 ± 0.13	-	0.44 ± 0.09
Pyrite	0.46 ± 0.29	-	0.29 ± 0.22
Chlorite	0.75 ± 0.05	2.45 ± 0.28	1.42 ± 0.04
Kaolinite	6.02 ± 1.81	46.30 ± 2.81	22.22 ± 1.51
Illite	12.63 ± 3.76	38.64 ± 4.65	23.05 ± 2.07
Illite/Smectite Mixed Layer	-	1.58 ± 0.27	0.64 ± 0.19